

1982

Structures and polarized electronic absorption spectra of dimolybdenum tetraformate crystals

Gary Alan Robbins
Iowa State University

Follow this and additional works at: <https://lib.dr.iastate.edu/rtd>

 Part of the [Inorganic Chemistry Commons](#)

Recommended Citation

Robbins, Gary Alan, "Structures and polarized electronic absorption spectra of dimolybdenum tetraformate crystals " (1982).
Retrospective Theses and Dissertations. 7529.
<https://lib.dr.iastate.edu/rtd/7529>

This Dissertation is brought to you for free and open access by the Iowa State University Capstones, Theses and Dissertations at Iowa State University Digital Repository. It has been accepted for inclusion in Retrospective Theses and Dissertations by an authorized administrator of Iowa State University Digital Repository. For more information, please contact digirep@iastate.edu.

INFORMATION TO USERS

This reproduction was made from a copy of a document sent to us for microfilming. While the most advanced technology has been used to photograph and reproduce this document, the quality of the reproduction is heavily dependent upon the quality of the material submitted.

The following explanation of techniques is provided to help clarify markings or notations which may appear on this reproduction.

1. The sign or "target" for pages apparently lacking from the document photographed is "Missing Page(s)". If it was possible to obtain the missing page(s) or section, they are spliced into the film along with adjacent pages. This may have necessitated cutting through an image and duplicating adjacent pages to assure complete continuity.
2. When an image on the film is obliterated with a round black mark, it is an indication of either blurred copy because of movement during exposure, duplicate copy, or copyrighted materials that should not have been filmed. For blurred pages, a good image of the page can be found in the adjacent frame. If copyrighted materials were deleted, a target note will appear listing the pages in the adjacent frame.
3. When a map, drawing or chart, etc., is part of the material being photographed, a definite method of "sectioning" the material has been followed. It is customary to begin filming at the upper left hand corner of a large sheet and to continue from left to right in equal sections with small overlaps. If necessary, sectioning is continued again—beginning below the first row and continuing on until complete.
4. For illustrations that cannot be satisfactorily reproduced by xerographic means, photographic prints can be purchased at additional cost and inserted into your xerographic copy. These prints are available upon request from the Dissertations Customer Services Department.
5. Some pages in any document may have indistinct print. In all cases the best available copy has been filmed.

**University
Microfilms
International**

300 N. Zeeb Road
Ann Arbor, MI 48106

8224247

Robbins, Gary Alan

STRUCTURES AND POLARIZED ELECTRONIC ABSORPTION SPECTRA OF
DIMOLYBDENUM TETRAFORMATE CRYSTALS

Iowa State University

PH.D. 1982

University
Microfilms
International 300 N. Zeeb Road, Ann Arbor, MI 48106

PLEASE NOTE:

In all cases this material has been filmed in the best possible way from the available copy.
Problems encountered with this document have been identified here with a check mark .

1. Glossy photographs or pages _____
2. Colored illustrations, paper or print _____
3. Photographs with dark background _____
4. Illustrations are poor copy _____
5. Pages with black marks, not original copy _____
6. Print shows through as there is text on both sides of page _____
7. Indistinct, broken or small print on several pages
8. Print exceeds margin requirements _____
9. Tightly bound copy with print lost in spine _____
10. Computer printout pages with indistinct print _____
11. Page(s) _____ lacking when material received, and not available from school or author.
12. Page(s) _____ seem to be missing in numbering only as text follows.
13. Two pages numbered _____. Text follows.
14. Curling and wrinkled pages _____
15. Other _____

University
Microfilms
International

**Structures and polarized electronic absorption
spectra of dimolybdenum tetraformate crystals**

by

Gary Alan Robbins

**A Dissertation Submitted to the
Graduate Faculty in Partial Fulfillment of the
Requirements for the Degree of
DOCTOR OF PHILOSOPHY**

**Department: Chemistry
Major: Inorganic Chemistry**

Approved:

Signature was redacted for privacy.

In Charge of Major Work

Signature was redacted for privacy.

For the Major Department

Signature was redacted for privacy.

For the Graduate College

Members of the Committee:

Signature was redacted for privacy.

**Iowa State University
Ames, Iowa**

1982

TABLE OF CONTENTS

	Page
INTRODUCTION	1
EXPERIMENTAL	33
Preparation	33
Crystal Optics and Spectra	34
Polarization Ratios	43
Crystallographic Indexing	45
X-ray Data Collection and Structure Solution	47
General	47
β -Mo ₂ (O ₂ CH) ₄	48
γ -Mo ₂ (O ₂ CH) ₄	50
RESULTS AND DISCUSSION	52
Description of Crystal Structures	52
Crystal Optics	90
Crystal Spectra	99
BIBLIOGRAPHY	138
ACKNOWLEDGMENTS	142
APPENDIX A: OBSERVED AND CALCULATED STRUCTURE FACTORS FOR β -Mo ₂ (O ₂ CH) ₄	143
APPENDIX B: OBSERVED AND CALCULATED STRUCTURE FACTORS FOR γ -Mo ₂ (O ₂ CH) ₄	151
APPENDIX C	154

LIST OF FIGURES

	Page
Figure 1. Structure of quadruply-bonded complexes showing the molecular axis system (axial ligands A may not be present)	3
Figure 2. General structure of dimolybdenum tetracarboxylate complexes	10
Figure 3. Energy levels calculated by SCF-X α -SW methods for Mo ₂ (O ₂ CH) ₄ and Mo ₂ Cl ₈ ⁴⁻ (orbitals containing at least 15% Mo character)	15
Figure 4. Polarized absorption spectra for Mo ₂ (O ₂ CH) ₄	18
Figure 5. The carboxylate π^* orbital	24
Figure 6. The behavior of polarized light entering a crystal face	36
Figure 7. Basic components of the polarizing microscope	38
Figure 8. Behavior of a crystal between perpendicular polarizers	40
Figure 9. Atom labelling system used in the structure solution of β -Mo ₂ (O ₂ CH) ₄ . Primes indicate atoms generated by an inversion center located at the center of the molecule	58
Figure 10. Atom labelling system used in the structure solution of γ -Mo ₂ (O ₂ CH) ₄ . Primes indicate atoms generated by an inversion center located at the center of the molecule	61
Figure 11. Intermolecular bonding in dimolybdenum tetracarboxylate complexes	63
Figure 12. The molecular structure of α -Mo ₂ (O ₂ CH) ₄	64
Figure 13. The molecular structure of β -Mo ₂ (O ₂ CH) ₄	65
Figure 14. The molecular structure of γ -Mo ₂ (O ₂ CH) ₄	66
Figure 15. Diagram showing the observed effects of axial coordination (some ligands are omitted for clarity). All atoms shown lie approximately in the plane of the paper	81

Figure 16.	Diagram of the Mo-O axial interaction showing orbital geometries	83
Figure 17.	The molecular structure of $\text{Mo}_2(\text{O}_2\text{CH})_4 \cdot \text{KCl}$	88
Figure 18.	A view of $\beta\text{-Mo}_2(\text{O}_2\text{CH})_4$ showing $0\bar{1}3$ lattice planes	93
Figure 19.	Polarized spectra of $\alpha\text{-Mo}_2(\text{O}_2\text{CH})_4$ showing the weak features	101
Figure 20.	Polarized spectra of a crystal of $\alpha\text{-Mo}_2(\text{O}_2\text{CH})_4$. The crystal thickness was $\sim 9 \mu\text{m}$.	106
Figure 21.	Polarized spectra of sublimed $\alpha\text{-Mo}_2(\text{O}_2\text{CH})_4$ (Group I crystals)	107
Figure 22.	Polarized spectra of sublimed $\alpha\text{-Mo}_2(\text{O}_2\text{CH})_4$ (Group II crystals). The crystal thickness was $5.1 \mu\text{m}$	108
Figure 23.	Polarized spectra of $\beta\text{-Mo}_2(\text{O}_2\text{CH})_4$	115
Figure 24.	Scale-expanded spectra of $\beta\text{-Mo}_2(\text{O}_2\text{CH})_4$	116
Figure 25.	Polarized spectra of $\beta\text{-Mo}_2(\text{O}_2\text{CH})_4$, showing weak vibrational progressions. The crystal thickness was $36 \mu\text{m}$	117
Figure 26.	Boltzman plot for hot bands in $\beta\text{-Mo}_2(\text{O}_2\text{CH})_4$	124
Figure 27.	Polarized spectra of $\gamma\text{-Mo}_2(\text{O}_2\text{CH})_4$. The crystal thickness was $50 \pm 10 \mu\text{m}$	126
Figure 28.	Polarized spectra of $\text{Mo}_2(\text{O}_2\text{CH})_4 \cdot \text{KCl}$	133

LIST OF TABLES

	Page
Table 1. Data from the polarized spectra of $\text{Mo}_2(\text{O}_2\text{CCH}_2\text{NH}_3)_4(\text{SO}_4)_2 \cdot 4\text{H}_2\text{O}$	13
Table 2. A summary of the electronic spectra of binuclear molybdenum complexes of bond order greater than three	26
Table 3. Calculated and observed $\delta \rightarrow \delta^*$ transition energies in $\text{Mo}_2\text{Cl}_8^{4-}$ and $\text{Mo}_2(\text{O}_2\text{CH})_4$	30
Table 4. Crystallographic parameters for the $\text{Mo}_2(\text{O}_2\text{CH})_4$ polymorphs and for $\text{Mo}_2(\text{O}_2\text{CH})_4 \cdot \text{KCl}$	53
Table 5. Final positional parameters and their estimated standard deviations for $\beta\text{-Mo}_2(\text{O}_2\text{CH})_4$	54
Table 6. Final thermal parameters and their estimated standard deviations for $\beta\text{-Mo}_2(\text{O}_2\text{CH})_4$	56
Table 7. Final positional parameters and their estimated standard deviations for $\gamma\text{-Mo}_2(\text{O}_2\text{CH})_4$	59
Table 8. Final thermal parameters and their estimated standard deviations for $\gamma\text{-Mo}_2(\text{O}_2\text{CH})_4$	60
Table 9. Interatomic distances and angles and their estimated standard deviations for $\beta\text{-Mo}_2(\text{O}_2\text{CH})_4$	68
Table 10. Interatomic distances and angles and their estimated standard deviations for $\gamma\text{-Mo}_2(\text{O}_2\text{CH})_4$	72
Table 11. Interatomic distances and angles illustrating the effects of axial coordination in several dimolybdenum tetracarboxylate complexes	77
Table 12. Comparison of interatomic distances and angles in the polymorphs of $\text{Mo}_2(\text{O}_2\text{CH})_4$	85
Table 13. Weak vibrational details of the low energy absorption band in crystals of $\alpha\text{-Mo}_2(\text{O}_2\text{CH})_4$ at 17 K	102
Table 14. Vibrational details in the crystal spectra of sublimed $\alpha\text{-Mo}_2(\text{O}_2\text{CH})_4$ at 6 K showing additional crystal sites	110

Table 15.	Reported vibrational details in the spectra of sublimed films of $\alpha\text{-Mo}_2(\text{O}_2\text{CH})_4$	112
Table 16.	Vibrational details in the crystal spectra of $\beta\text{-Mo}_2(\text{O}_2\text{CH})_4$ at 5 K	118
Table 17.	Weak vibrational details in the crystal spectra of $\gamma\text{-Mo}_2(\text{O}_2\text{CH})_4$ at 6 K	127
Table 18.	Vibrational progressions built upon A_0 in the crystal spectra of dimolybdenum tetracarboxylate complexes	130
Table 19.	Vibrational details in the crystal spectra of $\text{Mo}_2(\text{O}_2\text{CH})_4 \cdot \text{KCl}$ at 5 K	134

INTRODUCTION

In this work, spectra of $\text{Mo}_2(\text{O}_2\text{CH})_4 \cdot \text{KCl}$, along with crystal structures and spectra of two new polymorphs of dimolybdenum tetraformate are presented and analyzed. Data and results are discussed in relation to other quadruply-bonded molybdenum complexes, in particular the carboxylate complexes and including the original polymorph of dimolybdenum tetraformate (1). The author proposes that the original polymorph be designated $\alpha\text{-Mo}_2(\text{O}_2\text{CH})_4$, and the new polymorphs designated $\beta\text{-Mo}_2(\text{O}_2\text{CH})_4$ and $\gamma\text{-Mo}_2(\text{O}_2\text{CH})_4$.

In recent years, there has been considerable interest and controversy concerning the assignment of the lowest energy band of transitions in the dimolybdenum tetracarboxylate complexes. Polarized absorption spectroscopy has proven itself a useful technique in elucidation of the electronic structure of dimer complexes containing multiple metal-metal bonds. In favorable cases, it may lead to conclusive assignments of electronic transitions and the relative ordering of molecular orbitals. More often, however, data may be incomplete or lead to inconclusive results. In addition, many factors in such a study are frequently beyond experimental control: size and quality of crystals, molecular symmetry and orientation, and broadness and resolution of observed peaks. This particular study was undertaken to augment an earlier study of dimolybdenum tetraformate and clarify certain issues raised by other studies of binuclear tetracarboxylates.

The metal-metal quadruple bond was proposed by Cotton in 1964, to account for unusual features noted in the structure of $\text{K}_2\text{Re}_2\text{Cl}_8 \cdot 2\text{H}_2\text{O}$ (2-4). The $\text{Re}_2\text{Cl}_8^{2-}$ anion was found to consist of two square planar ReCl_4^- units in a rotationally eclipsed conformation approximating D_{4h} point group symmetry. An extremely short Re-Re distance of 2.24 Å was found and a magnetic susceptibility measurement showed the compound to be diamagnetic. Cotton used an approximate molecular orbital approach to describe the bonding qualitatively. Figure 1 shows the general molecular structure of binuclear metal complexes and the axis system most often used in group theoretical considerations of the bonding. This is the axis system Cotton used and the one we will use throughout our discussions of the bonding and spectra. The molecular z axis was defined by the metal-metal axis and the x and y axes were chosen to lie in M-L-L-M planes. Cotton assigned metal s , p_x , p_y , and $d_{x^2-y^2}$ orbitals to metal-ligand σ bonding. Overlap of the d_{z^2} , d_{xz} , and d_{yz} orbitals on the two metal centers would result in the formation of one σ and two π bonds, respectively. Similarly, overlap of the metal d_{xy} orbitals would form one δ bond, so designated since two nodal planes would pass through the metal interatomic axis. The metal p_z orbitals, which were neglected for the sake of simplicity, might also be involved in the metal-metal σ bonding. The metal p_z and d_{z^2}

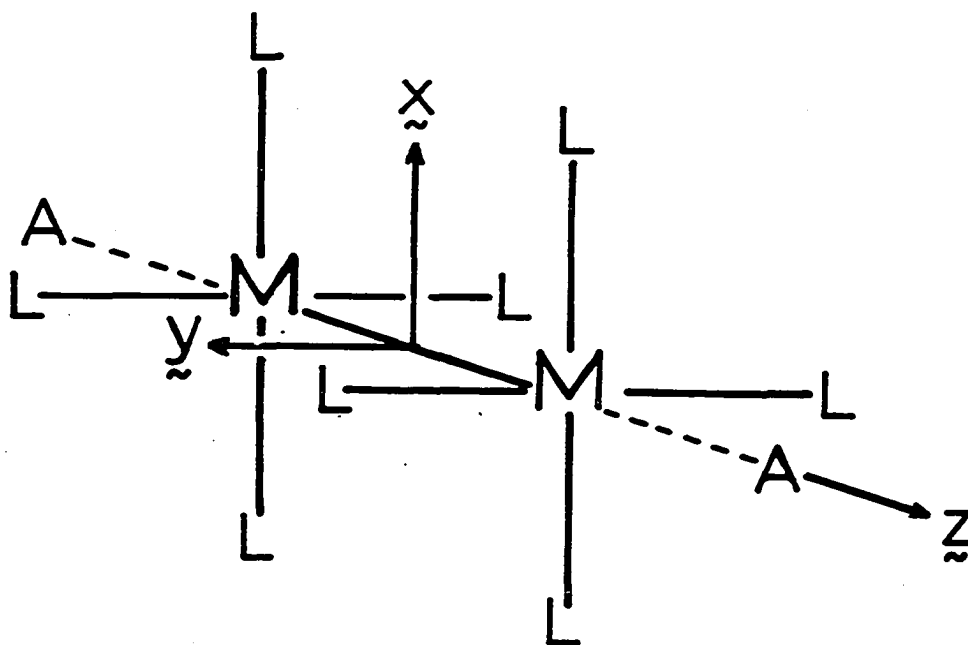


Figure 1. Structure of quadruply-bonded complexes showing the molecular axis system (axial ligands A may not be present)

orbitals would also be involved in bonding with any axial ligands (A in Figure 1). This bonding scheme did account for the observed diamagnetism, short Re-Re distance, and eclipsed conformation. Had $\text{Re}_2\text{Cl}_8^{2-}$ adopted a staggered conformation, the δ bond would have no net overlap while the σ and π bonds would not be affected.

It is noteworthy that in 1956, a δ bond was suggested by Figgis and Martin to explain the diamagnetic behavior of $\text{Cu}_2(\text{O}_2\text{CCH}_3)_4 \cdot 2\text{H}_2\text{O}$ and $\text{Cr}_2(\text{O}_2\text{CCH}_3)_4 \cdot 2\text{H}_2\text{O}$ (5). They proposed a similar formulation of the quadruple bond as that proposed later for $\text{Re}_2\text{Cl}_8^{2-}$. It is unfortunate that an inaccurate Cr-Cr distance of 2.64 Å (6) led to the conclusion that the bonding was quite weak in that complex. This distance was later found to be 2.39 Å (7).

Before we look at electronic spectra, it is important to consider the selection rules. The intensity of an electronic transition depends on the transition moment integral

$$\mu_{\nu} = \langle \psi_{e1}^{-} | (\hat{M}_x + \hat{M}_y + \hat{M}_z) | \psi_{e1}^{\circ} \rangle$$

The ground and excited state electronic wavefunctions are represented by ψ_{e1}° and ψ_{e1}^{-} , respectively, and \hat{M}_x , \hat{M}_y , and \hat{M}_z are components of the electric dipole operator \hat{M} . For example, $\hat{M}_x = \sum e\vec{x}_i$, where e is the charge on the electron and \vec{x}_i is the x component of the vector position of the i^{th} electron relative to the center of mass. The sum is taken

over all the electrons. We can use group theory to determine when the transition moment integral would vanish, without the need to evaluate the integral itself. For a non-vanishing integral, group theory requires that the symmetry product of all functions and operators involved in the integral contain the totally symmetric representation. For our case of D_{4h} , we have

$$\Gamma_{\psi_{el}} \circ \Gamma_{op} \cdot \Gamma_{\psi_{el}} \supset A_{1g},$$

where Γ_{op} represents the irreducible representation of \hat{M}_x , \hat{M}_y , or \hat{M}_z (treating each separately), and the Γ_{ψ} 's are the symmetry representations of the wavefunctions. Under D_{4h} , \hat{M}_z transforms as A_{2u} , and \hat{M}_x and \hat{M}_y form a degenerate pair transforming as E_u . If such a product involving \hat{M}_z gives A_{1g} then the transition is electric dipole-allowed for light plane-polarized in the z direction. Similarly, an A_{1g} product resulting from \hat{M}_x and \hat{M}_y indicated the transition is electric dipole-allowed with x, y polarization. A simpler, but equivalent expression of these selection rules is

$$\Gamma_{\psi_{el}} \circ \Gamma_{\psi_{el}} \supset A_{2u} \text{ for } z \text{ polarization and}$$

$$\Gamma_{\psi_{el}} \circ \Gamma_{\psi_{el}} \supset E_u \text{ for } x, y \text{ polarization.}$$

When transitions are electric dipole-forbidden, there is yet another mechanism which may allow certain transitions. This is the vibronic, or Hertzberg-Teller mechanism, producing

transitions which are, normally, much lower in intensity than electric dipole-allowed transitions. In our consideration of the transition moment integral it was assumed that the electronic and vibrational wavefunctions could be completely separated (although it was not stated). This was a mathematical simplification which does not strictly apply to the physical realm. In polyatomic molecules, vibrations with appropriate symmetries will produce mixing of wavefunctions with various symmetries. We now express the transition moment integral as

$$\mu_{\lambda} = \langle \psi_{\text{el}} \psi_{\text{vib}}' | (\hat{M}_x + \hat{M}_y + \hat{M}_z) | \psi_{\text{el}} \psi_{\text{vib}}^{\circ} \rangle$$

using the vibronic (vibrational-electronic) wavefunction $\psi_{\text{el}} \psi_{\text{vib}}$ in place of ψ_{el} used previously. The same requirement for a non-vanishing integral applies here, except that the symmetry representations of $\psi_{\text{vib}}^{\circ}$ and ψ_{vib}' must be included in the product. For room temperature and cryogenic measurements of spectra, the $v=0$ vibrational level is the most populated level in $\psi_{\text{vib}}^{\circ}$ and has A_{1g} symmetry. Including this in our treatment we obtain

$$\Gamma_{\psi_{\text{el}}^{\circ}} \cdot \Gamma_{\psi_{\text{el}}'} \cdot \Gamma_{\psi_{\text{vib}}^{\circ}} \cdot \Gamma_{\psi_{\text{vib}}'} \supset A_{2u} \text{ for } z \text{ polarization, and}$$

$$\Gamma_{\psi_{\text{el}}^{\circ}} \cdot \Gamma_{\psi_{\text{el}}'} \cdot \Gamma_{\psi_{\text{vib}}^{\circ}} \cdot \Gamma_{\psi_{\text{vib}}'} \supset E_u \text{ for } x, y \text{ polarization}$$

as our selection rules for vibronically-allowed electronic transitions.

These selection rules are valid only for spin-allowed transitions. Spin-forbidden transitions may be observed if

there is significant spin-orbit coupling. In this case, the ground and excited state wavefunctions must each include the mixed spin states. To account for the symmetry of the spin functions, double groups may be required. In any event, the polarization of a spin-forbidden transition may not be the same as its spin-allowed counterpart. Such a treatment will not be given here. Unless otherwise stated, comments concerning electronic transitions and assignments will refer to spin-allowed transitions only. In addition, no consideration will be given here to magnetic dipole or electric quadrupole mechanisms for electronic transitions. These transitions are usually not observed, due to their low intensity.

While Cotton's simple description readily explained the more striking observable characteristics of the quadruple bond, it did not seem to account for all features of the electronic spectrum of $\text{Re}_2\text{Cl}_8^{2-}$. Under D_{4h} symmetry, the δ bonding combination of d_{xy} orbitals has b_{2g} symmetry and the δ^* antibonding combination has b_{1u} symmetry. The spin-allowed electronic transition from a filled δ orbital to an empty δ^* orbital, denoted as $\delta(b_{2g}) \rightarrow \delta^*(b_{1u}) (^1A_{1g} \rightarrow ^1A_{2u})$, is electric dipole-allowed with \hat{z} polarization. Such an allowed transition would be expected to exhibit a high intensity in the absorption spectrum. The simple MO model gave the δ level as the highest occupied MO (HOMO) and the δ^* level as the lowest unoccupied MO (LUMO). This implies that the lowest energy electronic

transition for $\text{Re}_2\text{Cl}_8^{2-}$ should be $\delta \rightarrow \delta^*$. However, since this first band (observed at $\sim 14,000 \text{ cm}^{-1}$) had a low intensity, Cotton tentatively assigned it as $\delta(b_{2g}) \rightarrow \sigma_n(a_{1g}, a_{2u}) ({}^1A_{1g} \rightarrow {}^1B_{2g}, {}^1B_{1u})$. The empty σ_n orbitals were considered to be $d_{z^2}-p_z$ hybrid orbitals, not involved in the metal-metal σ bonding.

A more rigorous extended Hückel calculation for $\text{Re}_2\text{Cl}_8^{2-}$ by Cotton and Harris in 1967 predicted the LUMO to be σ_n , with δ^* slightly higher in energy (8). While the calculated transition energy was high by some $4,000 \text{ cm}^{-1}$, this calculation seemed to support the assignment of the low energy transition as $\delta \rightarrow \sigma_n$. Recent calculations by self-consistent-field $X\alpha$ scattered wave methods (SCF- $X\alpha$ -SW) have changed minor features of the bonding view (9). Results indicated no unfilled orbital which could be labelled as σ_n . Instead, the δ^* was calculated to be the LUMO. In general, calculations supported the original formulation of one σ , two π , and one δ bond for $\text{Re}_2\text{Cl}_8^{2-}$. However, the lowest energy transition was then predicted to be $\delta \rightarrow \delta^*$. This has been supported by further studies of the electronic spectra of $\text{Re}_2\text{Cl}_8^{2-}$, including polarized spectra in crystals (9-11). Application of SCF- $X\alpha$ -SW techniques to large molecules has been a fairly recent development, but has had success in calculating energies in good agreement with experiment. Although the method has theoretical advantages and disadvantages when compared with ab initio Hartree-Fock calculations, it will produce comparable calculations with much less computer time.

Let us now focus our attention on molybdenum complexes, and then to electronic spectra in particular. Since the recognition of the quadruple metal-metal bond, synthesis of new complexes with various metals has been an active and prolific area of research (12-14). Molybdenum seems to stand out, however, by having the greatest number of complexes containing triple and quadruple metal-metal bonds. The first report of a quadruply-bonded Mo complex came in 1965, not long after the $\text{Re}_2\text{Cl}_8^{2-}$ report. Cotton and Bratton (15) proposed quadruple bonding in dimolybdenum tetraacetate, whose molecular structure was reported concurrently by Lawton and Mason (16). In 1960, Bannister and Wilkinson had reported the production of this complex (referred to as molybdenum(II) acetate) by refluxing acetic acid, acetic anhydride, and molybdenum hexacarbonyl (17). The dimeric nature of the complex was recognized, however, before the complete structure was known (18). The molecular structure was found to be four carboxylate groups bridging the two metal atoms, as found in $\text{Cr}_2(\text{O}_2\text{CCH}_3)_4 \cdot 2\text{H}_2\text{O}$ (6-7) and illustrated in Figure 2 for the general case. The Mo-Mo distance of 2.11 Å found was remarkably shorter than the 2.9 Å expected from a reasonable estimate of the metal covalent radii. This provided good evidence for strong metal-metal bonding as noted in $\text{Re}_2\text{Cl}_8^{2-}$. At the time, a number of similar Mo(II) complexes had already been prepared with other carboxylic acids. Thus, the door was opened to the extensive chemistry which followed (a 1979 review (14) cites investigations of twenty-five

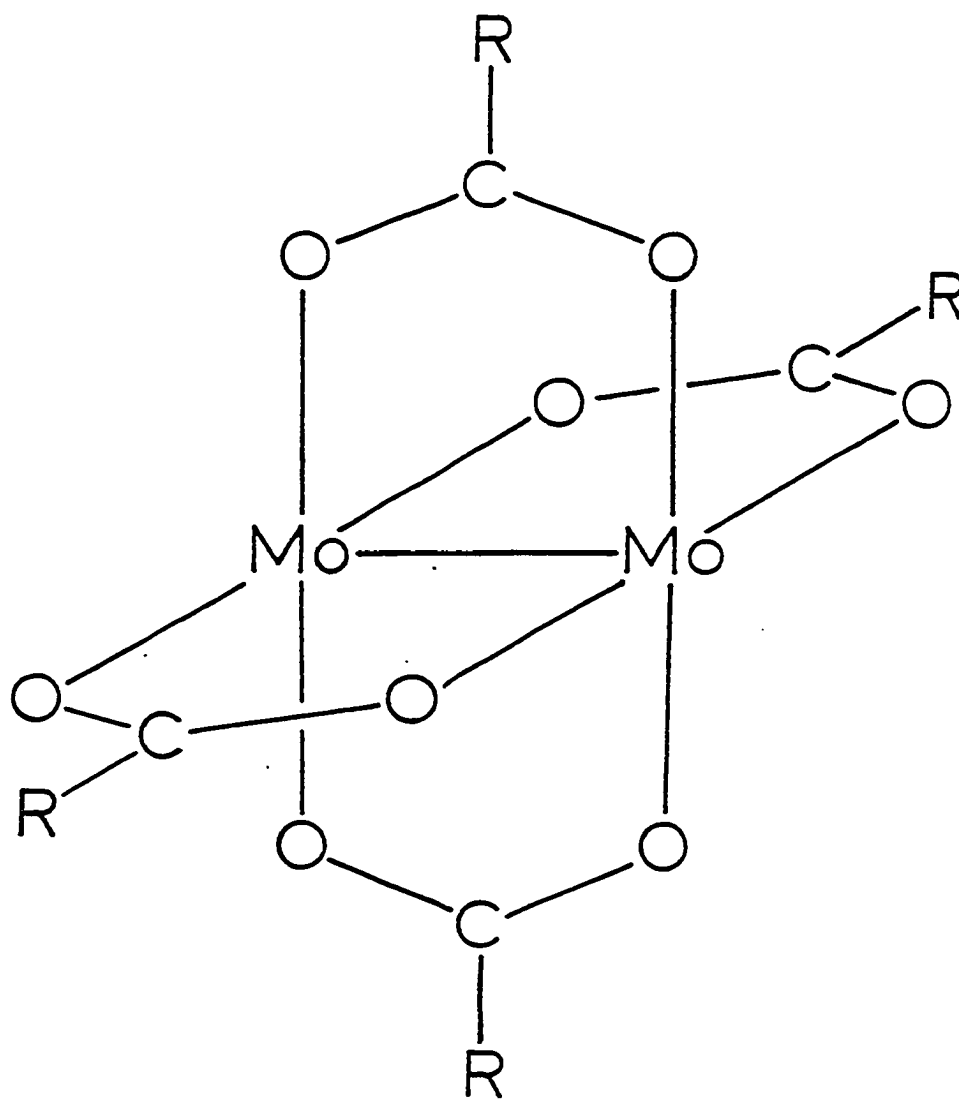


Figure 2. General structure of dimolybdenum tetracarboxylate complexes

crystal structures and more than forty-five reactions for Mo complexes containing quadruple bonds).

In 1969, Dubicki and Martin published the first MO calculation and electronic spectral studies for binuclear Mo complexes (19). The self-consistent charge and configuration molecular orbital (SCCC-MO) calculation was made for dimolybdenum tetraacetate. Few features of the resulting MO diagram differed from the extended Hückel Mo diagram for $\text{Re}_2\text{Cl}_8^{2-}$. One difference was a reversal in the relative order of the two empty A_{1g} and A_{2u} σ^* orbitals (labelled σ_n in $\text{Re}_2\text{Cl}_8^{2-}$). Also, a b_{1g} symmetry orbital designated $\delta\sigma^*(x^2-y^2)$ was calculated to be the LUMO. The latter orbital would be metal-ligand σ^* and metal-metal δ bonding. In order of increasing energy, the three lowest unfilled MO's were $\delta\sigma^*(x^2-y^2)(5b_{1g})$, $\sigma^*(z^2)(6a_{1g})$, and $\delta^*(xy)(2b_{1u})$, with $\delta(xy)(2b_{2g})$ as the HOMO. A number of closely-spaced ligand π levels were calculated to lie just below the δ level. Thus, the lowest energy transition would be $\delta(2b_{2g}) \rightarrow \delta\sigma^*(5b_{1g}) (^1A_{1g} \rightarrow ^1A_{2g})$ or $\delta(2b_{2g}) \rightarrow \sigma^*(6a_{1g}) (^1A_{1g} \rightarrow ^1B_{2g})$, either of which would be electric dipole-forbidden but could be vibronically allowed. The electric dipole-allowed transition $\delta(2b_{2g}) \rightarrow \delta^*(2b_{1u}) (^1A_{1g} \rightarrow ^1A_{2u})$ would then be somewhat higher in energy. Spectra of the acetate, benzoate, p-fluorobenzoate, and perfluorobutyrate complexes were obtained in 95% ethanol solution as absorption spectra and at 77 K as diffuse reflectance spectra of the powders. Dubicki and Martin observed a very weak band at $\sim 22,500 \text{ cm}^{-1}$, a very intense one

at $\sim 34,000 \text{ cm}^{-1}$, and an intense band at $\sim 43,000 \text{ cm}^{-1}$ for the acetate complex. Similar features were noted for the other complexes, with the observation that the energy of the second band was strongly ligand-dependent. They assigned the low energy band as a vibronically-allowed transition, either $\delta(2b_{2g}) \rightarrow \sigma^*(6a_{1g})$ or $L(\pi) \rightarrow \sigma^*(6a_{1g})$. The second band was assigned as the $\delta(2b_{2g}) \rightarrow \delta^*(2b_{1u})$ (${}^1A_{1g} \rightarrow {}^1A_{2u}$). The red shift in this band on changing from acetate to benzoate or perfluorobutyrate was thought to be due to weaker Mo-Mo bonding in the latter complexes. No assignment was made for the third band at $\sim 43,000 \text{ cm}^{-1}$. These assignments were similar to earlier ones made for $\text{Re}_2\text{Cl}_8^{2-}$, based on the extended Hückel and simple MO energy diagrams.

The first Mo dimer complex to be investigated using polarized absorption spectroscopy was the quadruply-bonded glycine complex in tetra- μ -glycine-dimolybdenum(II) sulfate tetrahydrate, $\text{Mo}_2(\text{O}_2\text{CCH}_2\text{NH}_3)_4(\text{SO}_4)_2 \cdot 4\text{H}_2\text{O}$. The molecular orientation was ideal as all Mo_2^{4+} units were found to be crystallographically equivalent and aligned parallel to the crystallographic c axis. The molecular symmetry, idealized as D_{4h} , is reduced to S_4 in the crystallographic site. However, the deviation from D_{4h} is small. Spectra polarized in the $c(z)$ and $a(x, y)$ directions were presented by Cotton et al. for the $20,000\text{-}25,000 \text{ cm}^{-1}$ region (20). The spectra taken at 15 K showed detailed vibrational structure. Table 1 gives the essential data obtained for the four observed vibrational

Table 1. Data from the polarized spectra of $\text{Mo}_2(\text{O}_2\text{CCH}_2\text{NH}_3)_4(\text{SO}_4)_2 \cdot 4\text{H}_2\text{O}$

First member of progression (cm^{-1})	Number of lines in progression	Mean separation (cm^{-1})	ϵ_{max} ($\text{M}^{-1}\text{cm}^{-1}$)	Polarization
20,570	4	343 ± 9	~ 20	$\xi(z)$
21,510	9	345 ± 10	~ 125	$\xi(z)$
21,790	7	342 ± 11	~ 100	$\eta(x,y)$
21,930	6	344 ± 8	~ 90	$\eta(x,y)$

progressions. It was proposed that the very weak ξ -polarized progression beginning at $20,570 \text{ cm}^{-1}$ be assigned to an electronic transition which is forbidden in D_{4h} symmetry, but allowed under the S_4 site symmetry. The transition would be ${}^1A_{1g} \rightarrow {}^1A_{1u}$, ${}^1B_{1g}$, or ${}^1B_{2g}$, but no specific MO's which might be involved were proposed. The remaining three progressions were attributed to that same electronic transition which is vibronically-allowed by three different vibrations. It was proposed that the vibrational separations averaging $340\text{-}345 \text{ cm}^{-1}$ correspond to the metal-metal stretching vibration. A transition from an Mo-Mo bonding orbital or to an antibonding Mo-Mo orbital would lower the vibrational frequency from the 393 cm^{-1} observed for the ground state. The most important result from this study is that an electric dipole-allowed $\delta \rightarrow \delta^*$ assignment seemed inconsistent with the data.

By 1975, SCF-X α -SW calculations for octachlorodimolybdate(II), Mo₂Cl₈⁴⁻, and dimolybdenum tetraformate, Mo₂(O₂CH)₄, had been reported by Norman and Kolarik (21, 22). An improved calculation for the formate and calculations for Mo₂ and Mo₂⁴⁺ were reported by Norman et al. in 1977 (23). It is convenient here to discuss the bonding in Mo dimers based on these calculations. Figure 3 shows the calculated energy levels Mo₂Cl₈⁴⁻ and Mo₂(O₂CH)₄ containing substantial Mo character. We note in each case levels identified as Mo-Mo σ , π , δ , δ^* , π^* , and σ^* . We must consider, however, that separating orbitals into Mo-Mo and Mo-L bonding categories is not entirely possible. For example, the 5e_u and 6e_u orbitals in Mo₂(O₂CH)₄ both participate in Mo-Mo and Mo-O π bonding. However, since the 6e_u level contains substantially more Mo character, it is more appropriately labelled "Mo-Mo π bonding". The simple MO concept of the quadruple bond is nonetheless supported quite well by the calculations. One important feature to note is that the SCF-X α -SW results show no nonbonding σ -type levels, which would lie in the region between the δ and π^* levels. The calculation thus differs from the SCCC-MO treatment of Dubicki and Martin. Furthermore, there were no levels calculated other than those pictured for the regions between Mo-Mo π and π^* levels in both dimolybdenum complexes. This restricts the number of possible assignments for the lower energy electronic transitions observed in spectra of these complexes. The calculations predict that the lowest energy transition

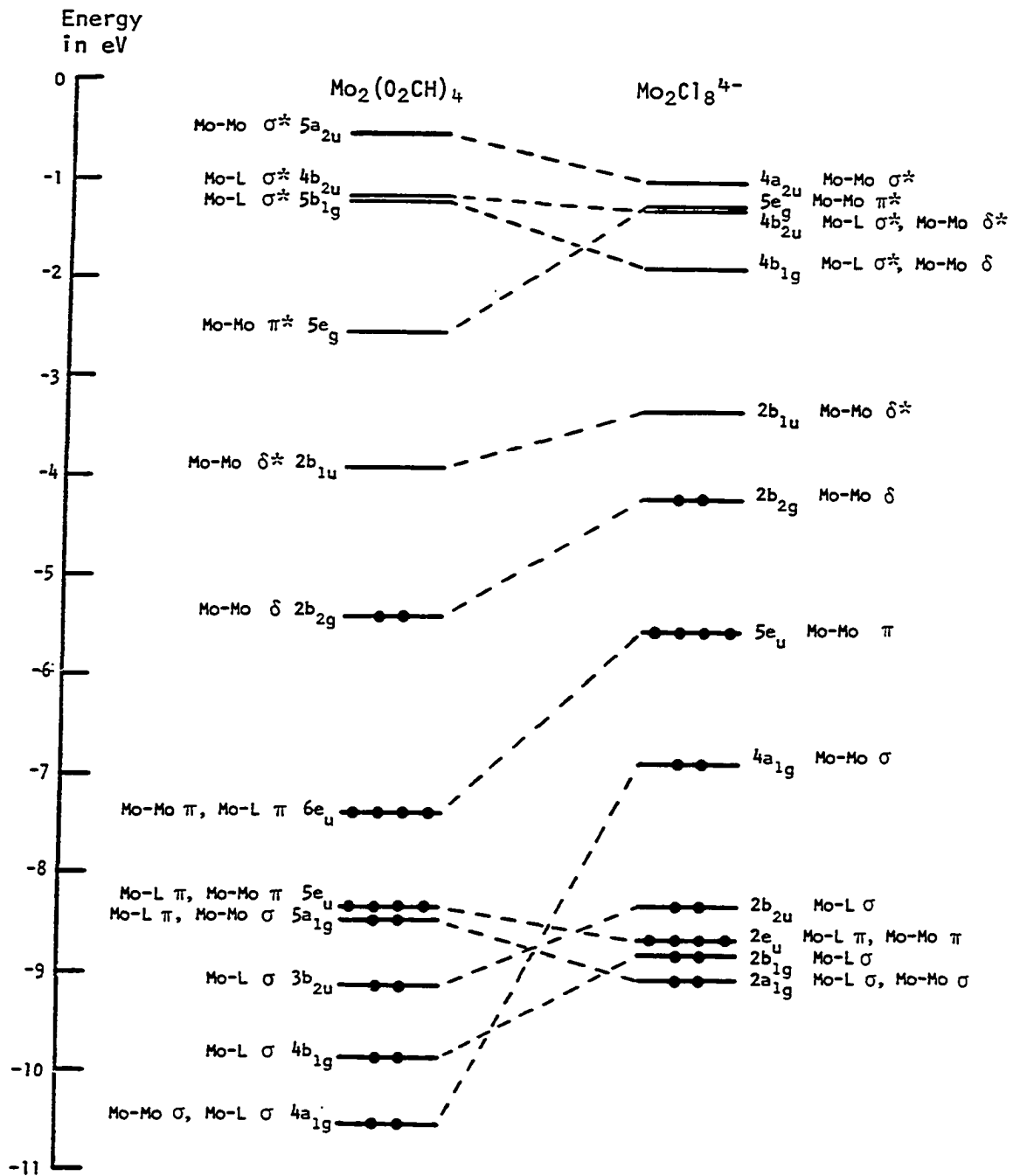


Figure 3. Energy levels calculated by SCF-X α -SW methods for $\text{Mo}_2(\text{O}_2\text{CH})_4$ and $\text{Mo}_2\text{Cl}_8^{4-}$ (orbitals containing at least 15% Mo character)

would be $\delta(b_{2g}) \rightarrow \delta^*({}^1A_{1g} \rightarrow {}^1A_{2u})$. Other electric dipole-allowed transitions at much higher energies would be $\pi(e_u) \rightarrow \pi^*(e_g)$ and $\pi(e_u) \rightarrow \text{Mo-L}\sigma^*(b_{1g})$, both ${}^1A_{1g} \rightarrow {}^1E_u$ and thus allowed in χ_v, χ polarization. In addition to these, almost any dipole-forbidden transition can be vibronically-allowed because of the large number and variety of vibrational modes available to these large complexes. Thus, vibronic transitions such as $\delta(b_{2g}) \rightarrow \pi^*(e_g)$ or $\pi(e_u) \rightarrow \delta^*(b_{1u})$, both ${}^1A_{1g} \rightarrow {}^1E_g$, are candidates for lower energy transitions.

The lowest energy band in $\text{Mo}_2\text{Cl}_8^{4-}$, found in pellet and mull samples of $\text{K}_4\text{Mo}_2\text{Cl}_8$ and $\text{K}_4\text{Mo}_2\text{Cl}_8 \cdot 2\text{H}_2\text{O}$ at $\sim 18,800 \text{ cm}^{-1}$, has been attributed to the $\delta \rightarrow \delta^*$ transition (10, 21). This assignment was later substantiated when Fanwick et al. showed that the band had χ_v polarization in crystals of the dihydrate form (24).

Polarized electronic spectra of $\text{Mo}_2(\text{O}_2\text{CH})_4$ and $\text{K}_4\text{Mo}_2(\text{SO}_4)_4 \cdot 2\text{H}_2\text{O}$ were studied in our group to determine the applicability of results obtained for the glycine complex to other carboxylate complexes (25). As the formate spectra are particularly relevant, they are presented here in some detail. Spectra were recorded polarized parallel to the ξ and ζ crystal axes for the 010 face of the formate complex. The Mo-Mo bond, which defines the molecular χ axis, is aligned 33.4° from the ζ axis. A χ_v -polarized molecular transition

would absorb in both the a and c crystal directions, with the greatest component in the c direction. The expected intensity ratio (referred to as the polarization ratio) I_c/I_a was calculated to be 4.3 for a z -polarized transition. For an x,y polarized molecular transition, I_c/I_a is expected to be 0.36. Polarized spectra for $\text{Mo}_2(\text{O}_2\text{CH})_4$ are presented in Figure 4 for the region from 21,400-25,000 cm^{-1} . This corresponds to the region studied in the glycine complex. We note three progressions, each with a separation of $350 \pm 10 \text{ cm}^{-1}$. The first progression begins at 21,870 cm^{-1} in a (21,880 cm^{-1} in c) and consists of the lowest energy line in each group (the first "group" containing only one line). The second progression consists of the next higher energy line in each group, beginning with the second group. The high energy lines of the third group onward comprise the third progression. While the intensities are higher in a than in c polarization in each component, the ratio I_c/I_a is larger for members of the second progression than for the other two. This was taken to imply z polarization for the second progression, which somehow showed enhanced intensity in the a direction. The other two progressions seemed clearly to have x,y polarization. It was concluded that the spectra must be due to an electric dipole-forbidden transition which is vibronically-allowed by three molecular vibrations. Each gives rise to a Franck-Condon

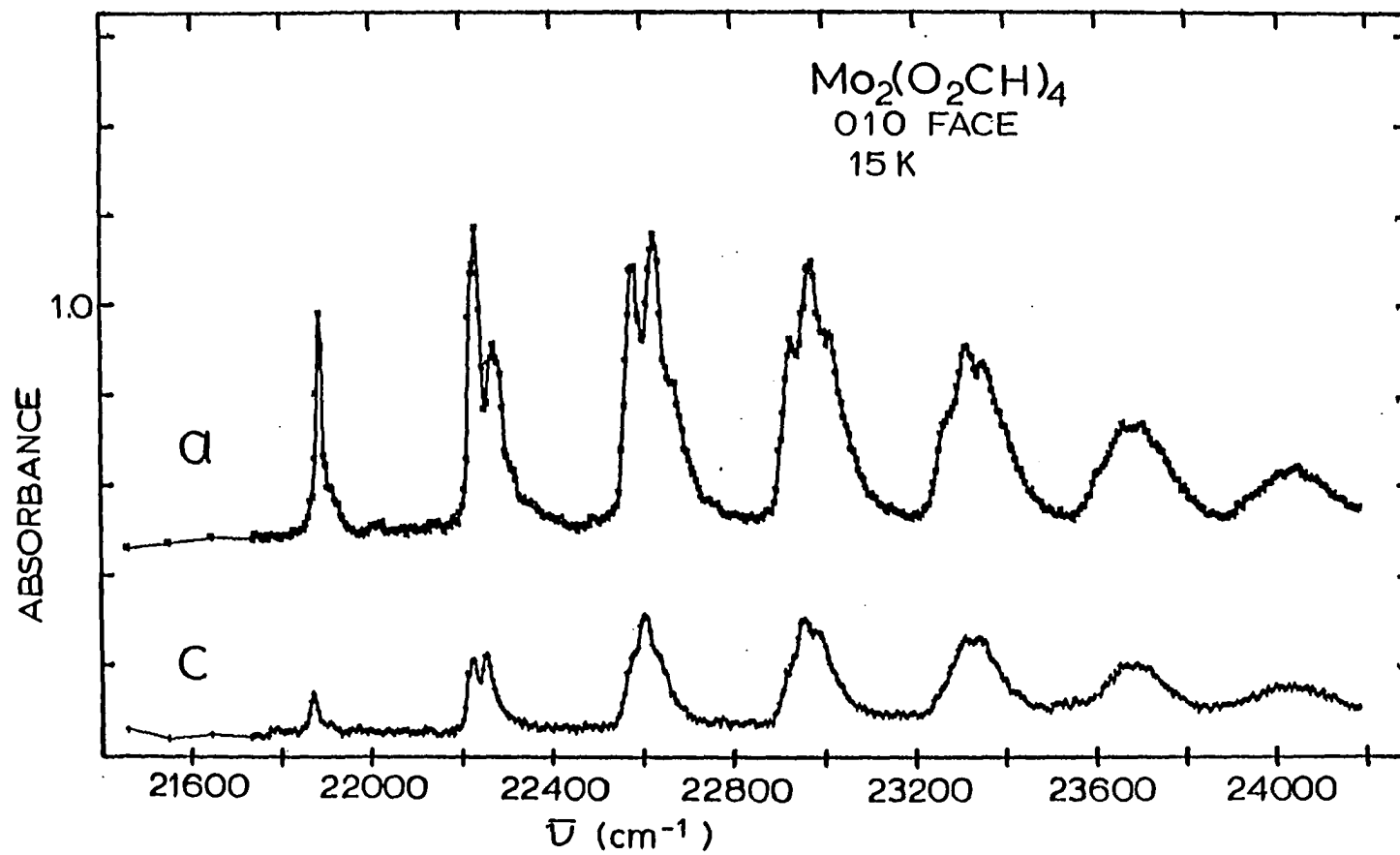


Figure 4. Polarized absorption spectra for $\text{Mo}_2(\text{O}_2\text{CH})_4$

progression based on a totally symmetric vibration with frequency 350 cm^{-1} in the excited state, presumed to be the metal-metal stretch. Two of the three vibrations apparently provide intensity for x, y -polarized transitions, and the other provides intensity for a z -polarized transition. Thus, these results agreed with those of the glycine complex, implying their generality for all of the carboxylate dimer complexes. The transition was assigned as $\delta \rightarrow X^*$ or $X \rightarrow \delta^*$, where X and X^* refer to molecular orbitals containing substantial contributions from carboxylate $p\pi$ orbitals.

The study of $\text{Mo}_2(\text{SO}_4)_4^{4-}$ was then necessary to determine if the carboxyl group (with possible π interactions with the Mo-Mo bonding) was unique in its influence on the spectra. The sulfate ion contains the same basic ligand feature as the carboxylates of two oxygen atoms connected through a bridging atom. Cotton, Martin and co-workers (25) studied the 100 face of $\text{K}_4\text{Mo}_2(\text{SO}_4)_4 \cdot 2\text{H}_2\text{O}$, obtaining spectra for polarizations along b and c . The molecular z axis lies 23.7° from the c axis, yielding $I_c/I_b = 5.2$ for a z -polarized transition and $I_c/I_b = 1/5.2$ for an x, y -polarized transition, in the ideal case. Experimentally, the band at $19,400 \text{ cm}^{-1}$ was found to be about four times as intense in c as in b polarization. This showed clearly that the band is z -polarized. It was also found that the band intensity did not change substantially on decreasing

the temperature from 300 K to 15 K. A vibronic band would lose intensity in this case due to depopulation of the allowing vibrational states (which are thermally populated according to the Boltzman distribution). The evidence supports an electric dipole-allowed transition, resulting in a $\delta \rightarrow \delta^*$ assignment for the low energy band. This implied that the carboxylate ligands had some special electronic feature that distinguished them from sulfate.

A later polarized spectral study of $K_3Mo_2(SO_4)_4 \cdot 3.5H_2O$ by Fanwick et al. also led to a $\delta \rightarrow \delta^*$ assignment (26). However, $Mo_2(SO_4)_4^{3-}$ has only one electron in the δ bonding orbital and represents a one-electron oxidized anion in relation to $Mo_2(SO_4)_4^{4-}$. Due to the weakened Mo-Mo bond, the lowest energy transition was observed at $\sim 7,000 \text{ cm}^{-1}$ instead of in the typical 19,000-22,000 cm^{-1} region.

Trogler et al. have assigned the band at $\sim 23,000 \text{ cm}^{-1}$ in the acetate, trifluoroacetate, and formate complexes to the vibronically-allowed $\delta \rightarrow \pi^* (^1A_{1g} \rightarrow ^1E_g)$ transition (27). Absorption spectra were observed for films of $Mo_2(O_2CCF_3)_4$, $Mo_2(O_2CCD_3)_4$ and $Mo_2(O_2CH)_4$. The emission spectrum of a film sample of the trifluoroacetate complex was obtained, as well as polarized spectra of crystals of the acetate complex. Their assignment was based primarily on observations from the acetate and trifluoroacetate complexes. The detailed vibrational progressions

showed three types of polarization behavior which were attributed to vibronic contribution by e_u and a_{2u} vibrations. It was proposed that the e_u vibrations gave rise to polarization $\parallel z_c$. The weak and strong polarizations $\perp z_c$ were attributed to a breaking of the degeneracy of the 1E_g excited state, due to a lowering of symmetry from D_{4h} to C_i in the crystal. This would result in nondegenerate x_c and y_c polarizations, hence the two types of polarizations $\perp z_c$. The experiments of Trogler et al. included analysis of hot bands. These are weak features of a spectrum which grow in upon increasing the temperature above ~ 20 K. They are due to transitions from higher energy ground state vibrational levels which are thermally populated. The hot bands are observed at energies below those of corresponding transitions from $v=0$ levels. They may provide information on the energy of a band's origin transition and frequencies of certain vibrations involved.

In spite of the extensive studies reported by Trogler et al., they did not adequately treat certain aspects of the crystal optics. A more thorough investigation of the polarized spectra of crystals of dimolybdenum tetraacetate was performed by Martin and co-workers (28). They did take into account the wavelength dependence of the crystal's polarization directions, which was not done in the previous study. This is always possible with certain crystallographic faces in certain

Bravais lattice types, but is not always large enough to produce an observable effect. In addition, polarized spectra were obtained for both the 100 and the 001 faces. This gave much more information than spectra obtained from just one face. It allowed the spacial orientation of the transition moment (a vector) to be determined. The transition moment would be found precisely $\parallel z_c$ or $\perp z_c$ in an ideal case (with no intermolecular interactions). However, it was determined to be oriented 33.9° from z_c for the first line in one dominant vibrational progression in the $23,000 \text{ cm}^{-1}$ band. This was considered to be a z_c -polarized transition with the molecular transition moment shifted from the z_c axis by crystal field perturbations. A second dominant progression, having different polarization behavior, was attributed to a degenerate pair of transitions with x_c, y_c polarization. The normal to such a degenerate pair was determined to lie 32.3° from z_c . Other progressions could be related to these based on observed polarization behavior. Along with studies of hot bands and relative intensities of successive members of the dominant progressions, this evidence led to a $\delta \rightarrow \delta^*$ assignment for the band. It was proposed that vibronic contributions to this electric dipole-allowed transition produced vibrational lines with only slightly less intensity than the dipole allowed features. It was suggested that the unusually low $\delta \rightarrow \delta^*$

intensity seen in the tetracarboxylate spectra was due to metal interactions with unfilled ligand orbitals. The lowest unfilled orbital in alkyl carboxylate anions is the π^* involving oxygen and carbon p orbitals, shown in Figure 5. This empty orbital can interact with the filled δ orbital, withdrawing electron density from it, thus reducing the intensity of the observed $\delta \rightarrow \delta^*$ band.

The foregoing results led to reevaluation of the assignments previously made for carboxylate spectra. Martin et al. noted similarities in the dominant features of polarized spectra of the acetate, trifluoroacetate, formate and glycine complexes. A $\delta \rightarrow \delta^*$ assignment was proposed for the low energy band in the latter three, based on the acetate results. Although they offered plausible explanations for observed discrepancies, unfortunately, few of the explanations have been experimentally verifiable. Spectral investigations of the trifluoroacetate complex have recently been completed in our group (29). The polarized spectra were shown to be in good agreement with the acetate spectra. In the case of the glycine complex, Martin et al. suggested that the low energy z_c -polarized progression was due to a defect or impurity. The first member of the stronger z_c -polarized progression would then represent the band's origin. Recent polarized spectra obtained by Bino, Cotton and Fanwick for the leucine complex showed three strong

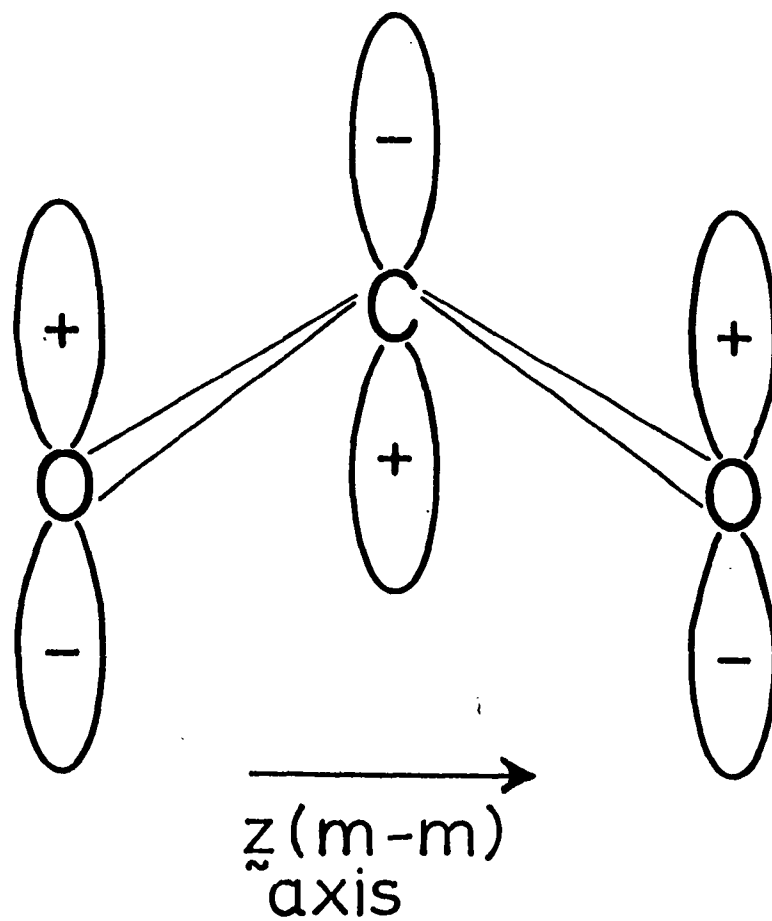


Figure 5. The carboxylate π^* orbital

progressions similar to those observed in the glycine spectra (30). No analogous weak progression was seen, however, lending support to a $\delta \rightarrow \delta^*$ assignment for the glycine and leucine complexes.

Table 2 summarizes the major spectral studies conducted to date for binuclear Mo complexes of bond order greater than three. Table 3 summarizes calculated and observed $\delta \rightarrow \delta^*$ transition energies. Most transition energies calculated by SCF-X α -SW techniques for metal dimer complexes have fallen within $\sim 15\%$ of the observed energies. However, the calculated energies for closed-to-open shell $\delta \rightarrow \delta^*$ transitions have been routinely low by 30-50%. This has been attributed to failure of the method to adequately account for the different electronic repulsions in the ground and excited states. One criticism of the method has been that it does not include sufficient electron correlation. The usual approach to the SCF-X α -SW calculations has been an MO approach, which assumes delocalization of the electrons. It was thought that the low δ -type overlap might result in electron localization, which the calculations did not allow for. Noodleman and Norman thus developed a valence bond (localized) approach to the calculations (39). A preliminary calculation of this type for Mo₂Cl₈⁴⁻ yielded the improved energy of 1.52 μm^{-1} listed in Table 3. In spite of this difficulty, the X α calculations

Table 2. A summary of the electronic spectra of binuclear molybdenum complexes of bond order greater than three

Complex	Sample Condition ^a
$M_2(O_2CC_3F_7)_4$	solution 95% EtOH
$M_2(O_2CC_3F_7)_4$	diffuse reflectance 77 K
$Mo_2(O_2CC_6H_5)_4$	diffuse reflectance 77 K, sol'n EtOH
$Mo_2(O_2CCH_3)_4$	solution 95% EtOH
	diffuse reflectance 77 K
	sublimed film, crystal 15 K
	crystal 5 K
$Mo_2(aq)^{4+}$	solution HSO_3CF_3
$Mo_2(en)_4Cl_4$	solution HSO_3CF_3
$K_4Mo_2Cl_8$	pellet 5 K
	solution 6 M HCl
	pellet 15 K
$K_4Mo_2Cl_8 \cdot 2H_2O$	mineral oil mull
	crystal 4 K
	pellet 4 K
$Mo_2(O_2CCH_2NH_3)_4(SO_4)_2 \cdot 4H_2O$	aqueous solution

^aAt room temperature unless otherwise noted.

^bOscillator strength.

^cExcited-state stretching energy.

^dReported for crystal--divide by 3 to compare with solution value.

^eBand origin.

$\bar{\nu}_{\max}$, cm^{-1}	Ref.	Year	ϵ_{\max} , $\text{M}^{-1}\text{cm}^{-1}$	f^b	Assignment	$\bar{\nu}(\text{Mo-Mo})^c$
22989	19	1969	100		L(π), $\delta \rightarrow \sigma^*$	
23120	19	1969			L(π), $\delta \rightarrow \sigma^*$	300
22450	19	1969			L(π), $\delta \rightarrow \sigma^*$	370
22727	19	1969	60		L(π), $\delta \rightarrow \sigma^*$	
22800	19	1969			L(π), $\delta \rightarrow \sigma^*$	350
22436	27	1977			$\delta \rightarrow \pi^*$	370
22820	28	1979	735 ^d	0.001	$\delta \rightarrow \delta^*$	375
19841	31	1974	337			
20921	31	1974	483			
17897 ^e	10	1973			$\delta \rightarrow \delta^*$	351
~19300	27	1977		0.015	$\delta \rightarrow \delta^*$	
18260	24	1977			$\delta \rightarrow \delta^*$	332
18800	21	1975			$\delta \rightarrow \delta^*$	
18804	24	1977	~7700 ^d	0.019	$\delta \rightarrow \delta^*$	336
18660	24	1977			$\delta \rightarrow \delta^*$	346
22422	32	1976	~100			

Table 2. Continued.

Complex	Sample Condition ^a
$\text{Mo}_2(\text{O}_2\text{CCH}_2\text{NH}_3)_4(\text{SO}_4)_2 \cdot 4\text{H}_2\text{O}$	crystal 15 K
$\text{Mo}_2(\text{O}_2\text{CH})_4$	90% HCO_2H solution
	crystal 15 K
	4:1 EtOH/MeOH 80 K
	sublimed film 15 K
$\text{K}_4\text{Mo}_2(\text{SO}_4)_4 \cdot 2\text{H}_2\text{O}$	crystal 15 K
$\text{K}_3\text{Mo}_2(\text{SO}_4)_4 \cdot 3.5\text{H}_2\text{O}^{\text{f}}$	KBr pellet 15 K
	crystal 5 K, 300 K
$\text{Mo}_2(\text{O}_2\text{CCD}_3)_4$	sublimed film 15 K
$\text{Mo}_2(\text{O}_2\text{CCF}_3)_4$	acetonitrile solution
	sublimed film 15 K
	crystal 6 K
$[\text{Li}(\text{Et}_2\text{O})]_4\text{Mo}_2(\text{CH}_3)_8$	Et_2O solution
$\text{Mo}_2\text{Cl}_4(\text{PEt}_3)_4$	CH_2Cl_2 solution
	KBr pellet 15 K
$\text{Mo}_2[(\text{CH}_2)_2\text{P}(\text{CH}_3)_2]_4$	THF solution
	KBr pellet 5 K
$\text{Mo}_2(\text{NCS})_8^{4-}$	solution 1 M KNCS
$\text{Mo}_2(\text{L-leucine})_4\text{Cl}_2(\text{pts})_2 \cdot 2\text{H}_2\text{O}^{\text{g}}$	crystal 5 K

^f Bond order 3.5.

^g pts = p-toluenesulfonate ion.

$\bar{\nu}_{\max}$, cm^{-1}	Ref.	Year	ϵ_{\max} , $\text{M}^{-1}\text{cm}^{-1}$	f^b	Assignment	$\bar{\nu}(\text{Mo-Mo})^c$
22570	20	1976	125		vibronic	343
22831	1	1976	100			
22220	25	1976			$\delta \rightarrow X^*$, $X \rightarrow \delta^*$	350
~22900	23	1977		0.0008	$\delta \rightarrow \pi^*$	
22616	27	1977			$\delta \rightarrow \pi^*$	360
19400	25	1976		0.0011	$\delta \rightarrow \delta^*$	
7117	33	1977	143		$\delta \rightarrow \delta^*$	357
7135	26	1978	228	0.0008	$\delta \rightarrow \delta^*$	350
22472	27	1977				370
22700	27	1977		0.0011		
22791	27	1977			$\delta \rightarrow \pi^*$	355
22810	29	1981			$\delta \rightarrow \delta^*$	360
19500	34	1977	1500		$\delta \rightarrow \delta^*$	
17094	35	1977	~3000		$\delta \rightarrow \delta^*$	
16955	35	1977			$\delta \rightarrow \delta^*$	320
20100	36	1978	660		$\delta \rightarrow \delta^*$	320
19956	37	1979			$\delta \rightarrow \delta^*$	346
14500	38	1979	2500		$\delta \rightarrow \delta^*$	
22904	30	1980			$\delta \rightarrow \delta^*$	347

Table 3. Calculated and observed $\delta \rightarrow \delta^*$ transition energies in $\text{Mo}_2\text{Cl}_8^{4-}$ and $\text{Mo}_2(\text{O}_2\text{CH})_4$.

Complex	Energy of $\delta \rightarrow \delta^*$ calculated ^a	transition, cm^{-1} observed	Reference	Year
$\text{Mo}_2\text{Cl}_8^{4-}$	13,700	18,800	21	1975
"	9,200 ^b	"	23	1977
"	15,200 ^c	"	39	1979
$\text{Mo}_2(\text{O}_2\text{CH})_4$	14,700	22,900	23	1977

^aCalculated by various modifications of SCF-X α -SW methods.

^bThis calculation had more theoretical merit than the prior one yielding 13,700 cm^{-1} .

^cSCF-X α -VB calculation.

have contributed greatly to our understanding of the multiple metal-metal bond, and the spectra of metal dimer complexes.

It was hoped that $\text{Mo}_2(\text{O}_2\text{CH})_4 \cdot \text{KCl}$ and the additional $\text{Mo}_2(\text{O}_2\text{CH})_4$ polymorphs would provide additional information on the nature of the low energy transition and orientation of the transition moment in dimolybdenum tetraformate. While the discovery of dimolybdenum tetraformate in additional crystalline environments was not premeditated, it was perhaps not without warning. Cotton et al. reported inconsistencies in solution of the structure of $\text{Mo}_2(\text{O}_2\text{CH})_4$ and in the product obtained by two preparative routes (1). While their route was to reflux

dimolybdenum tetraacetate in formic acid, Dr. E. H. Abbot had produced it directly by refluxing molybdenum hexacarbonyl in formic acid (Reference 1 and references contained therein).

Cotton et al. reported the following concerning the two products:

"Dr. Abbot has sent us samples of the compound made by this method in his laboratory. The X-ray powder pattern is similar to but not identical to that of our product."

The following comments pertain to crystallographic data taken from two crystals from the same preparation:

"It should be pointed out that the structural solution from the first crystal, refined to $R_1 = 0.078$, would not refine with the second data set. In fact, the structure had to be completely re-solved using the second data set and there is no crystallography allowed transformation for the atomic positions from crystal one to crystal two. There also appears to be no common scale factor relating the equivalent reflections between the two data sets. The problem, be it twinning or something else, results in two different crystals giving virtually identical unit cells, identical space groups, yet, two different structural solutions."

Thus, we see that in the original structural investigation there was some evidence of one or more additional polymorphs of $\text{Mo}_2(\text{O}_2\text{CH})_4$. Our discovery of anomalous dimolybdenum tetraformate spectra led to further spectral and structural investigations, which we detail herein.

EXPERIMENTAL

Preparation

$\text{Mo}_2(\text{O}_2\text{CH})_4 \cdot \text{KCl}$ was produced by reacting ~0.2 g freshly prepared $\text{K}_4\text{Mo}_2\text{Cl}_8$ with 20 ml of 90% formic acid at room temperature under N_2 . Nitrogen was bubbled through the formic acid prior to mixing. The solid was added and the mixture stirred yielding a cloudy red solution. A gradual color change resulted in a clear yellow solution after about 10 minutes. The solution was left under low N_2 flow for 3 days to allow evaporation of solvent and formation of crystals. The yellow crystalline product was suction-filtered, washed with hexane, and dried in a vacuum desiccator for several hours. The product did not appear uniform, but the best crystals which were chosen for our studies yielded consistent spectra and unit cell parameters. Crystals appeared as thick parallelepiped and thin platelike forms. Subsequent solution of the crystal structure indicated that the compound should be formulated as $\text{Mo}_2(\text{O}_2\text{CH})_4 \cdot \text{KCl}$. Solution of the structure has been described elsewhere (40).

The β -polymorph of $\text{Mo}_2(\text{O}_2\text{CH})_4$ was produced in an attempted recrystallization of $\text{Mo}_2(\text{O}_2\text{CH})_4 \cdot \text{KCl}$ from formic acid. As in the preparation of $\text{Mo}_2(\text{O}_2\text{CH})_4 \cdot \text{KCl}$, the solution was reduced in volume under N_2 over a few days' time. The yellow crystals were suction filtered and dried in a vacuum dessicator. Crystals had the form of plates or short needles. This polymorph was

characterized by visible absorption spectra and by solution of the crystal structure.

The γ -polymorph was obtained by subliming the original α -form of $\text{Mo}_2(\text{O}_2\text{CH})_4$ for 3 hours at $\sim 270^\circ \text{C}$ in a tube furnace with a flow of N_2 . This was done in an attempt to purify older material which had turned green. Yellow crystals were obtained as large needles or thin bladelike plates. This sublimation yielded three types of crystal groups by their absorption spectra. Group I was identified as the α -form, as the spectra were consistent with this form. Group II had polarized spectra similar to the α -form, but with certain unusual features. It has not been determined whether or not this type represents an additional polymorph. Polarized spectra of Group III crystals were distinctly different from the other two. The crystal structure of this group was solved. This type is referred to as the γ -polymorph. It appears that the thicker crystals from the sublimation are the Group III type of crystal, while the thin crystals consist of Groups I and II crystals.

Crystal Optics and Spectra

The electric vector of plane-polarized light incident on an anisotropic crystal face can be transmitted only in two mutually perpendicular directions. These directions are called the privileged directions for that crystal face. They are also referred to variously as the extinction, vibration, or polarization directions. Frequently, they are identified as slow (N) and fast

(n) directions, the slow direction having the larger index of refraction of the two. If any crystal axis lies in the face of an orthorhombic crystal, then one of the privileged directions must always lie parallel to it. The 100 (or b, c) face, for example, has b and c as the privileged directions. Similarly, if a face of a monoclinic crystal contains (is parallel to) the b axis, then b is one of the privileged directions. However, for all other faces of these two crystal systems and for all faces of a triclinic system, the privileged directions may vary with wavelength. This is the situation that Martin et al. found for dimolybdenum tetraacetate (28). It may happen that the wavelength-dependence of the privileged directions is so small that it is not observable. This was found to be the case for the experiments reported here.

If the plane of polarization of incident light is not aligned with either privileged direction, then the light is split into two components polarized along these directions. This is illustrated in Figure 6. These components pass through the crystal, then re-combine as they emerge. An absorption spectrum for one crystal polarization is obtained by using incident radiation which is plane-polarized along that particular polarization direction. This is then repeated for the other polarization direction. Any observed absorption must be at either a maximum or minimum along these directions. It is

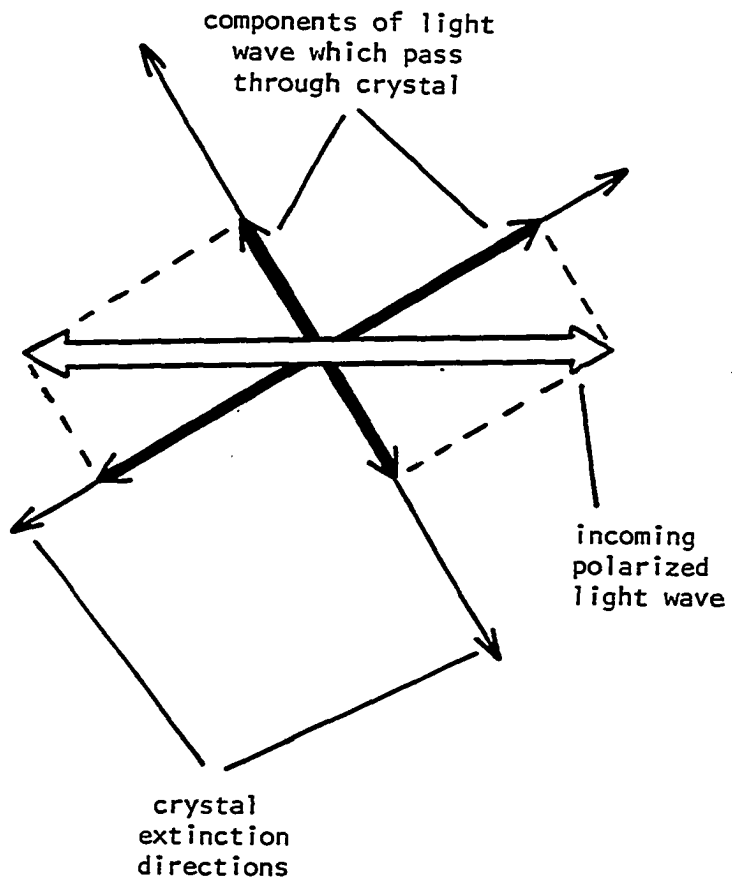


Figure 6. The behavior of polarized light entering a crystal face

possible under certain conditions for an absorbing crystal to produce an elliptically-polarized wave instead of transmitting a plane-polarized one. It is assumed here that any deviation from plane-polarization is small, and can be ignored.

In practice, the privileged directions are determined with the use of a polarizing microscope. Figure 7 presents the basic components of a polarizing microscope. Two polarizers are present, designated as the polarizer and analyzer. They are usually oriented with their planes of polarization perpendicular to each other. For certain applications, the analyzer orientation may be rotated or the analyzer may be removed from the optical path. Several accessories are available for placement in the optical path in order to characterize various optical properties. The sample crystal is placed on a glass slide which sits on a rotatable stage. This stage is calibrated for precise measurement of angles. To facilitate these measurements, the eyepiece (ocular) has perpendicular cross hairs with which a crystal edge, for example, may be aligned. An additional eyepiece is ruled to allow measurement of crystal dimensions.

With no sample in place and crossed (perpendicular) polarizers, one sees a dark field through the microscope. The polarizer polarizes the light in one direction which then cannot pass through the analyzer. If a crystal is placed on

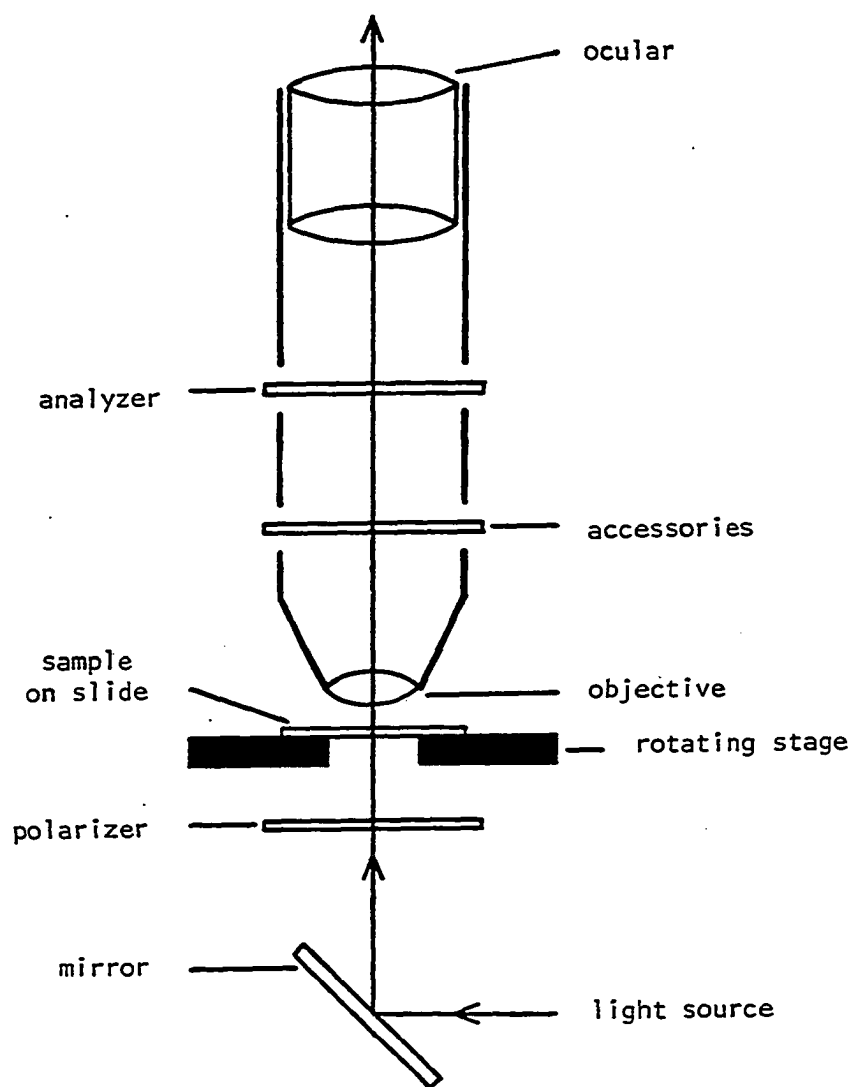
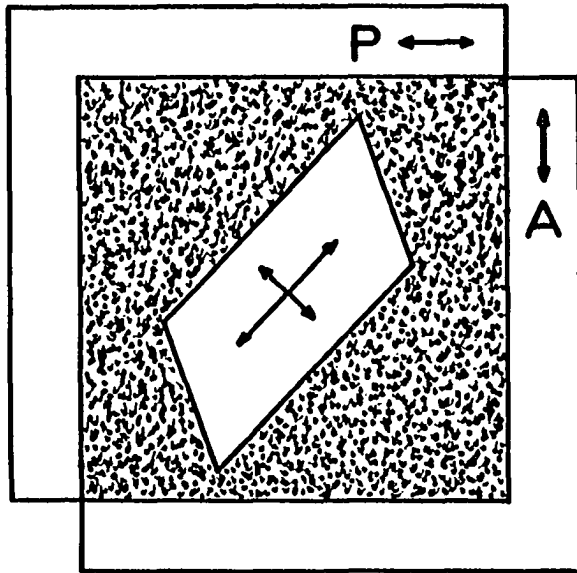
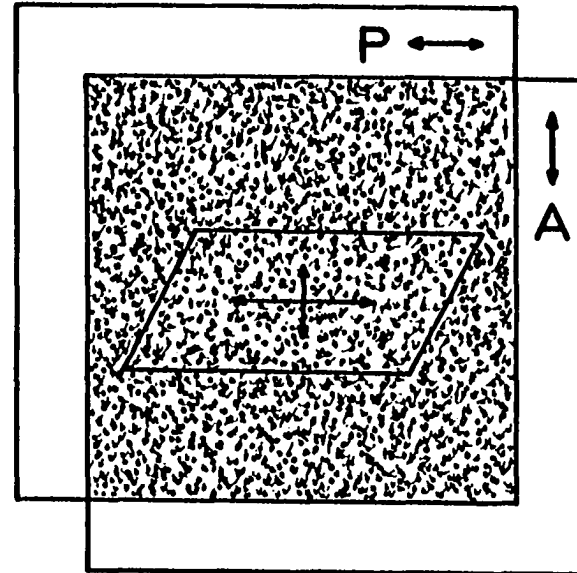


Figure 7. Basic components of the polarizing microscope

the stage with its privileged directions not aligned with the polarizers, then the crystal appears illuminated, while the remainder of the field of view is dark. As the polarized light enters the crystal, it is split into two components polarized along the privileged directions. Each of the two emerging polarized waves has a component in the plane of polarization of the analyzer. Thus, some of the light incident on the crystal is allowed to pass through the analyzer. This results in an illuminated crystal, while the rest of the field is dark. If the stage is rotated to orient the polarizer vibration direction with one of the crystal's vibration directions, the crystal also appears dark. Three successive 90° rotations from this orientation will also result in a dark field. This is the origin of the term "extinction directions", as the crystal appears to extinguish in these four orientations. In such an orientation, the incident polarized wave passes through the crystal without a change in its plane of polarization. It is then blocked out entirely by the analyzer, resulting in a dark crystal. Figure 8 illustrates the behavior of a crystal viewed through the polarizing microscope. The extinction directions in a crystal are thus identified by rotating the stage until the crystal extinguishes. The extinction directions would correspond to those indicated by the cross hairs in the eyepiece. One then



**General orientation of crystal
between crossed polarizers**



**Crystal extinction directions
aligned with polarizers**

Figure 8. Behavior of a crystal between perpendicular polarizers

relates these directions to a recognizable crystal edge, or to an axis of the spectroscopy sample holder.

All crystals used for spectroscopy or X-ray diffraction were thoroughly sketched in a notebook prior to mounting. Extinction directions were identified for the spectroscopy samples under the polarizing microscope. In some cases, crystal dimensions were measured with the ruled eyepiece. Calibration was obtained by viewing a millimeter rule through the microscope. A crystal thickness measurement was facilitated by standing a crystal on an edge. Crystals were manipulated under microscopic observation by sewing needles or sharpened tungsten wires. A conventional binocular microscope without a stage was used during mounting of samples. Each crystal was mounted over a pinhole produced in a small metal plate. Each plate was of approximate dimensions 1 cm x 2 cm x 3 mil and was made from either platinum or brass. A small amount of silicone high-vacuum grease would be placed adjacent to the pinhole, and the crystal placed over the pinhole so that the grease held it in place. If the mounting was done properly, only light which passed through the crystal would be transmitted through the pinhole. Pinholes as small as $\sim 20 \mu\text{m}$ were produced by a series of pin pricks, each followed by sanding with very fine emery cloth. The metal plate with the sample was placed in a brass sample holder and the extinction

directions of the crystal were re-determined in relation to the central axis of the sample holder. The sample holder was placed in position in a liquid helium dewar for spectroscopic measurements.

Samples were maintained at temperatures down to ~ 5 K in an Andonian cryogenics model MHD-3L-30N dewar equipped with quartz windows. A sample was cooled by a flow of helium vapor produced in the liquid helium reservoir. The vapor temperature could be controlled by heating it slightly prior to introduction into the sample compartment. Temperatures above and below 25 K were monitored by Pt and Ge resistance thermometers, respectively. These were located ~ 4 cm from the sample, with thermal contact maintained through the metal parts of the sample holder. A constant-current source supplied current to the resistors, whose resistances were recorded by a chart recorder. A temperature calibration chart was used to determine the sample temperature.

All spectra were recorded by a Cary model 14 spectrophotometer equipped with a special product number 50-025-000 Range Modifier. A model 1471200 high intensity tungsten-halogen light source and a Cary model 1460215 phototube were used. Various neutral density screens and/or pinholes were used to attenuate the reference beam. A range of ~ 3 absorbance units could be measured, if necessary. All spectral data were recorded on punched cards by an IBM model 29 keypunch linked to the

spectrophotometer via a Cary Digital System interface. Baselines were subtracted and the spectra were plotted on an incremental plotter by a computer program developed previously within the research group. Baselines were obtained by repeating the spectral experiments with a pinhole blank in place of the sample. Glan-Taylor-type calcite polarizers in the sample and reference compartments produced plane-polarized beams which then illuminated the samples and neutral density filters.

Polarization Ratios

In order to properly interpret polarized spectra, it is necessary to relate the crystal's extinction directions to the molecular axes. This requires knowledge of the crystal face examined (Miller indices), the orientation of the unit cell axes with respect to some identifiable morphological feature of the crystal (such as an edge), and coordinates of the important atoms in the unit cell. The first two are obtained by crystallographic indexing, which is discussed in another section. The third one requires at least a partially solved crystal structure. It is convenient to calculate polarization ratios in order to relate the molecular axes to the crystal extinctions (extinction directions). A polarization ratio is the ratio of the intensity of a transition along one extinction to its intensity along the other extinction. It is calculated for an ideal case and then compared with the observed value.

For the ideal \bar{z} -polarized case we consider the transition moment a unit vector coincident with the \bar{z} symmetry axis of the molecule studied. This is conveniently accomplished by computing the Mo-Mo vector, then converting it to unit length. We then define vectors to represent the crystal's extinction directions. We let \hat{z} , \hat{E}_1 and \hat{E}_2 represent the \bar{z} -transition moment and the two extinction directions, respectively. The angles between \hat{z} and \hat{E}_1 and between \hat{z} and \hat{E}_2 we shall call θ_1 and θ_2 , respectively. For the electric vector of a wave polarized along \hat{E}_1 , the amplitude along \hat{z} is $\epsilon \cos \theta_1$, where ϵ is the electric vector amplitude of the incident wave. Since intensity is given by the amplitude squared, the intensity absorbed from the light polarized along \hat{E}_1 is $\epsilon^2 \cos^2 \theta_1$. Similarly, an intensity of $\epsilon^2 \cos^2 \theta_2$ is absorbed from the \hat{E}_2 -polarized light for the \bar{z} -polarized transition. This yields an intensity or polarization ratio of $\frac{I_1}{I_2} = \frac{\cos^2 \theta_1}{\cos^2 \theta_2}$. These are obtained from the dot products by $\hat{z} \cdot \hat{E}_1 = \cos \theta_1$ and $\hat{z} \cdot \hat{E}_2 = \cos \theta_2$. The vectors involved in the initial steps of such a calculation are defined in unit cell coordinates. To facilitate the calculations, an orthogonal coordinate system is set up and these vectors are put into the new system. The vector calculations are then performed on a TI-59 calculator, using a program written in the research group. For a pair of degenerate and orthogonal \bar{x} and \bar{y} transition moments which are also orthogonal to \bar{z} , the

polarization ratio $\frac{I_1}{I_2} = \frac{\sin^2\theta_1}{\sin^2\theta_2}$ is obtained. For space groups which produce different orientations for each molecule in the unit cell, a variation of this calculation is used. If transition moment vectors $\hat{z}_1, \hat{z}_2, \hat{z}_3$ and \hat{z}_4 made angles of $\theta_1, \theta_2, \theta_3, \theta_4$ and $\phi_1, \phi_2, \phi_3, \phi_4$, respectively, with \hat{E}_1 and \hat{E}_2 , then the z polarization ratio would be given by

$$\frac{I_1}{I_2} = \frac{\cos^2\theta_1 + \cos^2\theta_2 + \cos^2\theta_3 + \cos^2\theta_4}{\cos^2\phi_1 + \cos^2\phi_2 + \cos^2\phi_3 + \cos^2\phi_4}$$

Crystallographic Indexing

Crystallographic indexing of samples by X-ray diffraction was performed for three reasons:

- (1) to confirm the identity of a crystal,
- (2) to determine the crystal face (Miller indices) examined spectroscopically, and
- (3) to relate the unit cell axes to some identifiable macroscopic feature of a crystal.

Careful sketches were made of samples prior to and after mounting for indexing. This was a necessary step, as crystals were inadvertently turned over or partially broken during the mounting procedure on many occasions. Frequently, a spectroscopic sample could be subsequently mounted for indexing. A crystal to be indexed was cemented to a glass fiber with a small amount of epoxy and placed in a goniometer head. If identification of a crystal face was desired, that face would be oriented

parallel to an easily recognized flat surface on the goniometer head. It was thus easy to determine the orientation of that face. The goniometer head was placed on the Ames Laboratory four-circle diffractometer, which was controlled by a PDP-15 computer. Automatic indexing was accomplished through the interactive program ALICE developed by Dr. R. A. Jacobson (41). Omega-oscillation photographs were taken at various phi settings. The coordinates of several diffraction spots were entered into the computer program. The program indexed the crystal, usually based on ten or more reflections, according to guidelines published in Crystal Data (42). When a sufficiently accurate set of unit cell parameters was obtained, each unit cell axis could be oriented vertically for an oscillation photograph. The axes could thus be related to identifiable crystal features. For identification of a crystal face, the computer would place various crystallographic planes into the diffracting position, by request of the operator. When the face to be identified was found in this position, it was assigned the Miller indices for the crystallographic plane requested. Accurate unit cell parameters could be compared to reported or previously determined values for the identity of a crystal.

X-ray Data Collection and Structure Solution

General

Those aspects of data collection and structure solution common to both polymorphs reported here are discussed in this section. The remaining details will be described in a section for each polymorph. Crystals were mounted and indexed on the Ames Laboratory diffractometer as described under Crystallographic Indexing. Graphite-monochromated Mo K α X-radiation was used with a take-off angle of 4.5° in all indexing and data collection. Data were collected at room temperature, using a scintillation counter for detection. A scan rate of 0.5 sec/step of 0.01° in omega was employed, with the scan range dependent on peak width. Peaks were scanned until background was encountered, as determined by the criterion count \leq background + σ (background). Stationary-crystal, stationary-counter background counts were taken at the beginning and end of each scan. All data collected were within a 2 θ sphere of 50°. As a check on electronic and crystal stability, the intensities of three standard reflections were remeasured every 75 reflections. The intensities of the standard reflections did not vary significantly throughout data collection.

The intensity data were corrected for Lorentz-polarization effects, but no absorption corrections were applied. Data reduction was made through locally written computer programs.

The estimated error in each intensity was calculated by

$\sigma_I^2 = C_T + K_t C_B + (0.03C_T)^2 + (0.03C_B)^2$, where C_T , K_t , and C_B are the total count, a counting time factor, and the background count, respectively. The factor 0.03 represents an estimate of non-statistical errors inherent in the measuring process.

The estimated deviations in the structure factors were calculated by the finite-difference method (43). The scattering factors used for all non-hydrogen atoms were those of Hanson et al. (44) for the β -form and those given in the International Tables (45) for the γ -form. Real and imaginary corrections for anomalous dispersion were obtained by linear interpolation of reported data (46). The hydrogen atom scattering factors used were those of Stewart et al. (47). The discrepancy factors used are given by $R_U = \Sigma ||F_O| - |F_C| | / \Sigma |F_O|$ and $R_W = (\Sigma w(|F_O| - |F_C|)^2 / \Sigma w |F_O|^2)^{1/2}$, where F_O and F_C are observed and calculated structure factors, respectively, and $w = 1/\sigma^2(F_O)$, with $\sigma(F_O)$ representing the estimated standard deviation in F_O . Plots depicting molecular structure were drawn by the ORTEP program (48).

β -Mo₂(O₂CH)₄

A crystal of the β -form of Mo₂(O₂CH)₄ was indexed to the following unit cell: $a = 12.368 \text{ \AA}$, $b = 19.866 \text{ \AA}$, $c = 5.490 \text{ \AA}$, $\alpha = 90.19^\circ$, $\beta = 90.07^\circ$, $\gamma = 90.02^\circ$, and $V = 1349.18 \text{ \AA}^3$. Data were collected for the $h\bar{k}l$ and $h\bar{k}\bar{l}$ octants using radiation

with $\lambda = 0.70954 \text{ \AA}$. A total of 2882 reflections were collected, of which 2492 independent reflections having $|F_o| \geq 3\sigma(F_o)$ were used in the structure solution. In order to follow the convention for monoclinic crystal systems, the data were transformed by

$$\begin{pmatrix} h' \\ k' \\ l' \end{pmatrix} = \begin{pmatrix} 0 & 0 & 1 \\ 1 & 0 & 0 \\ 0 & 1 & 0 \end{pmatrix} \begin{pmatrix} h \\ k \\ l \end{pmatrix}.$$

The program LATT (49) was used to calculate the following refined cell parameters based on $\pm 2\theta$ values of 12 reflections: $a = 5.485(1) \text{ \AA}$, $b = 12.365(2) \text{ \AA}$, $c = 19.862(4) \text{ \AA}$, $\beta = 90.24(2)^\circ$, and $V = 1347.1(5) \text{ \AA}^3$. The Howells, Phillips, and Rogers (50) test for a center of symmetry, based on one octant of data, indicated a centric unit cell. The monoclinic space group was identified as $P_{2_1/c}$, based on the systematic extinction of k odd of the $0k0$ reflections, and of l odd of the $h0l$ reflections.

The locations of all Mo atoms were found through Patterson superposition techniques. A series of electron density maps allowed location and subsequent block-diagonal least-squares refinement of all non-hydrogen atoms with anisotropic thermal parameters. Expected hydrogen atom positions were calculated, and an electron density map showed regions of electron density at or near these positions. No other atoms were found which were unaccounted for. The hydrogen atom positions were refined, while their isotropic thermal parameters were held

fixed. The variables were subjected to a final cycle of full-matrix refinement resulting in $R_u = 0.049$ and $R_w = 0.059$. The program LSQR2 (51) was used for least-squares refinement and Fourier synthesis was performed by the program ALFF (52). Interatomic distances, angles, and their standard deviations were calculated by a version of the program ORFFE (53).

γ -Mo₂(O₂CH)₄

A crystal of the γ -form of Mo₂(O₂CH)₄ was indexed to the following unit cell: $a = 14.834 \text{ \AA}$, $b = 11.179 \text{ \AA}$, $c = 5.526 \text{ \AA}$, $\beta = 90.41^\circ$, and $V = 916.45 \text{ \AA}^3$. Data were collected for the hkl , $\bar{h}\bar{k}l$, $\bar{h}k\bar{l}$, and $h\bar{k}\bar{l}$ octants using radiation with $\lambda = 0.71034 \text{ \AA}$. A total of 3935 reflections were collected, of which 743 independent reflections having $|F_o| \geq 3\sigma(F_o)$ were used in the structure solution. Since half of the data collected were considered unobserved, and an unusual systematic extinction was found, it was concluded that the unit cell used for data collection was not appropriate for structure solution. Therefore, the data were transformed by

$$\begin{pmatrix} h' \\ k' \\ l' \end{pmatrix} = \begin{pmatrix} 0.5 & 0 & -0.5 \\ 0 & 1 & 0 \\ 0 & 0 & 1 \end{pmatrix} \begin{pmatrix} h \\ k \\ l \end{pmatrix}.$$

The program LATT (49) was used to calculate the following refined cell parameters based on $\pm 2\theta$ values of 16 reflections: $a = 7.939(1) \text{ \AA}$, $b = 11.193(1) \text{ \AA}$, $c = 5.5270(9) \text{ \AA}$, $\beta = 110.86(2)^\circ$, and $V = 458.9(1) \text{ \AA}^3$. The Howells, Phillips, and Rogers (50)

test applied to 2 octants of data indicated a centric unit cell. The monoclinic space group was identified as $P_{2_1/a}$, based on the systematic extinction of k odd of the $0k0$ reflections, and of h odd of the $h0l$ reflections.

Initial Mo atom positions were obtained from a three-dimensional Patterson map. A subsequent electron density map yielded the positions of the remaining non-hydrogen atoms. The positional and anisotropic thermal parameters of the non-hydrogen atoms were subjected to several cycles of block-diagonal least-squares refinement. Expected hydrogen atom positions were then calculated. The hydrogen atoms were found on an electron density difference map, and no other atoms were found. The hydrogen atom positions were allowed to vary, while their isotropic thermal parameters were held fixed. The variables were subjected to two final cycles of full-matrix refinement resulting in $R_u = 0.032$ and $R_w = 0.041$. The program ALLS (54) was used for least-squares refinement and Fourier synthesis was performed by the program FOR (55). Interatomic distances, angles, and their standard deviations were calculated by the program DISTANCE (56).

RESULTS AND DISCUSSION

Description of Crystal Structures

Because of their similarity, the structures of the β - and γ -polymorphs of $\text{Mo}_2(\text{O}_2\text{CH})_4$ will be discussed together. In addition, the structure of $\text{Mo}_2(\text{O}_2\text{CH})_4 \cdot \text{KCl}$ will be described briefly, since it is important to the interpretation of the spectra. Table 4 summarizes crystallographic parameters for the three $\text{Mo}_2(\text{O}_2\text{CH})_4$ polymorphs and for $\text{Mo}_2(\text{O}_2\text{CH})_4 \cdot \text{KCl}$. Tables 5 and 6 give the final positional and thermal parameters, respectively, for β - $\text{Mo}_2(\text{O}_2\text{CH})_4$ and Figure 9 shows the atom labelling system. The positional and thermal parameters are listed for γ - $\text{Mo}_2(\text{O}_2\text{CH})_4$ in Tables 7 and 8, respectively, and the atom labelling system is shown in Figure 10. Observed and calculated structure factors are listed in Appendices A and B, respectively, for the β - and γ -polymorphs. The β -form has 6 molecules in the unit cell: 4 in general positions and 2 in the special positions $0,0,0$ and $0, \frac{1}{2}, \frac{1}{2}$. The latter two molecules are crystallographically equivalent and each has inversion symmetry. These will be referred to as site 1 molecules, while those in general positions will be designated site 2 molecules. The four site 2 molecules are equivalent, but they have no molecular symmetry imposed on them by the crystal lattice. The unit cell of γ - $\text{Mo}_2(\text{O}_2\text{CH})_4$ contains 2 molecules in the special positions $\frac{1}{2}, \frac{1}{2}, \frac{1}{2}$ and $0, 0, \frac{1}{2}$. Each of these molecules has inversion symmetry and the two molecules are equivalent.

Table 4. Crystallographic parameters for the $\text{Mo}_2(\text{O}_2\text{CH})_4$ polymorphs and for $\text{Mo}_2(\text{O}_2\text{CH})_4 \cdot \text{KCl}$

	$\alpha\text{-Mo}_2(\text{O}_2\text{CH})_4^{\text{a}}$	$\beta\text{-Mo}_2(\text{O}_2\text{CH})_4$	$\gamma\text{-Mo}_2(\text{O}_2\text{CH})_4$	$\text{Mo}_2(\text{O}_2\text{CH})_4 \cdot \text{KCl}$
Space Group	$P2_1 2_1 2_1$	$P2_1/c$	$P2_1/a$	$P\bar{1}$
Crystal System	Orthorhombic	Monoclinic	Monoclinic	Triclinic
a	12.288(4) Å	5.485(1) Å	7.939(1) Å	8.253(3) Å
b	12.930(5) Å	12.365(2) Å	11.193(1) Å	10.684(3) Å
c	5.500(1) Å	19.862(4) Å	5.5271(9) Å	6.769(3) Å
α	90.0°	90.0°	90°	89.52(5)°
β	90.0°	90.24(2)°	110.86(2)°	109.73(4)°
γ	90.0°	90.0°	90.0°	87.03(6)°
V	872.9(5) Å ³	1347.1(5) Å ³	458.9(1) Å ³	560.8(3) Å ³
Z	4	6	2	2
V/Z	218.2 Å ³ /molecule	224.5 Å ³ /molecule	229.5 Å ³ /molecule	280.4 Å ³ /molecule
Molecules on general positions (no symmetry)	4	4	0	0
Molecules on special positions (inversion symmetry)	0	2	2	2 ^b

^aReference 1.

^bThe molecules are crystallographically independent.

Table 5. Final positional parameters^a and their estimated standard deviations^b for β -Mo₂(O₂CH)₄

	x	y	z
Mo(1)	0.1611(1)	-0.01997(4)	0.02551(3)
Mo(2)	0.2720(1)	0.05052(4)	0.34210(3)
Mo(3)	0.5898(1)	-0.01654(4)	0.30189(3)
O(1)	0.1734(9)	-0.1737(4)	-0.0201(2)
O(2)	0.3727(8)	0.0459(4)	-0.0547(2)
O(3)	0.1694(9)	0.1309(4)	0.0743(3)
O(4)	-0.0276(9)	-0.0882(4)	0.1074(2)
O(5)	0.2370(9)	0.1562(4)	0.2593(3)
O(6)	0.4654(9)	0.1705(4)	0.3954(2)
O(7)	0.295(1)	-0.0495(4)	0.4283(3)
O(8)	0.0554(9)	-0.0682(4)	0.2907(2)
O(9)	0.5755(9)	0.0841(4)	0.2166(2)
O(10)	0.8065(8)	0.1002(4)	0.3541(2)
O(11)	0.6312(9)	-0.1201(4)	0.3853(2)
O(12)	0.3951(8)	-0.1372(4)	0.2486(2)
C(1)	0.002(2)	-0.1950(7)	-0.0605(4)
C(2)	0.258(1)	0.0856(6)	0.1038(4)
C(3)	0.395(2)	0.1492(6)	0.2147(4)
C(4)	0.694(1)	0.1688(6)	0.3892(4)

^aGiven in fractional coordinates.

^bGiven in parentheses for the least significant figure.

Table 5. Continued

	x	y	z
C(5)	0.475(2)	-0.1117(6)	0.4305(4)
C(6)	0.167(1)	-0.1373(6)	0.2553(4)
H(1)	0.02(2)	-0.264(8)	-0.081(4)
H(2)	0.34(2)	0.129(8)	-0.138(4)
H(3)	0.37(2)	0.206(7)	0.173(4)
H(4)	0.79(2)	0.236(7)	0.411(4)
H(5)	0.47(2)	-0.162(7)	0.471(4)
H(6)	0.05(2)	-0.205(7)	0.242(4)

Table 6. Final thermal parameters^a and their estimated standard deviations^b for β -Mo₂(O₂CH)₄

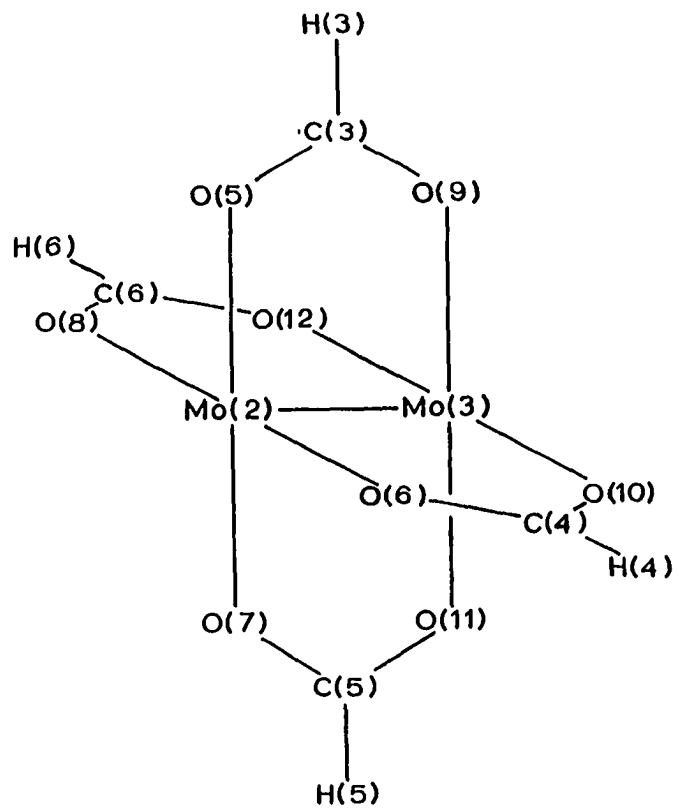
	B ₁₁	B ₂₂	B ₃₃	B ₁₂	B ₁₃	B ₂₃
Mo(1)	0.97(2)	1.95(3)	2.10(3)	0.09(2)	-0.40(2)	0.08(2)
Mo(2)	1.04(2)	1.87(2)	2.51(3)	0.08(2)	-0.01(2)	-0.35(2)
Mo(3)	0.97(2)	1.68(3)	2.12(3)	0.06(2)	-0.05(2)	-0.10(2)
O(1)	2.2(2)	2.6(2)	4.0(2)	0.4(2)	-0.3(2)	-0.5(2)
O(2)	1.4(2)	3.0(2)	2.6(2)	0.1(2)	-0.2(2)	0.4(2)
O(3)	2.0(2)	2.9(2)	4.0(2)	0.0(2)	-1.1(2)	-1.1(2)
O(4)	2.0(2)	3.1(2)	2.8(2)	0.1(2)	-0.3(2)	0.6(2)
O(5)	2.1(2)	2.5(2)	3.6(2)	0.0(2)	-0.9(2)	0.1(2)
O(6)	1.9(2)	3.1(2)	3.4(2)	0.4(2)	0.1(2)	-1.2(2)
O(7)	2.8(2)	3.2(2)	2.8(2)	0.1(2)	0.7(2)	0.1(2)
O(8)	1.6(2)	2.5(2)	3.8(2)	-0.3(2)	-0.2(2)	-0.7(2)
O(9)	2.6(2)	2.8(2)	2.5(2)	-0.2(2)	0.0(2)	0.2(2)
O(10)	1.2(2)	2.8(2)	3.4(2)	-0.2(2)	-0.3(2)	-0.7(2)
O(11)	2.3(2)	2.6(2)	2.7(2)	0.5(2)	-0.1(2)	0.4(2)
O(12)	1.8(2)	2.1(2)	3.2(2)	0.0(2)	-0.1(2)	-0.6(2)

C(1)	3.6(4)	2.8(3)	4.5(4)	0.5(3)	-0.7(3)	-1.4(3)
C(2)	2.3(3)	2.2(3)	3.3(3)	0.0(2)	0.1(3)	0.5(3)
C(3)	3.9(4)	2.0(3)	3.0(3)	-0.6(3)	-0.8(3)	-0.1(3)
C(4)	2.3(3)	2.4(3)	3.5(3)	-0.3(3)	-0.5(3)	-0.9(3)
C(5)	3.7(4)	2.7(3)	2.9(3)	-0.4(3)	-0.5(3)	0.1(3)
C(6)	2.2(3)	2.1(3)	3.1(3)	-0.2(3)	-0.1(3)	-0.3(2)
H(1)	2.0 ^c					
H(2)	2.0 ^c					
H(3)	2.0 ^c					
H(4)	2.0 ^c					
H(5)	2.0 ^c					
H(6)	2.0 ^c					

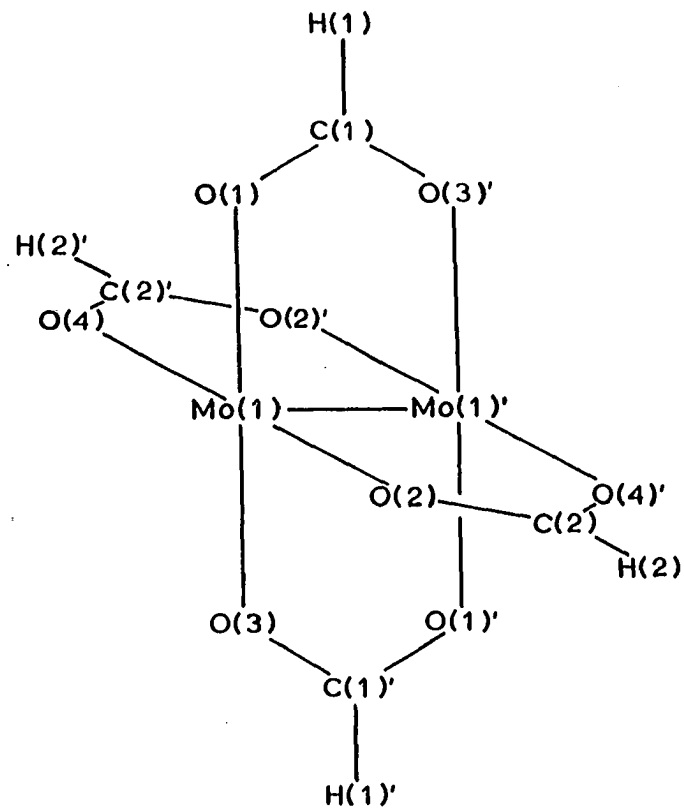
^aThe B_{ij} 's are defined by $T = \exp[-\frac{1}{4}(B_{11}h^2a^{*2} + B_{22}k^2b^{*2} + B_{33}l^2c^{*2} + 2B_{12}hka^*b^* + 2B_{13}hla^*c^* + 2B_{23}klb^*c^*)]$.

^bGiven in parentheses for the least significant figure.

^cIsotropic B which was not refined and is defined by $T = \exp[-\frac{B}{4}(h^2a^{*2} + k^2b^{*2} + l^2c^{*2} + 2hka^*b^* + 2hla^*c^*\cos\gamma^* + 2klb^*c^*)]$.



General Positions $\beta\text{-Mo}_2(\text{O}_2\text{CH})_4$



Special Positions $\beta\text{-Mo}_2(\text{O}_2\text{CH})_4$

Figure 9. Atom labelling system used in the structure solution of $\beta\text{-Mo}_2(\text{O}_2\text{CH})_4$. Primes indicate atoms generated by an inversion center located at the center of the molecule

Table 7. Final positional parameters^a and their estimated standard deviations^b for $\gamma\text{-Mo}_2(\text{O}_2\text{CH})_4$

	x	y	z
Mo	0.51056(6)	0.54768(4)	0.34326(7)
O(1)	0.2308(5)	0.5833(4)	0.1970(7)
O(2)	0.4674(5)	0.3891(4)	0.1163(6)
O(3)	0.7899(5)	0.5172(4)	0.4667(8)
O(4)	0.5564(6)	0.7100(3)	0.5486(7)
C(1)	0.1417(9)	0.5437(5)	0.328(1)
C(2)	0.4429(9)	0.2943(6)	0.221(1)
H(1)	0.01(1)	0.562(6)	0.26(2)
H(2)	0.40(1)	0.227(7)	0.10(2)

^aGiven in fractional coordinates.

^bGiven in parentheses for the least significant figure.

Table 8. Final thermal parameters^a and their estimated standard deviations^b for γ -Mo₂(O₂CH)₄

	B ₁₁	B ₂₂	B ₃₃	B ₁₂	B ₁₃	B ₂₃
Mo	2.82(3)	2.55(3)	1.55(2)	-0.06(1)	1.13(2)	0.17(1)
O(1)	3.3(2)	4.3(2)	2.4(2)	0.5(1)	1.0(1)	0.6(1)
O(2)	5.0(2)	3.4(2)	1.9(1)	-0.3(1)	1.6(1)	-0.6(1)
O(3)	3.1(2)	4.7(2)	2.8(2)	-0.2(1)	1.5(1)	0.4(1)
O(4)	5.8(2)	2.7(2)	3.0(2)	-0.5(1)	2.1(2)	0.0(1)
C(1)	3.2(3)	4.7(3)	2.8(3)	0.2(2)	1.3(2)	0.0(2)
C(2)	5.6(3)	3.4(3)	3.2(3)	-0.7(2)	2.0(3)	-1.2(2)
H(1)	3.5 ^c					
H(2)	3.5 ^c					

^aThe B_{ij}'s are defined by $T = \exp[-\frac{1}{4}(B_{11}h^2a^{*2} + B_{22}k^2b^{*2} + B_{33}l^2c^{*2} + 2B_{12}hka^{*}b^{*} + 2B_{13}hla^{*}c^{*} + 2B_{23}klb^{*}c^{*})]$.

^bGiven in parentheses for the least significant figure.

^cIsotropic B which was not refined and is defined by $T = \exp[-\frac{B}{4}(h^2a^{*2} + k^2b^{*2} + l^2c^{*2} + 2hka^{*}b^{*} + 2hla^{*}c^{*}\cos\gamma^{*} + 2klb^{*}c^{*})]$.

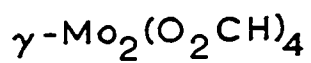
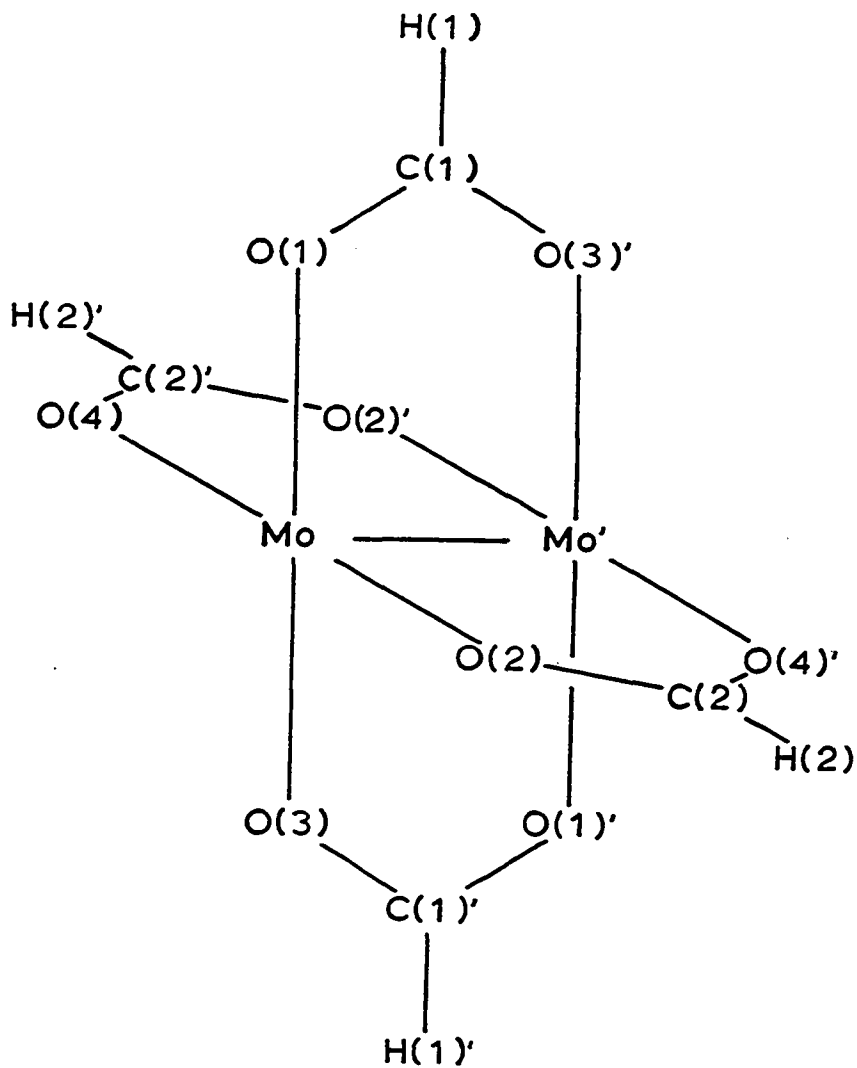


Figure 10. Atom labelling system used in the structure solution of $\gamma\text{-Mo}_2(\text{O}_2\text{CH})_4$. Primes indicate atoms generated by an inversion center located at the center of the molecule

Before interatomic distances and angles are presented, it is useful to consider an aspect of the molecular structure common to the three polymorphs. Note in Table 4 that each polymorph has one cell dimension which is ~ 5.5 Å in length. Each 5.5 Å axis is a molecular stacking axis in that particular polymorph. In addition to bonding with oxygens on four bridging carboxylates, each Mo atom is involved in weak axial coordination to an oxygen from an adjacent molecule. This intermolecular interaction produces chains of molecules, as depicted in Figure 11. The three polymorphs have this same basic stacking arrangement, as do the dimolybdenum complexes of acetate, trifluoroacetate, and benzoate. Dimolybdenum tetrapivalate also has intermolecular axial coordination, but it adopts a different stacking configuration.

The polymorphs of dimolybdenum tetraformate differ by the number and arrangement of the chains running through one unit cell. An ORTEP view along the stacking axis (showing one layer of molecules) is shown for each of the α -, β -, and γ -forms, respectively, in Figures 12, 13, and 14. In this view, each molecule shown represents one chain. The three figures are drawn to the same scale for comparison. Note that each molecule is oriented approximately the same with respect to the viewing (stacking) axis, in all three polymorphs. Note also that the chains pack approximately in a hexagonal (close-packed) arrangement in each case. It is evident from the drawings that the basic

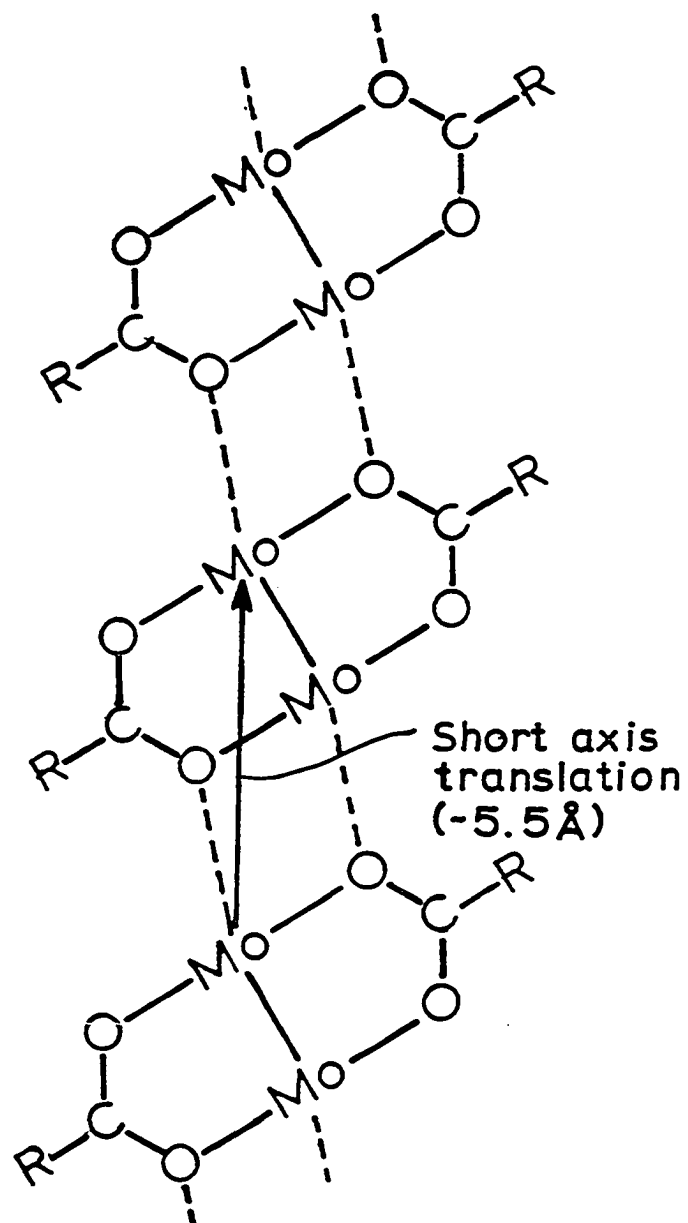


Figure 11. Intermolecular bonding in dimolybdenum tetracarboxylate complexes

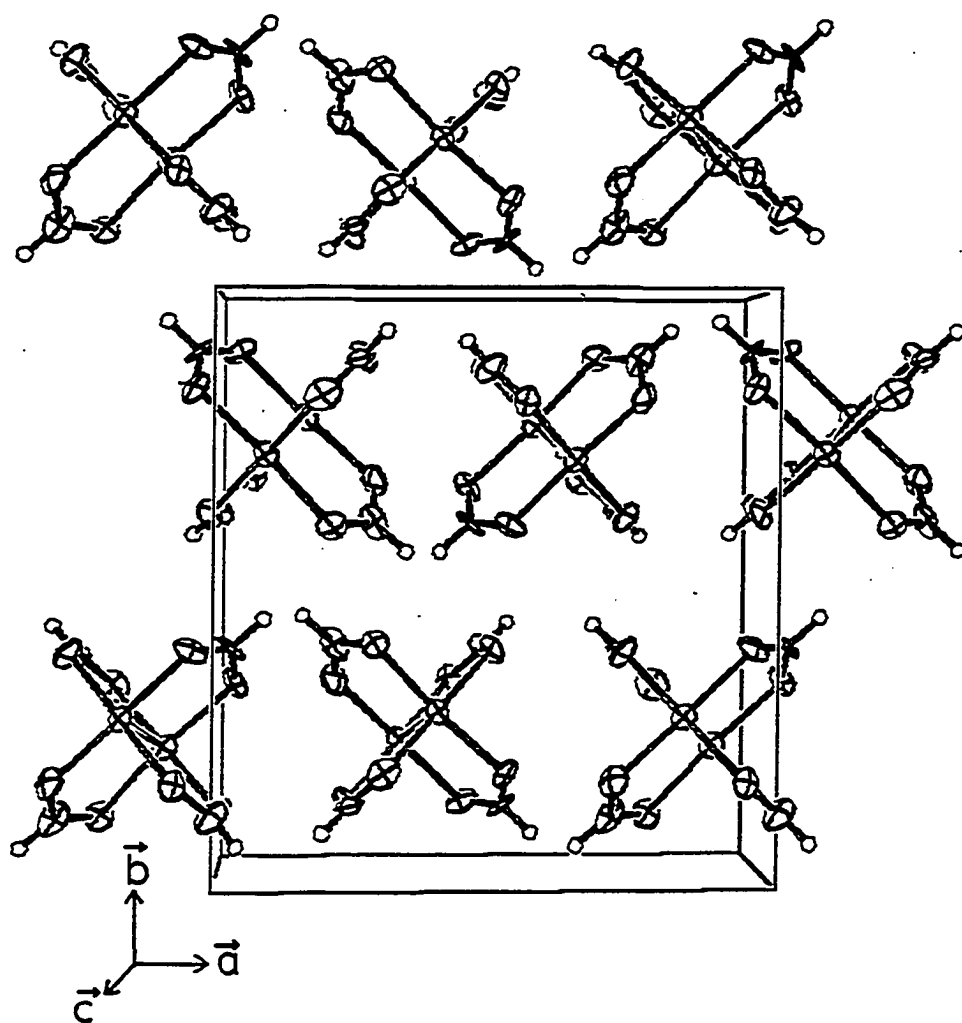


Figure 12. The molecular structure of $\alpha\text{-Mo}_2(\text{O}_2\text{CH})_4$

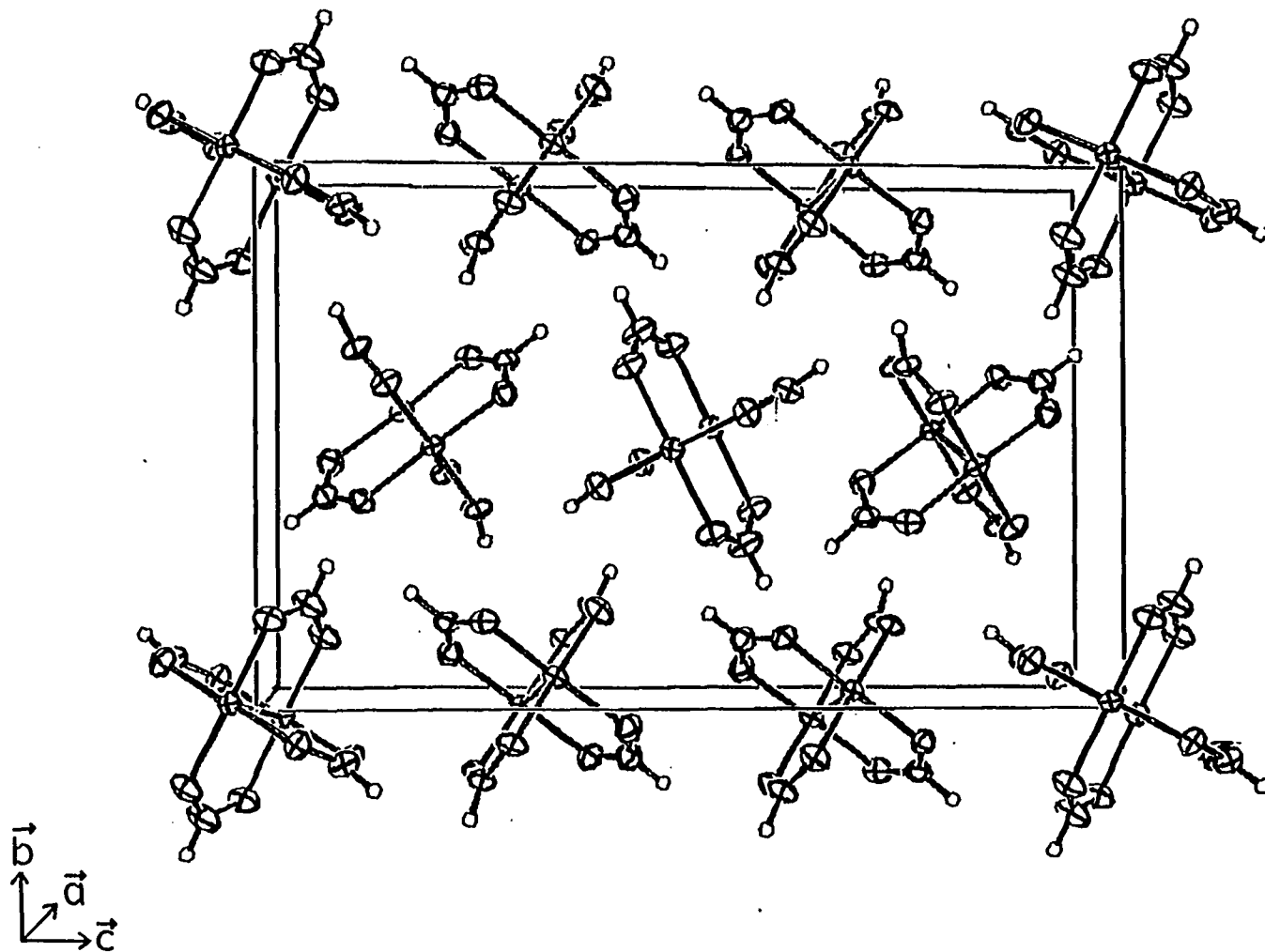


Figure 13. The molecular structure of $\beta\text{-Mo}_2(\text{O}_2\text{CH})_4$

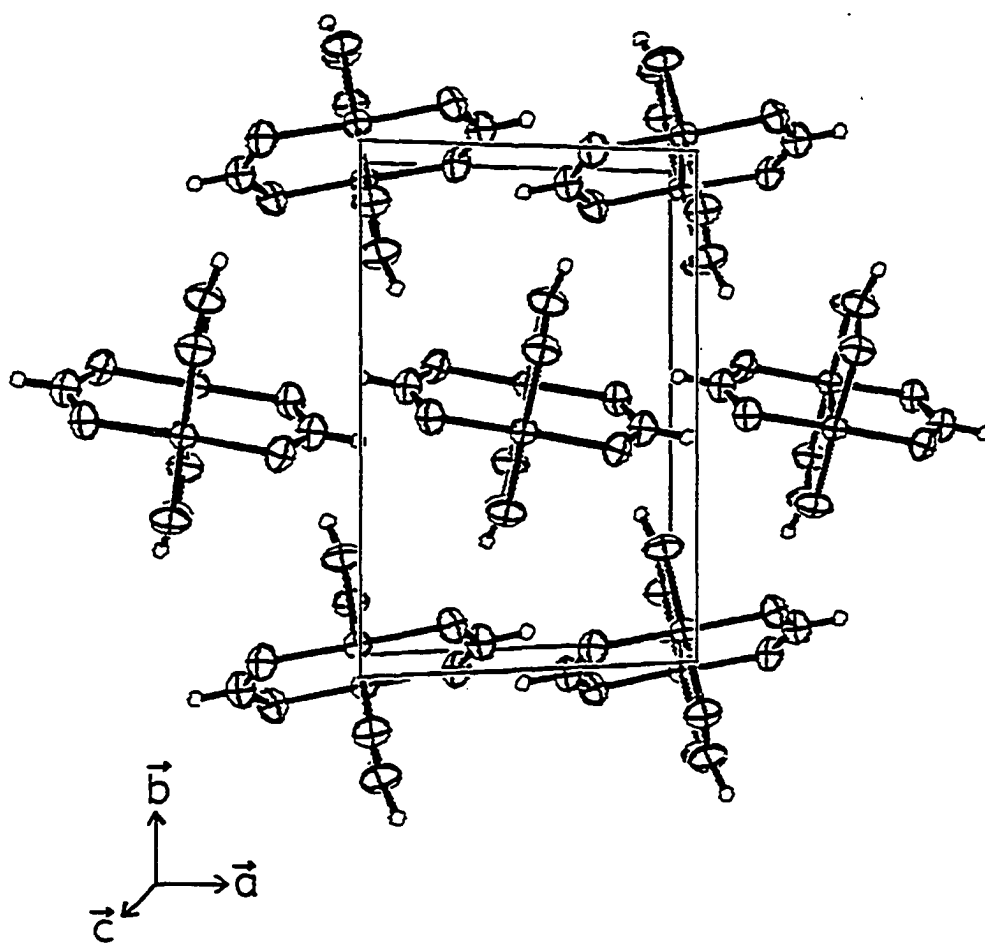


Figure 14. The molecular structure of $\gamma\text{-Mo}_2(\text{O}_2\text{CH})_4$

features of the structures are very similar, but that the chain packing varies somewhat from one polymorph to another.

For comparison of distances and angles, two values will be considered significantly different if their difference is greater than or equal to $3\sigma(\text{difference})$. Where averages are given, the estimated standard deviation (e.s.d.) in the average was taken as the larger of $\frac{S_{\max}}{\sqrt{n}}$ and $\frac{S}{\sqrt{n}}$, where n is the number of values used in the average, S_{\max} is the largest e.s.d. associated with an individual value, and $S = \sqrt{\frac{\sum_{i=1}^n (x_i - \bar{x})^2}{n - 1}}$. The important interatomic distances and angles are listed in Table 9 for $\beta\text{-Mo}_2(\text{O}_2\text{CH})_4$ and in Table 10 for $\gamma\text{-Mo}_2(\text{O}_2\text{CH})_4$. For $\beta\text{-Mo}_2(\text{O}_2\text{CH})_4$, it is apparent that only in one case do the analogous distances and angles in Table 9 differ significantly from site 1 to site 2. This case consists of the Mo-Mo-O (axial) angles, which are $161.9(1)^\circ$ for site 1 and $159.2(1)^\circ$ and $159.3(1)^\circ$ for site 2. The C-H bonds appear to be shorter for site 1 than site 2, but because of the large uncertainties associated with these, it is questionable to call this a real effect.

Note, however, that trends appear which vary between certain groups of atoms, but not between sites. One-half of the O-C-H angles are greater than 120° , while one-half are less than 120° . Furthermore, each carbon-hydrogen bond is associated with one angle of each type. In the site 1 molecules, this occurs with inversion symmetry such that the C(1)-H(1) and C(2)-H(2) bonds

Table 9. Interatomic distances and angles and their estimated standard deviations^a for β -Mo₂(O₂CH)₄

Site 1	
Mo(1)-Mo(1)	2.093(1)
Mo(1)-O(2) (axial)	2.639(5)
Mo(1)-O(1)	2.107(5)
-O(2)	2.136(5)
-O(3)	2.102(5)
-O(4)	2.109(5)
C(1)-O(1)	1.263(9)
-O(3)	1.257(9)
C(2)-O(2)	1.259(8)
-O(4)	1.265(0)
C(1)-H(1)	0.95(9)
C(2)-H(2)	0.96(9)
Mo(1)-Mo(1)-O(1)	91.9(1)
-O(2)	90.5(1)
-O(3)	91.7(1)
-O(4)	93.0(1)
Mo(1)-Mo(1)-O(2) (axial)	161.9(1)

^aGiven in parentheses for the least significant figure.

 Site 2

Distances, Å

Mo(2)-Mo(3)	2.0916(9)		
Mo(2)-O(10) (axial)	2.638(5)	Mo(3)-O(8) (axial)	2.643(5)
Mo(2)-O(5)	2.108(5)	Mo(3)-O(9)	2.103(5)
-O(6)	2.107(5)	-O(10)	2.136(4)
-O(7)	2.115(5)	-O(11)	2.105(5)
-O(8)	2.145(5)	-O(12)	2.116(4)
C(3)-O(5)	1.245(9)	C(5)-O(7)	1.251(10)
-O(9)	1.276(9)	-O(11)	1.249(9)
C(4)-O(6)	1.263(9)	C(6)-O(8)	1.266(8)
-O(10)	1.259(8)	-O(12)	1.259(8)
C(3)-H(3)	1.10(9)	C(5)-H(5)	1.02(9)
C(4)-H(4)	1.07(9)	C(6)-H(6)	1.07(9)

Angles, Degrees

Mo(3)-Mo(2)-O(5)	91.2(1)	Mo(2)-Mo(3)-O(9)	92.6(1)
-O(6)	93.0(1)	-O(10)	90.5(1)
-O(7)	91.7(1)	-O(11)	91.6(1)
-O(8)	90.4(1)	-O(12)	92.9(1)
Mo(2)-Mo(3)-O(8) (axial)	159.2(1)	Mo(3)-Mo(2)-O(10) (axial)	159.3(1)

Table 9. Continued

Site 1	
O(1)-Mo(1)-O(2)	90.3(2)
O(2)-Mo(1)-O(3)	89.7(2)
O(3)-Mo(1)-O(4)	90.5(2)
O(4)-Mo(1)-O(1)	89.3(2)
O(1)-Mo(1)-O(3)	176.4(2)
O(2)-Mo(1)-O(4)	176.4(1)
Mo(1)-O(1)-C(1)	115.9(5)
-O(2)-C(2)	117.1(4)
-O(3)-C(1)	116.4(5)
-O(4)-C(2)	116.1(5)
O(1)-C(1)-O(3)	124.1(7)
O(2)-C(2)-O(4)	123.4(7)
O(1)-C(1)-H(1)	111(5)
O(2)-C(2)-H(2)	123(5)
O(3)-C(1)-H(1)	124(5)
O(4)-C(2)-H(2)	113(5)

Site 2

O(5)-Mo(2)-O(6)	90.0(2)	O(9)-Mo(3)-O(10)	90.6(2)
O(6)-Mo(2)-O(7)	88.7(2)	O(10)-Mo(3)-O(11)	88.3(2)
O(7)-Mo(2)-O(8)	90.9(2)	O(11)-Mo(3)-O(12)	91.0(2)
O(8)-Mo(2)-O(5)	90.2(2)	O(12)-Mo(3)-O(9)	89.8(2)
O(5)-Mo(2)-O(7)	176.8(2)	O(9)-Mo(3)-O(11)	175.7(2)
O(6)-Mo(2)-O(8)	176.5(2)	O(10)-Mo(3)-O(12)	176.5(2)
Mo(2)-O(5)-C(3)	116.8(5)	Mo(3)-O(9)-C(3)	115.0(5)
-O(6)-C(4)	115.9(4)	-O(10)-C(4)	116.9(4)
-O(7)-C(5)	115.6(5)	-O(11)-C(5)	116.3(5)
-O(8)-C(6)	117.3(4)	-O(12)-C(6)	116.6(5)
O(5)-C(3)-O(9)	124.4(7)	O(7)-C(5)-O(11)	124.7(7)
O(6)-C(4)-O(10)	123.7(6)	O(8)-C(6)-O(12)	122.8(7)
O(5)-C(3)-H(3)	115(5)	O(9)-C(3)-H(3)	121(5)
O(6)-C(4)-H(4)	114(5)	O(10)-C(4)-H(4)	122(5)
O(7)-C(5)-H(5)	113(5)	O(11)-C(5)-H(5)	122(5)
O(8)-C(6)-H(6)	113(5)	O(12)-C(6)-H(6)	123(5)

Table 10. Interatomic distances and angles and their estimated standard deviations^a for γ -Mo₂(O₂CH)₄

Distances, Å			
Mo ⁺ -Mo	2.0910(8)	O(1)-C(1)	1.261(7)
Mo-O(1)	2.114(4)	O(2)-C(2)	1.258(8)
-O(2)	2.130(4)	O(3)-C(1) ⁺	1.266(7)
-O(3)	2.103(4)	O(4)-C(2) ⁺	1.272(7)
-O(4)	2.104(4)	C(1)-H(1)	1.03(8)
Mo-O(2) ⁺ (axial)	2.701(3)	C(2)-H(2)	0.98(8)
Angles, degrees			
Mo ⁺ -Mo-O(1)	91.7(1)	Mo-O(1)-C(1)	116.2(4)
-O(2)	91.1(1)	Mo-O(2)-C(2)	116.8(4)
-O(3)	92.0(1)	Mo-O(3)-C(1) ⁺	116.4(4)
-O(4)	92.5(1)	Mo-O(4)-C(2) ⁺	116.5(4)
Mo ⁺ -Mo-O(2) ⁺ (axial)	164.45(9)	O(1)-C(1)-O(3) ⁺	123.7(6)
O(1)-Mo-O(2)	90.3(2)	O(2)-C(2)-O(4) ⁺	123.1(6)
O(2)-Mo-O(3)	89.2(2)	O(1)-C(1)-H(1)	117(5)
O(3)-Mo-O(4)	90.3(2)	O(2)-C(2)-H(2)	115(5)
O(4)-Mo-O(1)	90.0(2)	O(3) ⁺ -C(1)-H(1)	120(5)
O(1)-Mo-O(3)	176.3(2)	O(4) ⁺ -C(2)-H(2)	120(5)
O(2)-Mo-O(4)	176.4(1)		

^aGiven in parentheses for the least significant figure.

bend toward the Mo(1) end in each molecule and the C(1)-H(1) and C(2)-H(2) bonds bend toward the Mo(1) end. In the site 2 molecules, the four C-H bonds bend toward the Mo(2) end of each molecule. The O-C-H bond angles average to $113(2)^\circ$ and $123(2)^\circ$ over the crystallographic sites.

Note, also, that certain of the bonding parameters are different for O(2), O(8), and O(10) when compared to the remainder of the oxygen atoms. The Mo-O bond lengths of ~ 2.14 Å for those three atoms are significantly longer than the bond lengths of ~ 2.10 - 2.12 Å containing the remaining nine oxygen atoms. The Mo-Mo-O angles are significantly smaller for O(2), O(8), and O(10) than for the other oxygen atoms, as well. Note also that the Mo-Mo-O angles are significantly larger for O(4), O(6), and O(12) than for the other oxygen atoms. These three atoms are found on the same formate ligand as O(2), O(8), and O(10), respectively. Thus, the values of the Mo-Mo-O angles fall into three distinct groups: of $\sim 90.5^\circ$ angles involving O(2), O(8), and O(10); of $\sim 93.0^\circ$ angles involving O(4), O(6), and O(12); and of $\sim 91.7^\circ$ angles involving the remaining oxygen atoms. Two other trends of this nature are apparent, though not meeting the criterion of statistical significance. The three largest Mo-O-C angles contain O(2), O(8), and O(10), as do the three smallest O-C-O angles. Note, however, that the $92.6(1)^\circ$ Mo(2)-Mo(3)-O(9) angle seems large since the Mo-Mo-O angles involving O(1), O(3), O(5), O(7), and O(11) (in

the group with ligands not involved in axial coordination) lie in the range $91.2(1)^\circ$ - $91.9(1)^\circ$. On further inspection of Table 9 other observations are noted for O(9). The longest C-O bond length of $1.276(9)$ Å involves O(9). Of the eight O-Mo-O angles of $\sim 176^\circ$, the one involving O(9) is obviously low. The smallest Mo-O-C angle contains O(9). No intermolecular interaction with O(9) is evident, and it is not clear why this oxygen might have an environment different from otherwise similar oxygen atoms. However, this serves to illustrate the subtle nature of crystal packing forces and the difficulties in grouping or identifying "equivalent" distances and angles in the solid state.

Like the β -form, γ -Mo₂(O₂CH)₄ seems to show a larger and a smaller O-C-H angle at each carbon atom, as Table 10 shows. The C(1)-H(1) and C(2)-H(2) bonds bend toward the Mo end, and the C(1)'-H(1)' and C(2)'-H(2)' bonds bend toward the Mo' end of each molecule. These give averages of $116(4)^\circ$ and $120(4)^\circ$, though their statistical validity is low, and the effect may not be real. If the effect is real, there is no consistent pattern of C-H bond deflection exhibited in the β - and γ -forms. Hydrogen positions were not refined in the α -form, so nothing can be said concerning such behavior in that polymorph. The O-C-H behavior at best represents only minor packing variations which may depend on a hydrogen atom's proximity to an oxygen or hydrogen atom on a nearby molecule.

Those axial coordination effects observed in the β -polymorph are also the same observed in γ - $\text{Mo}_2(\text{O}_2\text{CH})_4$, in which O(2) is the axially coordinated oxygen atom, and O(4)' is located on the same ligand as O(2). As in the β -form, a long Mo-O(2) bond length, a small Mo'-Mo-O(2) angle, and a large Mo'-Mo-O(4) angle are found relative to the corresponding values observed for the other oxygen atoms (Table 10). These differences are statistically significant. The trends noted in the Mo-O-C and O-C-O angles of the β -form are followed in the γ -form, again without statistical significance. Because of the small number of values for any particular type of distance or angle in the γ -form, it would be questionable to draw conclusions based on that data alone. However, since the β -form yields the same results based on more values, then the results appear to be real, and the possible implications will be considered. Furthermore, these same trends are observed in α - $\text{Mo}_2(\text{O}_2\text{CH})_4$, $\text{Mo}_2(\text{O}_2\text{CCH}_3)_4$, and $\text{Mo}_2(\text{O}_2\text{CCF}_3)_4$. They are not completely general, however, since they are not observed in $\text{Mo}_2(\text{O}_2\text{CC}_6\text{H}_5)_4$. The phenyl group in the benzoate is much larger than the methyl or trifluoromethyl group, which might account for the difference. With the exception of the lengthened Mo-O bonds, the trends mentioned here have gone unnoticed until now. Cotton and Thompson recently noted the Mo-O bond lengthening effect of axial coordination in several dimolybdenum carboxylate complexes (57).

Distances and angles which demonstrate the effects of axial Mo-O coordination are summarized in Table 11 for the polymorphs of the formate complex and for the acetate and trifluoroacetate complexes. Each compound may not show every trend, but there seems to be sufficient general support to indicate that the effects are real. These effects of axial coordination are shown graphically in Figure 15. It appears from the drawing that the oxygen atom is pushed or held away from the molybdenum atom to which it is weakly coordinated. This is a surprising result, but it has a simple explanation. As Figure 11 indicates, each intermolecular bonding region is described structurally by a Mo-O-Mo-O ring which approximates a parallelogram. (For those cases in which the dimolybdenum tetracarboxylate molecule has inversion symmetry, it is a true parallelogram.) The length of the shorter of the two diagonals is the O-O distance. A parallelogram with sides 2.14 Å and 2.70 Å and acute (O-Mo---O) angles of 70° is representative of the situation found in the formate polymorphs and the acetate and trifluoroacetate complexes of dimolybdenum. This corresponds to a Mo-Mo-O axial angle of $\sim 160^\circ$. The law of cosines then tells us that the O-O distance is 2.85 Å. Since the ionic radius of an oxygen atom is 1.4 Å, the oxygen atoms are evidently in contact. To keep the oxygens apart, the ligands then distort slightly, resulting in the effects observed. The Mo-O axial bonding interaction is sufficiently strong to produce this distortion.

Table 11. Interatomic distances and angles illustrating the effects of axial coordination in several dimolybdenum tetracarboxylate complexes

Category	$\alpha\text{-Mo}_2(\text{O}_2\text{CH})_4^{\text{a}}$		$\beta\text{-Mo}_2(\text{O}_2\text{CH})_4$	
	Distance, Å	Average ^{d,e} and Range ^f	No. of Values	Average and Range
Mo-O(b) ^g	2.14(1) 2.122-2.140(14)	2	2.139(3) 2.136-2.145(5)	3
Mo-O(nb) ^h	2.101(15) 2.072-2.125(14)	6	2.108(2) 2.102-2.116(5)	9
<u>Angle, degrees</u>				
Mo-Mo-O(b)	90.3(2) 90.2-90.4(3)	2	90.47(6) 90.4-90.5(1)	3
Mo-Mo-O(adj) ⁱ	93.3(3) 93.2-93.3(4)	2	92.97(6) 92.9-93.0(1)	3
Mo-Mo-O(nb) ^j	92.3(2) 91.6-92.7(4)	4	91.8(2) 91.2-92.6(1)	6

^aReference 1.

^bReference 58.

^cReference 59.

^dThe averaged values presented here are convenient and concise, but in some cases lack statistical credibility in regard to grouping of data. The range of observed values is included as an alternative means of illustrating the trends.

^eThe e.s.d. in the mean is given in parentheses.

^fThe largest individual e.s.d. is given in parentheses.

^gO(b) designates an oxygen atom involved in axial coordination.

^hO(nb) designates an oxygen atom not involved in axial coordination.

ⁱO(adj) designates an oxygen atom located on the same ligand as O(b).

^jO(nb) in this case does not include O(adj).

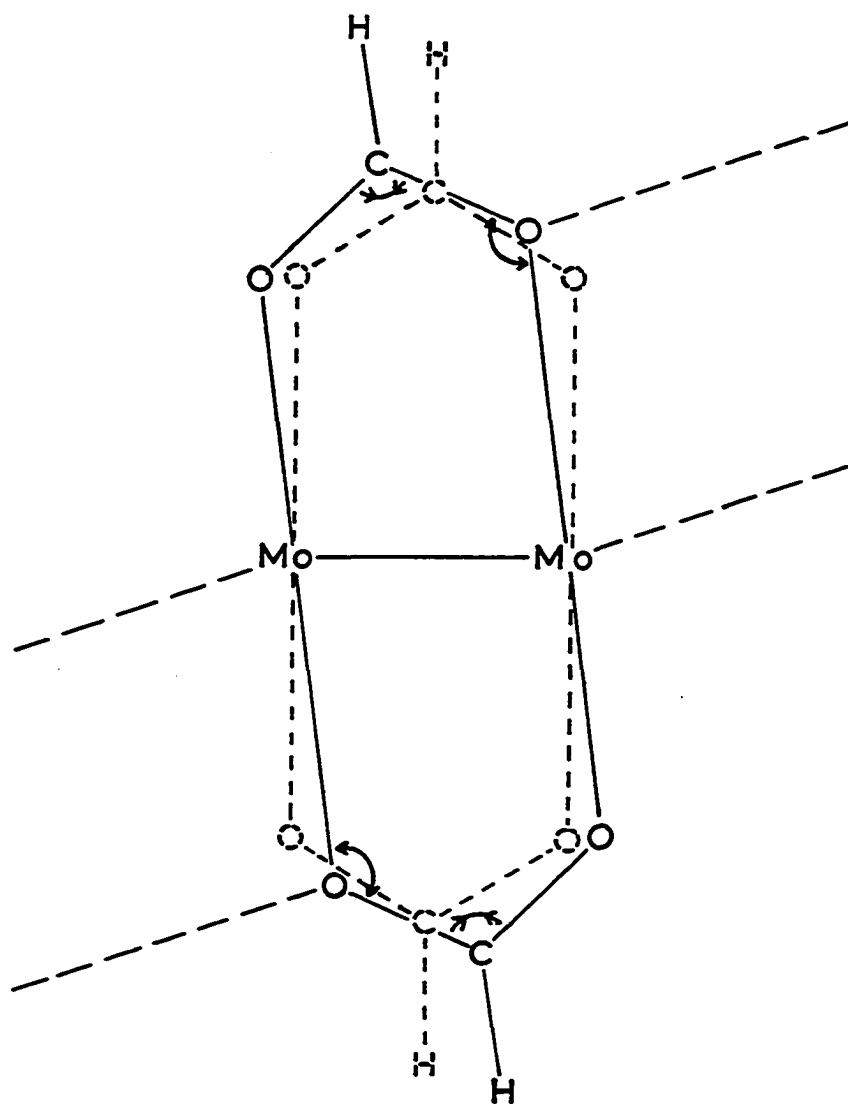
$\gamma\text{-Mo}_2(\text{O}_2\text{CH})_4$		$\text{Mo}_2(\text{O}_2\text{CCH}_3)_4^b$		$\text{Mo}_2(\text{O}_2\text{CCF}_3)_4^c$	
<u>Average and Range</u>	<u>No. of Values</u>	<u>Average and Range</u>	<u>No. of Values</u>	<u>Average and Range</u>	<u>No. of Values</u>
2.130(4) ---	1	2.137(4) ---	1	2.14(2) ---	1
2.107(4) 2.103-2.114(4)	3	2.113(6) 2.107-2.121(4)	3	2.03(5) 1.97-2.11(2)	3
91.1(1) ---	1	90.4(1) ---	1	90.6(4) ---	1
92.5(1) ---	1	93.2(1) ---	1	92.5(5) ---	1
91.9(2) 91.7-92.0(1)	2	91.9(2) 91.7-92.0(1)	2	92.7(4) 92.5-92.9(5)	2

Table 11. Continued.

Category	$\alpha\text{-Mo}_2(\text{O}_2\text{CH})_4$		$\beta\text{-Mo}_2(\text{O}_2\text{CH})_4$	
<u>Angle, degrees</u>	<u>Average and Range</u>	<u>No. of Values</u>	<u>Average and Range</u>	<u>No. of Values</u>
Mo-O(b)-C	119.5(7) 119-120(1)	2	117.1(2) 116.9-117.3(4)	3
Mo-O(nb)-C	116.3(6) 114-117(1)	6	116.1(2) 115.0-116.8(5)	9
O-C-O(b)	120(2) ---	1 ^k	123.3(4) 122.8-123.7(7)	3
O-C-O(nb)	122(2) 120-124(2)	2	124.4(4) 124.1-124.4(7)	3

^kA second value was omitted from the original paper.

$\gamma\text{-Mo}_2(\text{O}_2\text{CH})_4$		$\text{Mo}_2(\text{O}_2\text{CCH}_3)_4$		$\text{Mo}_2(\text{O}_2\text{CCF}_3)_4$	
<u>Average and Range</u>	<u>No. of Values</u>	<u>Average and Range</u>	<u>No. of Values</u>	<u>Average and Range</u>	<u>No. of Values</u>
116.8(4) ---	1	118.5(4) ---	1	118(2) ---	1
116.4(2) 116.2-116.5(4)	3	117.2(2) 117.1-117.3(4)	3	114(1) 112-117(2)	3
123.1(6) ---	1	120.8(5) ---	1	123(2) ---	1
123.7(6) ---	1	121.8(6) ---	1	129(2) ---	1





 angle has become smaller
 angle has become larger

Figure 15. Diagram showing the observed effects of axial coordination (some ligands are omitted for clarity). All atoms shown lie approximately in the plane of the paper

One must then inquire why the parallelogram does not distort to further reduce the oxygen repulsions. Distortion to a rectangle, for example, would produce a diagonal distance of 3.45 Å which should minimize O-O and Mo-Mo contacts. The answer is evident when the orbital geometries at the Mo and O atoms are considered. The axial interaction involves the Mo-Mo σ and σ^* orbitals, which extend beyond the Mo atoms along the Mo-Mo quadruple bond axis. The O lone pair is directed $\sim 120^\circ$ away from the intramolecular Mo-O and O-C bonds. Figure 16 illustrates the axial interaction involving these Mo and O orbitals. An important fact is evident from the illustration: the parallelogram structure must be adopted to produce good orbital overlap. The observed Mo-Mo-O axial angle of $\sim 160^\circ$ is misleading since the interaction occurs away from the Mo-O axis as a bent "banana" bond.

The differences between the polymorphic forms of the formate complex (in terms of distances and angles) will be considered here. Note in Table 11 that a few trends appear when considering these forms. While the Mo-Mo-O(nb) angle does not change, the Mo-Mo-O(b) angle gets larger, and the Mo-Mo-O(adj) angle gets smaller from the α -, to the β -, then to the γ -form. Put another way, from the α -, to the β -, to the γ -form there is a narrowing of the range covered by the two extreme Mo-Mo-O angles labelled (nb) and (adj). The implication is that the axial coordination

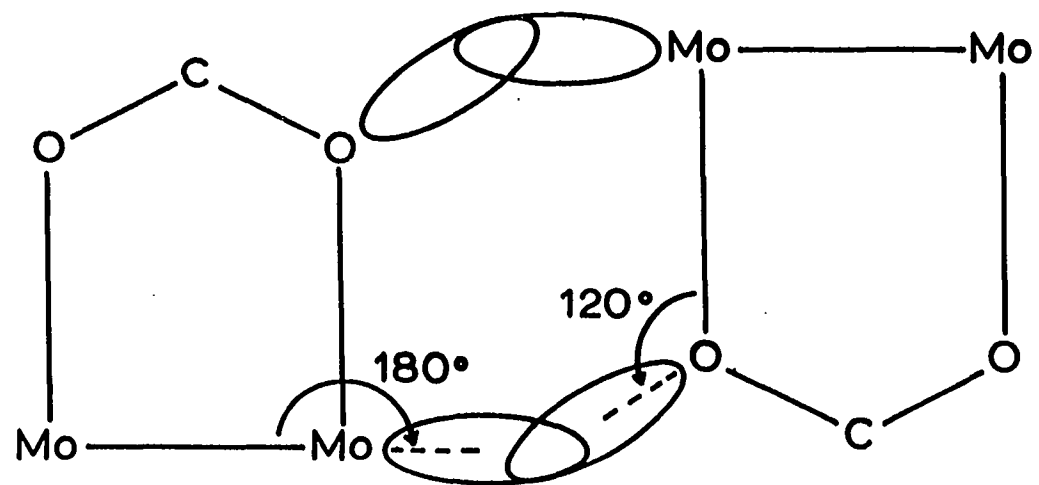


Figure 16. Diagram of the Mo-O axial interaction showing orbital geometries

has decreasing influence (produced by decreasing bond strength) in the order $\alpha > \beta > \gamma$. This is also reflected in the Mo-O(b)-C angle, which appears to follow a similar trend, though perhaps not significantly.

Further support for this conclusion is found in Table 12. Note that the gross features of the intramolecular bonds are virtually identical for the three polymorphs (as reflected by averaged values). However, variations in the intermolecular bonding are evident. Furthermore, for each type of intermolecular distance or angle listed, one of the extreme values (maximum or minimum) is found in γ -Mo₂(O₂CH)₄. It is apparent that the γ -form contains the weakest axial bonds, and that the α -form contains the strongest ones. Considering β_1 and β_2 molecules separately, we observe definite trends in the O-O distances and Mo-O-Mo(axial) angles. The Mo-O(axial) distances are indistinguishable between α , β_1 , and β_2 molecules, and the Mo-Mo-O(axial) angles are likewise identical in the α and β_2 cases. Note, however, that the set of Mo-O(axial) distances and Mo-Mo-O(axial) angles do not contradict the other two trends. It appears that the O-O distances and Mo-O-Mo(axial) angles are more sensitive indicators of differences in the metal-axial ligand bond strength. The data suggest the order $\gamma < \beta_1 < \beta_2 < \alpha$ in Mo---O bond strength.

Table 12. Comparison of interatomic distances and angles in the polymorphs of $\text{Mo}_2(\text{O}_2\text{CH})_4^a$

	α^b	β_1	β_2	β	γ
<u>Intramolecular</u>					
			<u>Distances, Å</u>		
Mo-Mo	2.091(2) ^c	2.093(1) ^c	2.0916(9) ^c	2.0923(7)	2.0919(8) ^c
O-C	1.29(1)	1.261(5)	1.269(4)	1.259(3)	1.264(4)
C-H	0.97	0.96(6)	1.07(5)	1.03(4)	1.01(6)
			<u>Angles, degrees</u>		
O-Mo-O	90.0(4)	90.0(3)	89.9(3)	89.9(2)	90.0(3)
O-Mo-O	175.8(5)	176.4(1)	176.4(2)	176.4(1)	176.4(1)
O-C-H	119 ^d	112(4)	114(3)	113(2)	116(4)
O-C-H	---	124(4)	122(3)	123(2)	120(4)
<u>Intermolecular</u>					
			<u>Distances, Å</u>		
Mo-O(axial)	2.645(8)	2.639(5)	2.641(4)	2.640(3)	2.701(3) ^c
O-O ^e	2.743	2.816	2.793	2.805	2.924

		<u>Angles, degrees</u>			
Mo-O-Mo(axial)	110.8(4)	108.6(2)	109.4(1)	109.0(2)	106.6(2) ^c
Mo-Mo-O(axial)	159.2(2)	161.9(2)	159.25(7)	160.6(1)	164.45(9) ^c

^aAveraged values except where denoted otherwise.

^bReference 1.

^cSingle value.

^dHydrogen positions were not refined.

^eRepresents a repulsive intermolecular contact.

The relation of the intermolecular distances and angles to the axial bond strength needs clarification, however. The inverse relationship between the Mo---O distance and bond strength needs no explanation. Weakening of the Mo---O bonds will cause the O-O distance to lengthen due to relaxation and decreased strain of the Mo-O-Mo-O parallelogram. The Mo-Mo-O(axial) and Mo-O-Mo(axial) angles approach 180° and 90° , respectively. These two values represent a situation of low axial Mo-O orbital overlap.

The structure of $\text{Mo}_2(\text{O}_2\text{CH})_4 \cdot \text{KCl}$ consists of $\text{Mo}_2(\text{O}_2\text{CH})_4$ molecules bridged by chloride ions with potassium ions present as counter ions (40, 60). Two crystallographically independent molecules are present, each of which possesses inversion symmetry. They are centered at special positions $0,0,0$ and $\frac{1}{2}, \frac{1}{2}, \frac{1}{2}$. The independence of these two sites is exhibited in the Mo-Mo distances and Mo-Mo-Cl angles of $2.109(2) \text{ \AA}$, $2.848(2) \text{ \AA}$, and $169.6(1)^\circ$ for site 1 and $2.102(1) \text{ \AA}$, $2.880(2) \text{ \AA}$, and $174.94(7)^\circ$ for site 2. Each chloride ion asymmetrically bridges two non-equivalent dimolybdenum tetraformate molecules, as Figure 17 illustrates. The structure thus contains a system of zigzag chains of alternating chloride ions and dimolybdenum tetraformate molecules. This type of structure is analogous to the zigzag chains in $\text{Ru}_2(\text{O}_2\text{CC}_3\text{H}_7)_4\text{Cl}$, where the chloride ions bridge

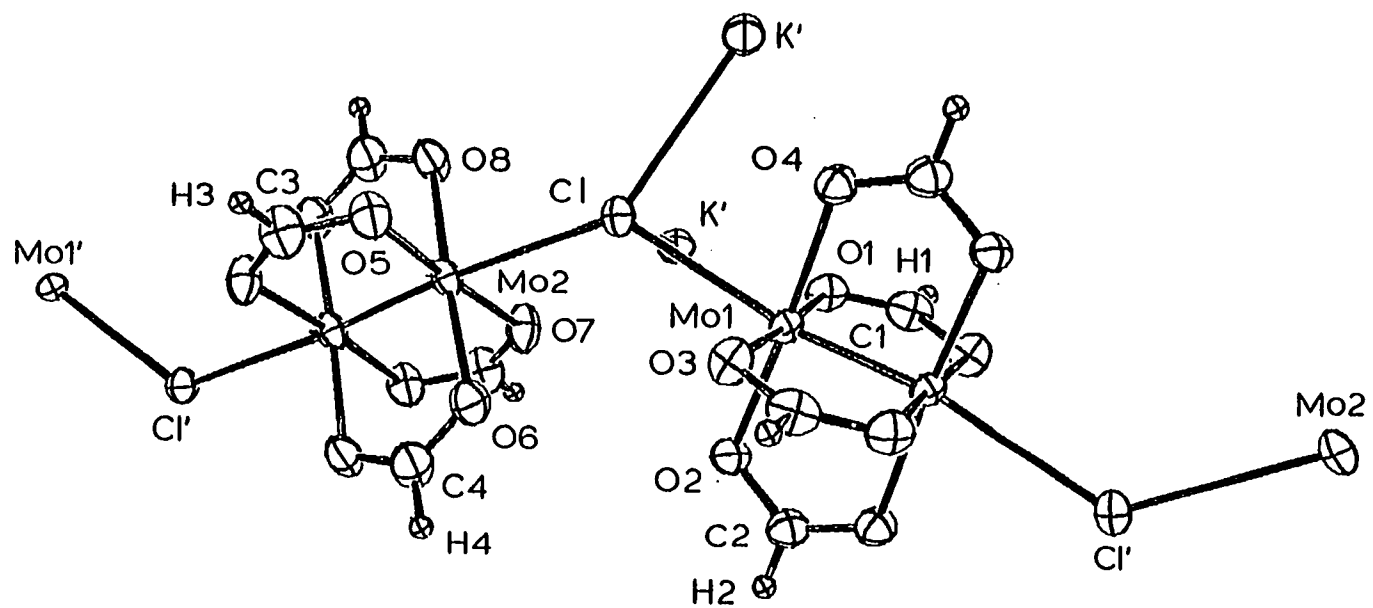


Figure 17. The molecular structure of $\text{Mo}_2(\text{O}_2\text{CH})_4 \cdot \text{KCl}$

symmetrically, however. This structure appears to be the only example of a metal carboxylate dimer with an asymmetric bridging chloride ion.

The K-Cl distances of 3.096(3) Å and 3.260(3) Å and K-O distances of ranging from 2.73 Å to 2.91 Å implies substantial potassium interaction with the oxygen atoms and chloride ions. It is thus possible that the potassium ion produces the assymetry in the chloride bridging.

The interatomic distances and angles are essentially the same for the two sites, except for the Mo-Mo and Mo-Cl distances, and the Mo-Mo-Cl angles. The differences in Mo-Mo and Mo-L_{axial} distances between the two sites and between Mo₂(O₂CH)₄·KCl and α-Mo₂(O₂CH)₄ show a slight lengthening (weakening) of the Mo-Mo bond with increasing axial coordination. The Mo-Mo bond is weaker in the KCl complex than in the α-polymorph as shown by the Mo-Mo bond length of 2.091(2) Å in the α-form and corresponding bond lengths 2.109(2) Å. Molecular volumes (V/Z) of α-Mo₂(O₂CH)₄ and KCl are additive to yield almost exactly the molecular volume of Mo₂(O₂CH)₄·KCl (218.2 + 61.9 = 280.1 ~ 280.4, all in Å³). This seems to imply that the Mo-Cl interactions are nonetheless weak ones.

Crystal Optics

The relevant details of the crystal optics will be presented here for the polymorphic forms of $\text{Mo}_2(\text{O}_2\text{CH})_4$, and then for $\text{Mo}_2(\text{O}_2\text{CH})_4 \cdot \text{KCl}$. Crystals of dimolybdenum tetraformate invariably exhibited an extinction axis coincident with the needle or stacking ($\sim 5.5 \text{ \AA}$) axis, within the experimental uncertainty of $\pm 2^\circ$. Crystallographic indexing confirmed that $\alpha\text{-Mo}_2(\text{O}_2\text{CH})_4$ crystals permitted spectroscopic study of the 010 faces. For convenience, all vector calculations were performed in an orthogonal coordinate system with unit direction vectors \hat{i} , \hat{j} , and \hat{k} . For the orthorhombic crystal system, this is trivial if we define $\hat{i} = \hat{a}$, $\hat{j} = \hat{b}$, and $\hat{k} = \hat{c}$, where \hat{a} , \hat{b} , and \hat{c} are unit direction vectors along the crystallographic axes. Any vector in the fractional coordinates x, y, z in the α -polymorph crystal system could thus be expressed by

$$\underline{v} = xa\hat{i} + yb\hat{j} + zc\hat{k}$$

where a , b , and c are the unit cell axis lengths. The molecular z axis vector was defined along the Mo-Mo bond and found to be 33.4° away from \hat{c} . For extinctions along \hat{a} and \hat{c} (\hat{i} and \hat{k}), the expected polarization ratio I_c/I_a is 4.3 for a molecular z -polarized transition, and 0.36 for a molecular x, y -polarized transition.

In crystals where the unit cell contains symmetry-equivalent molecules, exciton bands of states for these molecules interact to produce Davydov states. The resultant

Davydov states have characteristic symmetry properties and are subject to polarization effects. Selection rules for transitions to these Davydov states may be derived from the known crystal structure and crystal optics. The results will be presented for $\alpha\text{-Mo}_2(\text{O}_2\text{CH})_4$; however, the entire analysis is detailed for $\beta\text{-Mo}_2(\text{O}_2\text{CH})_4$ in Appendix C. For a transition occurring in molecule 1 (there are four equivalent molecules), the transition moment is given by $\mu_{\nu 1} = \langle \phi_1' | \mu_1 | \phi_1^{\circ} \rangle$, where ϕ_1° and ϕ_1' are the ground and excited state wavefunctions and μ_1 is the electric dipole operator for molecule 1. Transition moments $\mu_{\nu 2}$, $\mu_{\nu 3}$, and $\mu_{\nu 4}$ are similarly defined for the other molecules. The four transition moments may be expressed as the following four vectors, which are equivalent by the crystallographic symmetry:

$$\mu_{\nu 1} = x\hat{a} + y\hat{b} + z\hat{c}$$

$$\mu_{\nu 2} = -x\hat{a} - y\hat{b} + z\hat{c}$$

$$\mu_{\nu 3} = x\hat{a} - y\hat{b} - z\hat{c}$$

$$\mu_{\nu 4} = -x\hat{a} + y\hat{b} - z\hat{c}.$$

Transitions to four Davydov states have the transition moments

$$\mu_{\nu I} = 0$$

$$\mu_{\nu II} = 2\sqrt{N} z\hat{c}$$

$$\mu_{\nu III} = 2\sqrt{N} x\hat{a}$$

$$\mu_{\nu IV} = 2\sqrt{N} y\hat{b},$$

where N is the number of unit cells in the crystal. The \sqrt{N} factor arises from normalization of the exciton wavefunction,

and may be ignored for our purposes. For extinctions along \hat{a} and \hat{c} , only one transition moment is allowed polarized in each of these directions. These transitions could occur at slightly different energies in the two directions. If such an energy difference is observed, it is referred to as a Davydov splitting.

Crystallographic indexing of two $\beta\text{-Mo}_2(\text{O}_2\text{CH})_4$ crystals indicated that the spectroscopic faces were the $0\bar{1}3$ faces. This was quite surprising, since experience with other inorganic compounds has shown that faces suitable for spectroscopy are usually principal faces (i.e., all indices are -1, 0, or 1). This is not unreasonable, however, on further consideration of the crystal structure. Figure 18 shows a view along the a axis of the β -polymorph unit cell (parallel projection). Lines are shown which represent the $0\bar{1}3$ planes. These planes pass approximately through the center of each molecule. Crystallographers have observed that the largest faces of a crystal frequently contain the highest density of atoms. This would then explain the $0\bar{1}3$ face of $\beta\text{-Mo}_2(\text{O}_2\text{CH})_4$.

For a vector expressed as $\underset{\sim}{v} = xa\hat{a} + yb\hat{b} = zc\hat{c}$ in the β -polymorph unit cell, the relations

$$\hat{a} = \hat{i}$$

$$\hat{b} = \hat{j}$$

$$\hat{c} = -0.0041888\hat{i} + 0.999999\hat{k}$$

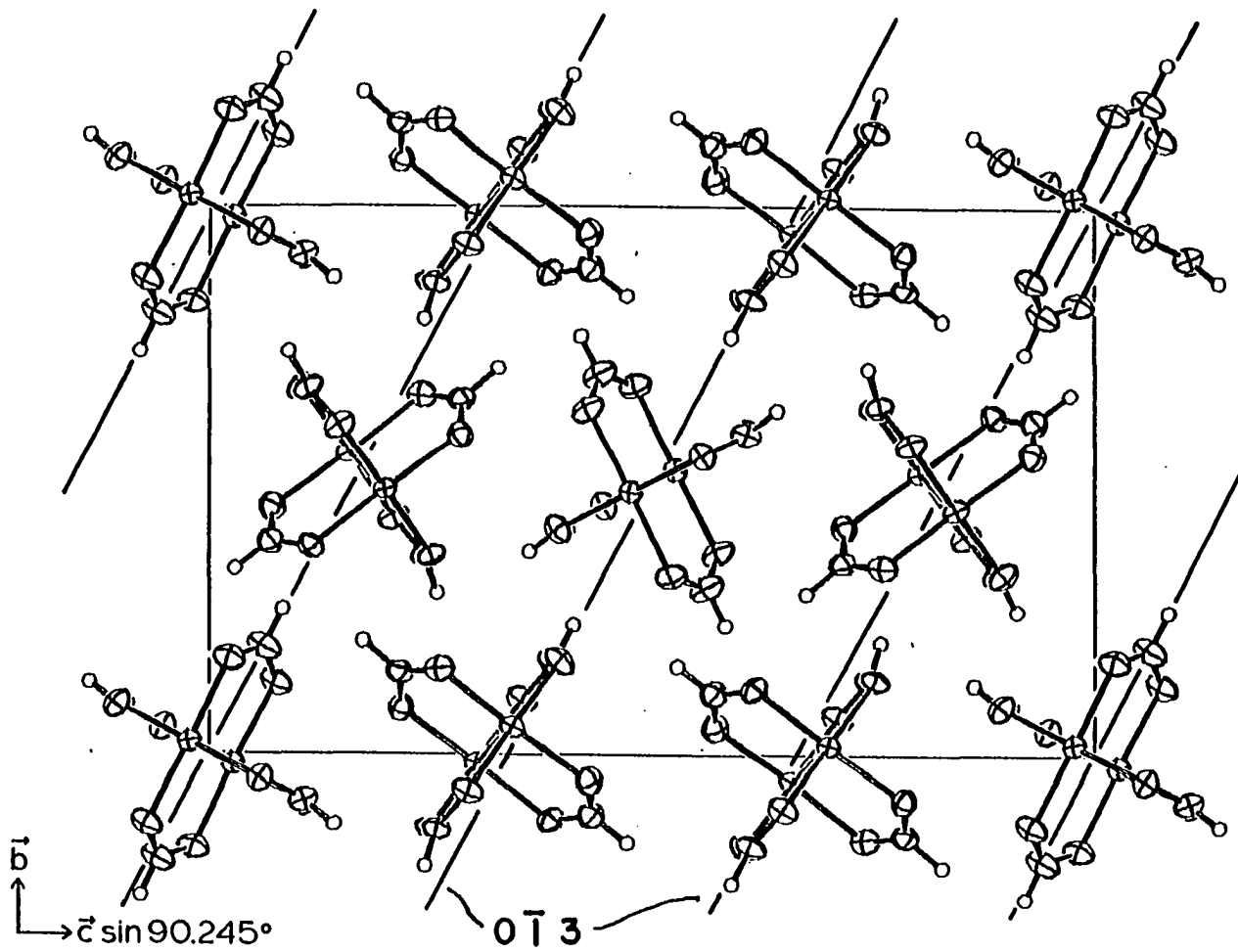


Figure 18. A view of $\beta\text{-Mo}_2(\text{O}_2\text{CH})_4$ showing $0\bar{1}3$ lattice planes

were used to transform it into an orthogonal system. Molecular \hat{z} axis vectors were defined along the Mo-Mo bonds and represented \hat{z} -polarized transition moments in the ideal case. These are listed below:

$$\hat{z}_1 = 0.84250\hat{i} - 0.23600\hat{j} + 0.48425\hat{k}$$

$$\hat{z}_2 = 0.84250\hat{i} + 0.23600\hat{j} + 0.48425\hat{k} \text{ (special positions)}$$

$$\hat{z}_3 = -0.83492\hat{i} + 0.39640\hat{j} + 0.38180\hat{k}$$

$$\hat{z}_4 = 0.83492\hat{i} - 0.39640\hat{j} - 0.38180\hat{k}$$

$$\hat{z}_5 = 0.83492\hat{i} + 0.39640\hat{j} - 0.38180\hat{k}$$

$$\hat{z}_6 = -0.83492\hat{i} - 0.39640\hat{j} + 0.38180\hat{k} \text{ (general positions).}$$

Wavelength-dependent extinction directions are possible for a monoclinic crystal face which does not contain the \hat{b} axis. (The $0\bar{1}3$ face contains \hat{a} , but does not contain \hat{b} .) However, crystals of $\beta\text{-Mo}_2(\text{O}_2\text{CH})_4$ gave no evidence of wavelength-dependent extinctions. The observed crystal extinction directions are given by:

$$\hat{E}x_1 = \hat{i} \quad (\parallel \text{ stacking axis})$$

$$\hat{E}x_2 = -0.88158\hat{j} - 0.47203\hat{k} \quad (\perp \text{ stacking axis}).$$

The following expected polarization ratios (I_1/I_2) were calculated for $\beta\text{-Mo}_2(\text{O}_2\text{CH})_4$:

special positions - \hat{z}	8.81
special positions - \hat{x}, \hat{y}	0.316
general positions - \hat{z}	4.48
general positions - \hat{x}, \hat{y}	0.359.

Treatment of the Davydov states in $\beta\text{-Mo}_2(\text{O}_2\text{CH})_4$ is presented in Appendix C. The results will be discussed here. For the special positions, $\mu_{\nu I} = \sqrt{2N} (x\hat{a} + z\hat{c})$ and $\mu_{\nu II} = \sqrt{2N} (y\hat{b})$. These were put into orthogonal coordinates and dotted into the vectors $\hat{E}x_1$ and $\hat{E}x_2$. These results are shown below:

$$\mu_{\nu I} \cdot \hat{E}x_1 = \sqrt{2N}(x - 0.0041888z)$$

$$\mu_{\nu I} \cdot \hat{E}x_2 = -\sqrt{2N}(0.47203z)$$

$$\mu_{\nu II} \cdot \hat{E}x_1 = 0$$

$$\mu_{\nu II} \cdot \hat{E}x_2 = -\sqrt{2N}(0.88158y).$$

This shows that $\hat{E}x_1$ will show only $\mu_{\nu I}$, while $\hat{E}x_2$ can show both $\mu_{\nu I}$ and $\mu_{\nu II}$.

For the general positions (site 2), the following Davydov transition moments result:

$$\mu_{III} = 0$$

$$\mu_{IV} = 0$$

$$\mu_V = 2\sqrt{N} y\hat{b}$$

$$\mu_{VI} = 2\sqrt{N} (x\hat{a} + z\hat{c}).$$

Thus, we see that the polarization properties of the Davydov transition for site 2 will be the same as those obtained for site 1. The extinction $\hat{E}x_1$ will allow $\mu_{\nu VI}$, and $\hat{E}x_2$ will allow both $\mu_{\nu V}$ and $\mu_{\nu VI}$.

Crystals of $\gamma\text{-Mo}_2(\text{O}_2\text{CH})_4$ were found to have $1\bar{1}0$ as the spectroscopic face. No evidence was found for wavelength dependent extinctions. The following relationships were used

to transform vectors defined in the crystallographic system to orthogonal coordinates:

$$\hat{a} = 0.93445\hat{i} - 0.35609\hat{k}$$

$$\hat{b} = \hat{j}$$

$$\hat{c} = \hat{k}.$$

The following vectors represented ideal case z transition moments for the two molecules:

$$\hat{z}_1 = 0.07490\hat{i} + 0.51023\hat{j} - 0.85677\hat{k}$$

$$\hat{z}_2 = 0.07490\hat{i} - 0.51023\hat{j} - 0.85677\hat{k}.$$

The observed extinctions were represented by the following vectors:

$$\hat{E}x_1 = \hat{k}$$

$$\hat{E}x_2 = -0.55246\hat{i} - 0.83354\hat{j}.$$

Note that, for the three polymorphs, $\hat{E}x_1$ was consistently taken as the extinction parallel to the needle axis and $\hat{E}x_2$ was the extinction perpendicular to that axis. The expected polarization ratios I_1/I_2 were calculated to be 4.0 for z polarization and 0.33 for x, y polarization.

Transitions to the two equivalent molecules in the γ -form result in the Davydov transition moments

$$\mu_{\sim I} = \sqrt{2N} (x\hat{a} + z\hat{c}) \text{ and}$$

$$\mu_{\sim II} = \sqrt{2N} (y\hat{b}), \text{ or}$$

$$\mu_{\sim I} = \sqrt{2N} (0.93445x\hat{i} + (z - 0.35609x)\hat{k}) \text{ and}$$

$$\mu_{\sim II} = \sqrt{2N} (y\hat{j})$$

in orthogonal coordinates. The following results are obtained when we take dot products of the transition moments with the extinction vectors:

$$\mu_{\nu I} \cdot \hat{E}x_1 = \sqrt{2N} (z - 0.35609x)$$

$$\mu_{\nu I} \cdot \hat{E}x_2 = -\sqrt{2N} (0.51625x)$$

$$\mu_{\nu II} \cdot \hat{E}x_1 = 0$$

$$\mu_{\nu II} \cdot \hat{E}x_2 = -\sqrt{2N} (0.83354y).$$

Thus, we find that $\hat{E}x_1$ should show only $\mu_{\nu I}$, while $\hat{E}x_2$ should show both $\mu_{\nu I}$ and $\mu_{\nu II}$.

Three separate attempts were made to index the same Group II (see Preparation) crystal. None of the attempts was without difficulty and ambiguity. Apparently, the difficulties were due to the crystal thinness (<10 μm), which resulted in weak reflections, and twinning or intergrowth of more than one crystal. All of the attempts gave evidence of a unit cell approximating that of the α -polymorph, but with the b axis doubled in some cases. For this unit cell, the face was identified as 010, just as in the α -polymorph. In the two diffractometer attempts (the other used precession photographs), this cell was obtained only with a subset (6 reflections) of the observable reflections (19 reflections). Other subsets containing 6-8 reflections would indicate other unit cells. The parameters obtained for many of these unit cells were undoubtedly in great error, since the diffractometer could not properly tune on

these weak reflections. In one case, however, a subset of reflections gave a unit cell resembling that of the γ -polymorph.

For $\text{Mo}_2(\text{O}_2\text{CH})_4 \cdot \text{KCl}$, the spectroscopic face was identified as $1\bar{1}0$. The crystal optics calculations proved more difficult for the triclinic crystal system. The \hat{c} axis is contained in the crystal face, and the extinction designated $\hat{E}x_1$ was found to lie 71° from it. No wavelength dependence was found for the extinction directions.

The following expressions relate the crystallographic coordinates to an orthogonal system:

$$\hat{a} = 0.94129\hat{i} - 0.33759\hat{k}$$

$$\hat{b} = 0.058049\hat{i} + 0.99828\hat{j} + 0.0083775\hat{k}$$

$$\hat{c} = \hat{k}.$$

Molecular \hat{z} transition moments were represented ideally by the vectors:

$$\hat{z}_1 = 0.80812\hat{i} + 0.155373\hat{j} + 0.20078\hat{k} \text{ and}$$

$$\hat{z}_2 = 0.13613\hat{i} + 0.92251\hat{j} + 0.36116\hat{k}.$$

The extinctions in the $1\bar{1}0$ face are given by

$$\hat{E}x_1 = 0.58453\hat{i} + 0.74319\hat{j} + 0.32557\hat{k} \text{ and}$$

$$\hat{E}x_2 = -0.20127\hat{i} - 0.25590\hat{j} + 0.94552.$$

For molecular \hat{z} polarization, we expect $I_1/I_2 = 87.5$ and for \hat{x}, \hat{y} polarization, we expect $I_1/I_2 = 0.1614$.

The molecular chains in the $\text{Mo}_2(\text{O}_2\text{CH})_4 \cdot \text{KCl}$ unit cell run along the body diagonal from 0,0,0 to 1,1,1. On considering

the orientation of the body diagonal in relation to the extinction directions, it was found that the body diagonal lies in the $1\bar{1}0$ face and that it was only 2.3° away from $\hat{E}x_1$. This result was deemed more than coincidental. The logical conclusion is that the body diagonal is the actual extinction direction, determined experimentally with an error of $\sim 2^\circ$. This is unexpected, though perhaps not surprising. The three polymorphic forms of the formate complex and the acetate and trifluoroacetate complexes each has the chain stacking axis in the spectroscopic face and an extinction is observed close to that axis. (The acetate complex had a second spectroscopic face, however, with an extinction $\sim 12^\circ$ from the stacking axis.)

Crystal Spectra

As stated in the Introduction, Martin et al. found three strong progressions in the polarized spectra of $\alpha\text{-Mo}_2(\text{O}_2\text{CH})_4$ (25). These were later designated A, C, and E progressions, analogous to the major progressions in the acetate complex (28). The C and E progression origins were found 400 cm^{-1} and 790 cm^{-1} above the A origin (identified as the band origin). Although weak progressions were mentioned, details of them in crystal spectra have not been discussed. They were included in the data of Trogler et al. (27, 61), taken from sublimed film spectra, but they were not discussed in any detail. We present now the details of the weak progressions observed in thicker

crystals of $\alpha\text{-Mo}_2(\text{O}_2\text{CH})_4$. Figure 19 shows the low-temperature polarized spectra obtained from a crystal $\sim 9 \mu\text{m}$ thick. Several weak progressions are evident, whose intensities are roughly one-fourth to one-half that of the A_0 line in the c polarization. Note in particular the lines at 21,990, 22,060 and 22,130 cm^{-1} . It is clear that these display three different polarization behaviors which we can designate as strong \perp , weak \parallel , and weak \perp , respectively, in relation to the crystal needle axis, c . Other progressions are present which are not obvious in the Figure.

The vibrational details are given in Table 13 as obtained from spectra of a crystal estimated to be 22 μm thick. Due to wavelength imprecision, the $\bar{\nu}$ values given in the Table are $\sim 24 \text{ cm}^{-1}$ higher than those shown on Figure 19. The origins of several progressions are listed, though the higher energy members were obscured for most of them. The separation of progression members is $\sim 353 \text{ cm}^{-1}$, presumably representing the Mo-Mo stretch in the excited state. The hot band indicates a ground state frequency of $\sim 378 \text{ cm}^{-1}$. The A through E labels given in the Table are used by analogy to the progressions observed in the acetate complex (28).

The indicated ground state frequency of 378 cm^{-1} is slightly low compared to the Raman frequency of the Mo-Mo stretch, measured at 406 cm^{-1} (1). This may result from difficulty in identifying the maximum in the weak, broad hot band. However, the Raman spectrum also shows Mo-O stretches at 393 and 371 cm^{-1} , one of which might

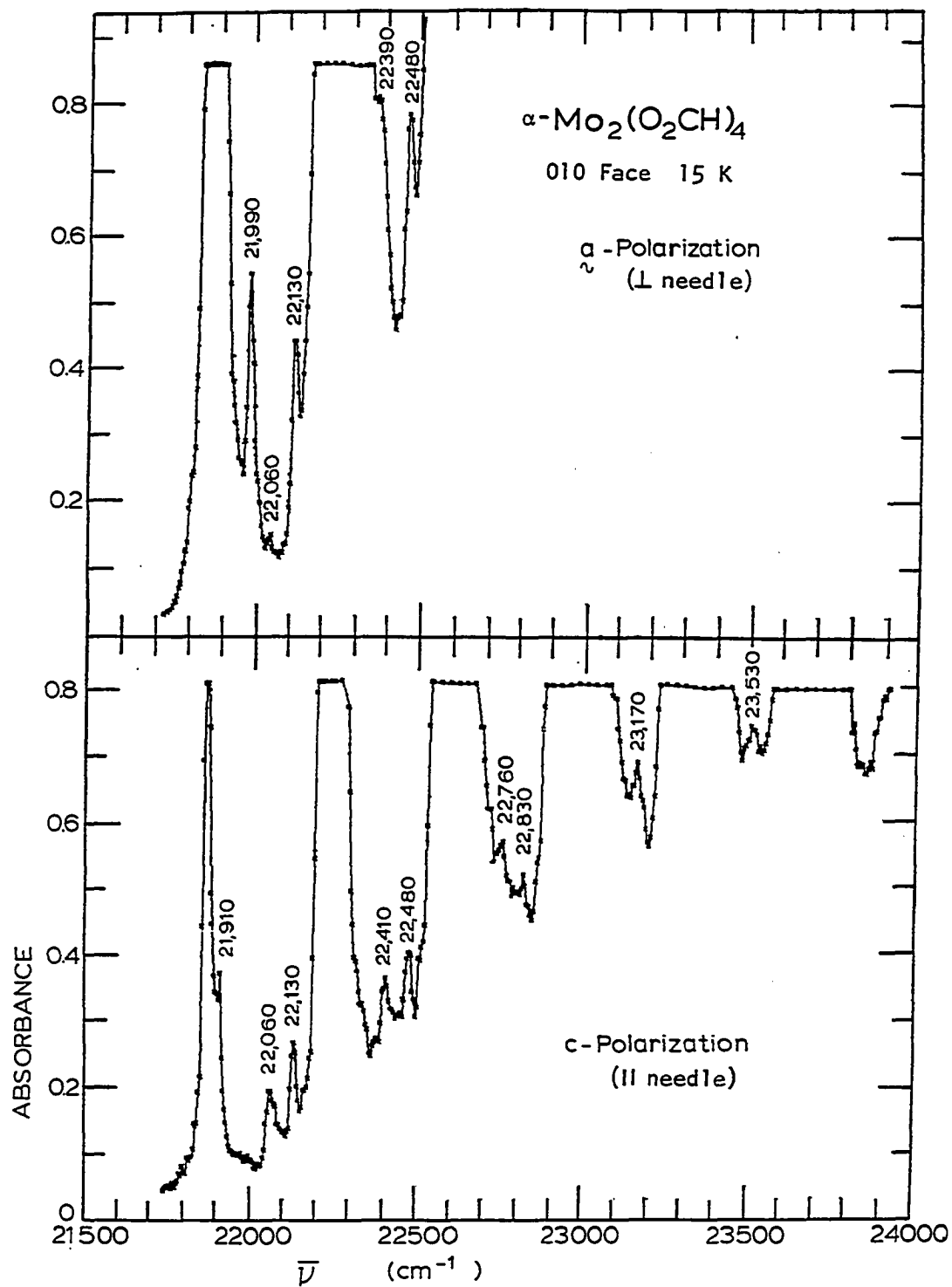


Figure 19. Polarized spectra of $\alpha\text{-Mo}_2(\text{O}_2\text{CH})_4$ showing the weak features

Table 13. Weak vibrational details of the low energy absorption band in crystals of $\alpha\text{-Mo}_2(\text{O}_2\text{CH})_4$ at 17 K

Assignment	$\bar{\nu}^a$, cm^{-1}	$\Delta\bar{\nu}(0-0)^b$, cm^{-1}	I_{\perp}/I_{\parallel}	$\Delta\bar{\nu}(\text{progression})^c$
A ₋₁	21316 ^d	(-378)	~ 4	
A ₀	21894	0	est. 5.5 ^e	
a ₀	21911	17		
b ₀	21925	31		
c ₀	21951	58	2.6	
d ₀	21988	94	~ 3.5	
e ₀	22017	123	7.5	
B ₀	22085	191	0.80	
f ₀	22135	241		
C ₀	22153	259	1.9	
D ₀	22190	296	~ 2.2	
d ₁	22346			358
e ₁	22364			347
E ₀	22414	520	~ 3	
B ₁	22437			352
f ₁	22489			354
C ₁	22506			353

^aListed values are $\pm 15 \text{ cm}^{-1}$ for $\bar{\nu}$ and $\pm 5 \text{ cm}^{-1}$ for $\Delta\bar{\nu}$.

^bDifference of the progression origin frequency and the A₀ frequency.

^cFrequency separation from preceding member of progression.

^dHot band observed at temperatures above 80 K.

^eBased on polarization ratios measured in thinner crystals.

be assigned as A_{1g} . If the Mo-Mo and Mo-O vibrations are strongly coupled, the Mo-O vibration contains significant Mo-Mo character. Thus, the observed progression spacings could represent an Mo-O stretch in the excited state. The progression frequency of $\sim 353 \text{ cm}^{-1}$ is lower than those found in the trifluoroacetate and acetate complexes, which are 360 and 375 cm^{-1} , respectively. This does indicate that the electronic and/or vibrational wavefunctions involved in the transition in the α -formate complex could differ substantially from those of the other complexes.

The assignment made for C_0 and E_0 differs from that suggested for $\alpha\text{-Mo}_2(\text{O}_2\text{CH})_4$ by Martin and co-workers in the latter part of the acetate paper. The polarization behavior of A_0 , B_0 , and C_0 in the α -formate complex appears to closely approximate that in the acetate complex, though B_0 and C_0 are much weaker in the formate, in relation to A_0 . It was not possible to reliably determine the E_0 polarization ratio. On considering the Raman and infrared data reported for the formate, acetate, and trifluoroacetate complexes (1, 59, 62, 63), it appeared that the vibrational details in the electronic spectra might not differ as much as previously thought between the three compounds. A C_0 - A_0 separation of $\sim 400 \text{ cm}^{-1}$ for the formate seemed unlikely when compared to the separations of 275 and 255 cm^{-1} , respectively, for the acetate and trifluoroacetate complexes. The E_0 - A_0

separation of 790 cm^{-1} was viewed with like suspicion, compared with 545 and 511 cm^{-1} . The new assignments were made for B_0 and C_0 on the basis of their polarization behaviors and separations from A_0 . E_0 was assigned on the basis of its separation from A_0 , alone. These will be supported by spectra to follow.

The B_0 and C_0 progressions can be accounted for by Raman lines at 195 and 293 cm^{-1} in the ground state. There are many Raman lines in the region of $84 - 420\text{ cm}^{-1}$ to account for the observed progressions whose separation from A_0 falls into this range. However, there is no reported Raman or infrared line corresponding to the E_0-A_0 separation of $\sim 520\text{ cm}^{-1}$. Weak Raman lines at either 795 or 782 cm^{-1} , and at 420 cm^{-1} would correspond to vibrations exciting the 790 and 400 cm^{-1} progressions, respectively. These are, most likely, some type of deformation in the first case, and an Mo-O stretch in the second case.

The assignments suggested here are in agreement with the conclusion drawn from the acetate study, that the $\delta \rightarrow \delta^*$ transition is allowed with comparable intensity by both the electric dipole and vibronic mechanisms. In the formate complex, the C and E progressions occur with very low intensity, but different vibrations interact appropriately to produce the more intense vibronic progressions at 400 cm^{-1} and 790 cm^{-1} . The consistent dominance of the A progression, in relation to the others (which vary from complex to complex), may be taken as evidence that the A progression

represents the dipole-allowed component of the transition. Its intensity is thus not particularly sensitive to the nature of the ligand, in contrast to the vibronic components. Conclusions drawn concerning the orientation of the transition moment in the acetate complex also seem to apply here, since the observed A_0 polarization is opposite its expected behavior (that is, A_0 is stronger in $\hat{E}x_2$ than in $\hat{E}x_1$).

The polarized spectra of a crystal of $\alpha\text{-Mo}_2(\text{O}_2\text{CH})_4$ which was ~ 3 years old are shown in Figure 20. Although the spectra involve a thicker sample than the spectra of Martin et al. (reproduced in Figure 4), it appears that the two sets of spectra are consistent. None of the spectra displayed an observable Davydov splitting. Figure 21 shows the spectra of another crystal of the formate complex. Note in this figure that the lines at 21920 and 21935 cm^{-1} are more intense in relation to the line at 21900 cm^{-1} than in Figure 20. This crystal was obtained from the sublimation of ~ 1 year old $\alpha\text{-Mo}_2(\text{O}_2\text{CH})_4$ crystals and is designated as a Group I crystal (see Preparation). The $\alpha\text{-Mo}_2(\text{O}_2\text{CH})_4$ material was yellow-green (an indication of decomposition) before sublimation, but resulted in yellow sublimed crystals. The polarized spectra obtained from a Group II crystal from the same sublimation are shown in Figure 22. The low energy group at $\sim 21920 \text{ cm}^{-1}$ clearly shows three components having comparable intensities. The spectra of five such Group II

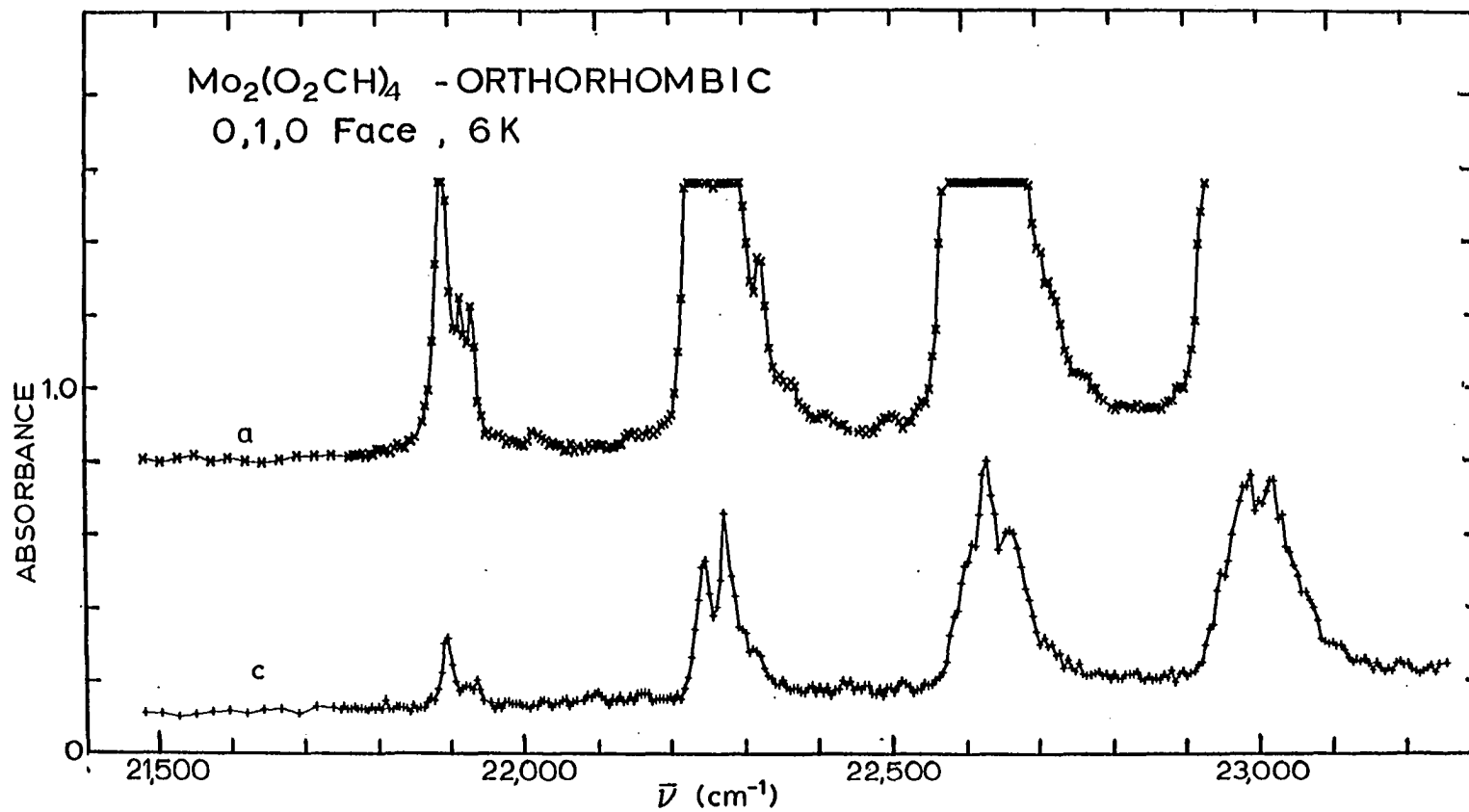


Figure 20. Polarized spectra of a crystal of $\alpha\text{-Mo}_2(\text{O}_2\text{CH})_4$. The crystal thickness was $\sim 9 \mu\text{m}$

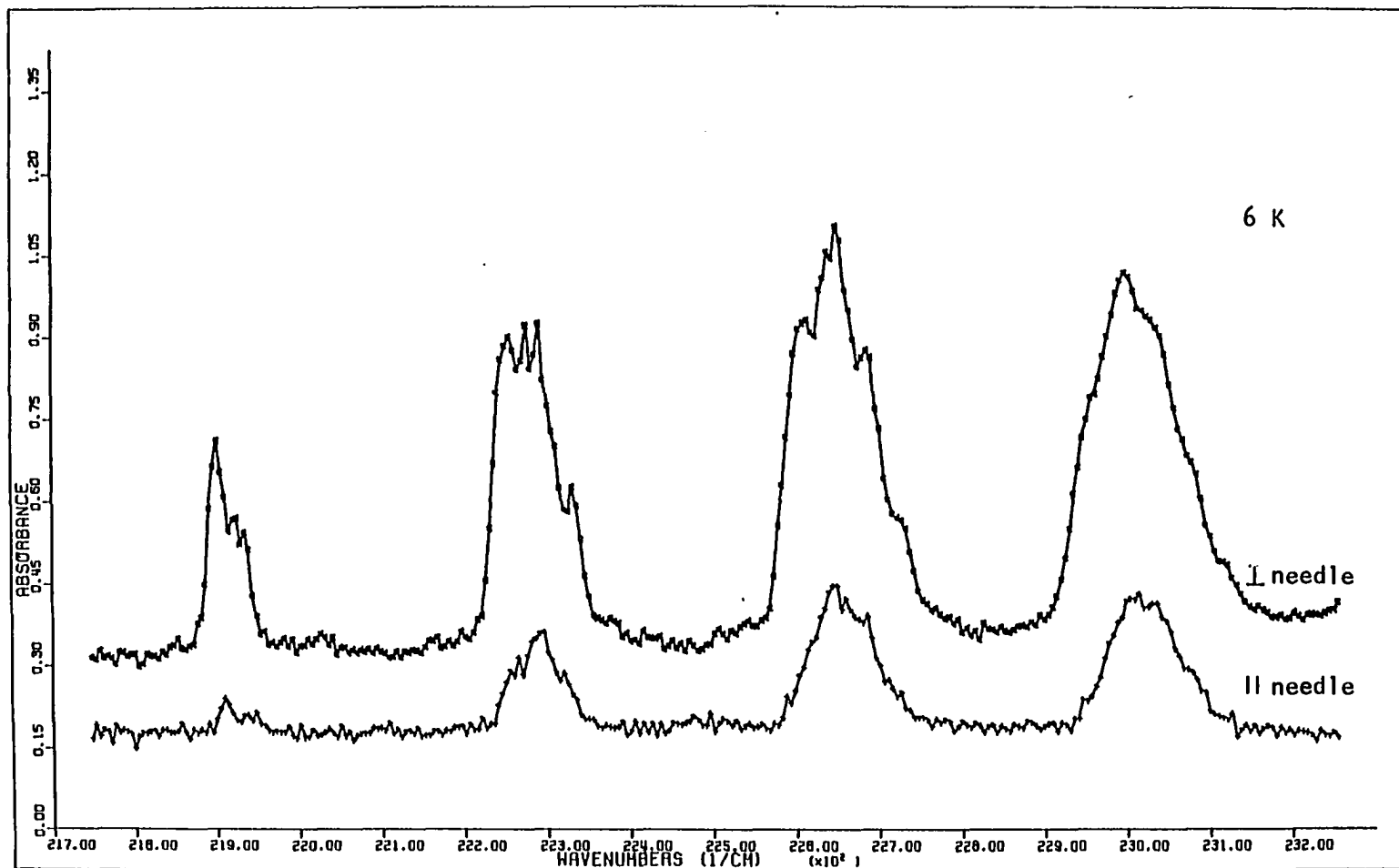


Figure 21. Polarized spectra of sublimed $\alpha\text{-Mo}_2(\text{O}_2\text{CH})_4$ (Group I crystals)

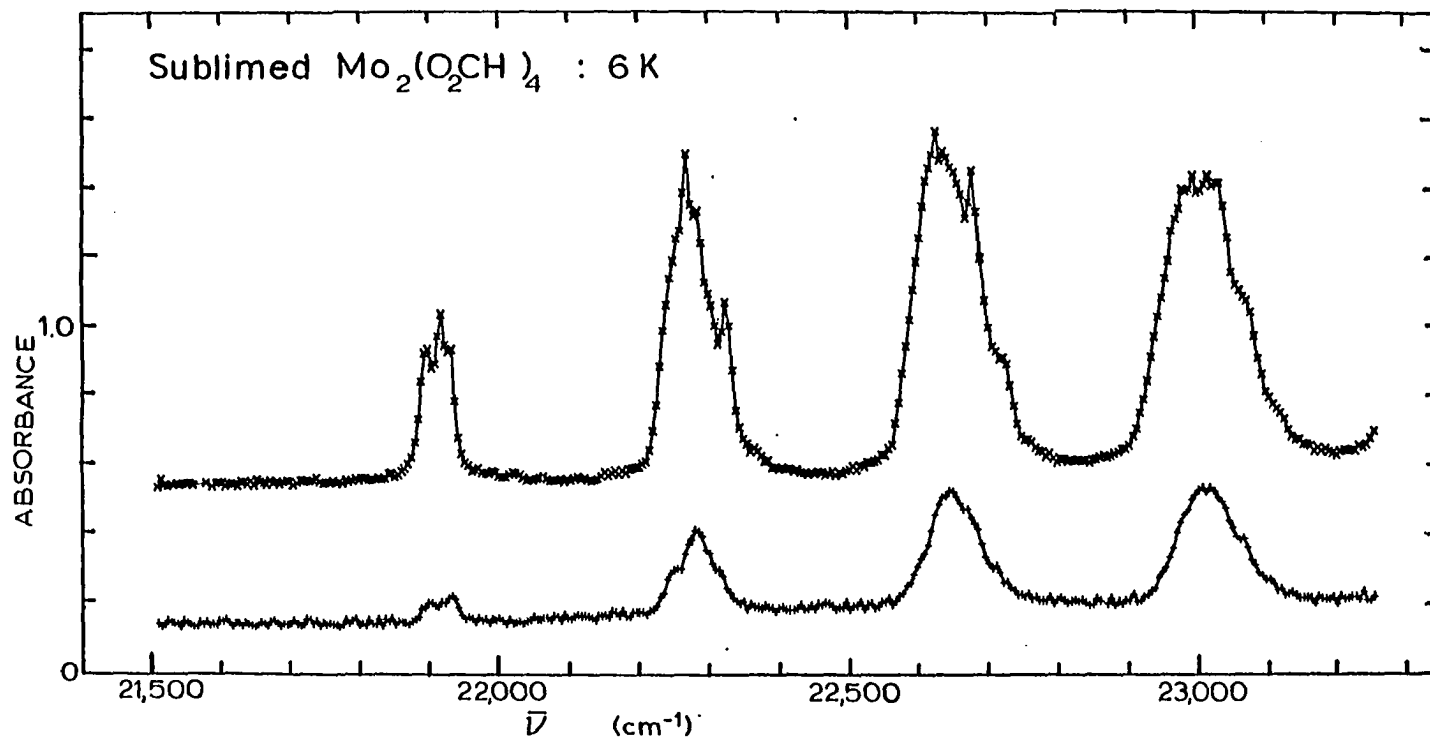


Figure 22. Polarized spectra of sublimed $\alpha\text{-Mo}_2(\text{O}_2\text{CH})_4$ (Group II crystals). The crystal thickness was $5.1 \mu\text{m}$

crystals were recorded. The intensity of the low energy component (presumably $\alpha\text{-Mo}_2(\text{O}_2\text{CH})_4$) relative to the other two was slightly different in two of the crystals. However, the intensities of the two components at 21920 and 21935 cm^{-1} relative to each other did not appear to vary in the crystals studied. It is evident from the Figure that the three components show slightly different polarization behavior. These two components appear to represent additional crystal sites of some type.

Table 14 gives the details of the crystal spectra of the Group II sublimed crystals. A_0 , A_0' , and A_0'' , respectively, represent the α -polymorph and the two unspecified crystal sites. It appears that only one e progression is present and it is assigned to $\alpha\text{-Mo}_2(\text{O}_2\text{CH})_4$. Note that the two strong vibronic progressions are labelled H and J. This allowed other progressions to be labelled as consistently as possible with the acetate spectra. The progressions labelled a and b in Table 13 can now be assigned as A' and A'' for the two crystal sites.

These sites were observed by Trogler et al. in sublimed films, but were not identified (27, 61). The sites are listed in their table of vibrational components, and the spectrum which they published (61) shows that they were only slightly less intense than $\alpha\text{-Mo}_2(\text{O}_2\text{CH})_4$. The data of Trogler et al. are listed in Table 15 with assignments. No clear assignments were made in the original paper. It is evident that their spectra are consistent with those obtained in this laboratory.

Table 14. Vibrational details in the crystal spectra of sublimed α - $\text{Mo}_2(\text{O}_2\text{CH})_4$ at 6 K showing additional crystal sites

Assignment	$\bar{\nu}^a$, cm^{-1}	$\Delta\bar{\nu}(0-0)^b$, cm^{-1}	I_{\perp}/I_{\parallel}	$\Delta\bar{\nu}(\text{progression})^c$, cm^{-1}	$\Delta\bar{\nu}(\text{site})^d$, cm^{-1}
A_{-1}	21468 ^e	(-428)			
A_0	21896		8.0		
A_0'	21914		9.4		18
A_0''	21928		5.0		14
c_0	21942	46			
c_0'	21957	43			15
c_0''	21971	45			14
e_0	22016	120			
C_0	22153	257			
C_0'	22169	255			16
C_0''	22185	259			16
A_1	22251			355	
A_1'	22269			355	18
$A_1'' + H_0$	22282	386			13
H_0'	22301	387			19

H_0''	22323	395	.16.7		22
e_1	22360			346	
A_2'	22625			356	
$A_2'' + H_1$	22639			357	14
H_1'	22660			359	21
$H_1'' + J_0$	22676	780		353	16
J_0''	22717	789			
	23004 ^f				
	23364 ^f			360	
	23724 ^f			360	
	24084 ^f			360	

^aListed values are $\pm 15 \text{ cm}^{-1}$ for $\bar{\nu}$ and $\pm 5 \text{ cm}^{-1}$ for $\Delta\bar{\nu}$.

^bDifference of the progression origin frequency and the A_0 frequency for a particular site.

^cFrequency separation from preceding member of progression.

^dFrequency separation from adjacent site, such as $\bar{\nu}(A_0') - \bar{\nu}(A_0)$ or $\bar{\nu}(A_0'') - \bar{\nu}(A_0')$.

^eHot band observed at 130 K.

^fCenter of a broad band of many unresolved components.

Table 15. Reported vibrational details in the spectra of sublimed films of $\alpha\text{-Mo}_2(\text{O}_2\text{CH})_4$ ^a

Assignment	$\bar{\nu}$, cm^{-1}	$\Delta\bar{\nu}(0-0)$, cm^{-1}	$\Delta\bar{\nu}(\text{progression})$, cm^{-1}
A ₋₁	21493	(-375) ^b	
A ₀	21868	0	
A ₀ '	21892	24	
A ₀ ''	21906	38	
e ₀	21995	127	
C ₀	22127	259	
D ₀	22163	295	
A ₁	22231		363
A ₁ '	22259		367
A ₁ ''	22280		374
d ₁	22305 ^c		
e ₁	22345		350
C ₁	22482		355
D ₁	22518		355
A ₂	22579		348
A ₂ '	22616		357
A ₂ ''	22653		373
e ₂	22700		355

^aReference 27.

^bHot band.

^cFirst member of progression not observed.

The evidence suggests that the two additional spectral components are due to a fourth polymorph of $\text{Mo}_2(\text{O}_2\text{CH})_4$, as yet unidentified. This accounts for the observation that the relative intensities of the two sites do not vary. The intensity differences between this polymorph and the α -polymorph would then be due to variations in crystal intergrowth along the crystal's needle axis. Since the needle axis cell dimensions are all $\sim 5.5 \text{ \AA}$ for the known polymorphs, it is logical to expect this to hold for the fourth polymorph. Two forms could conceivably grow and share this axis in common. Since this represents a crystal extinction, such a twinned crystal would appear single under the polarizing microscope. Different relative proportions of one polymorph to the other in the entire crystal would account for the differences in the observed spectral intensities.

It is impossible to rule out some sort of crystallographic defect to account for the spectral observations. Defects in the chain orientation and stacking can certainly occur. Any such defect would have to result in two spectral components, however, and explain the other observations. An additional polymorph seems to more readily account for all the observations.

Perhaps a bit more can be said about this polymorph, if it exists. It should have two independent crystallographic sites, to account for the two spectral components. It is likely to have slightly weaker axial Mo-O bonding (and thus stronger Mo-Mo

bonding), since A_0' and A_0'' occur at higher frequencies than A_0 . This latter claim will appear less speculative after the β - and γ - $\text{Mo}_2(\text{O}_2\text{CH})_4$ spectra are discussed. The polymorph will probably more closely resemble the α -form in terms of bonding parameters, than the other two forms.

The polarized crystal spectra of a crystal of β - $\text{Mo}_2(\text{O}_2\text{CH})_4$ are shown in Figure 23. A crystal site splitting of $\sim 25 \text{ cm}^{-1}$ is observed, but no Davydov splitting is seen. The lower energy component is found to lie 60 - 65 cm^{-1} higher in frequency than A_0 in the α -form. As in the previous set of spectra, the resulting complexity of the spectra makes assignment of individual components difficult beyond the first two major bands. The lower energy portion of Figure 23 is shown expanded in Figure 24. Figure 25 shows the spectra obtained from a thick crystal and some of the weak features are evident here.

Table 16 lists the vibrational components identified in spectra of β - $\text{Mo}_2(\text{O}_2\text{CH})_4$ crystals at 5 K. A weak feature is noted, about 75 cm^{-1} lower in frequency than A_0 . This feature is presumed to be due to an impurity or defect, likely resulting from decomposition of the crystals. This was demonstrated to be the case for similar weak features in the trifluoroacetate complex (29). The vibrational components of the $\delta \rightarrow \delta^*$ transition are assigned similarly to α - $\text{Mo}_2(\text{O}_2\text{CH})_4$, as given previously. The spectra of the two polymorphs are quite similar in terms

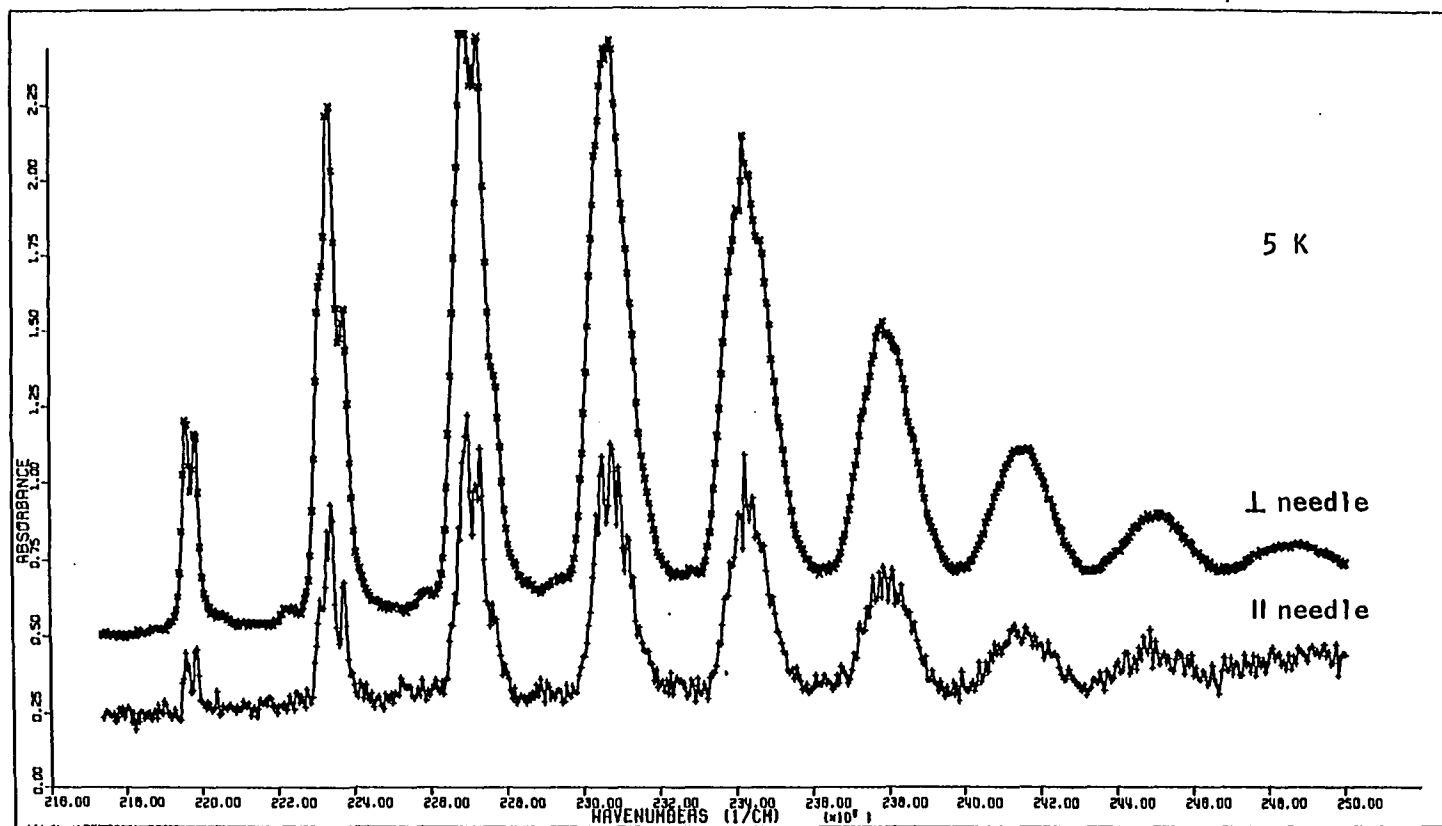


Figure 23. Polarized spectra of $\beta\text{-Mo}_2(\text{O}_2\text{CH})_4$

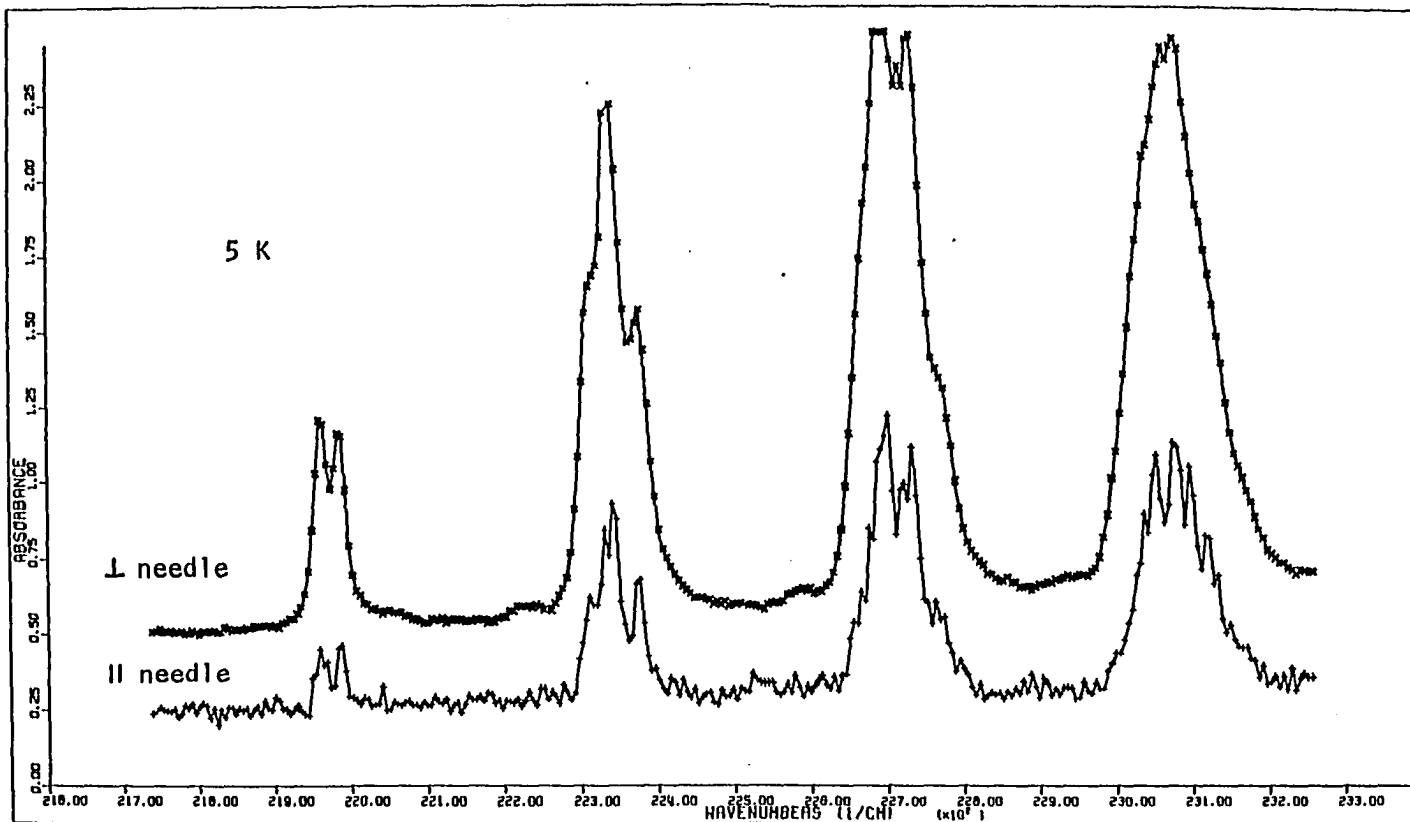


Figure 24. Scale-expanded spectra of $\beta\text{-Mo}_2(\text{O}_2\text{CH})_4$

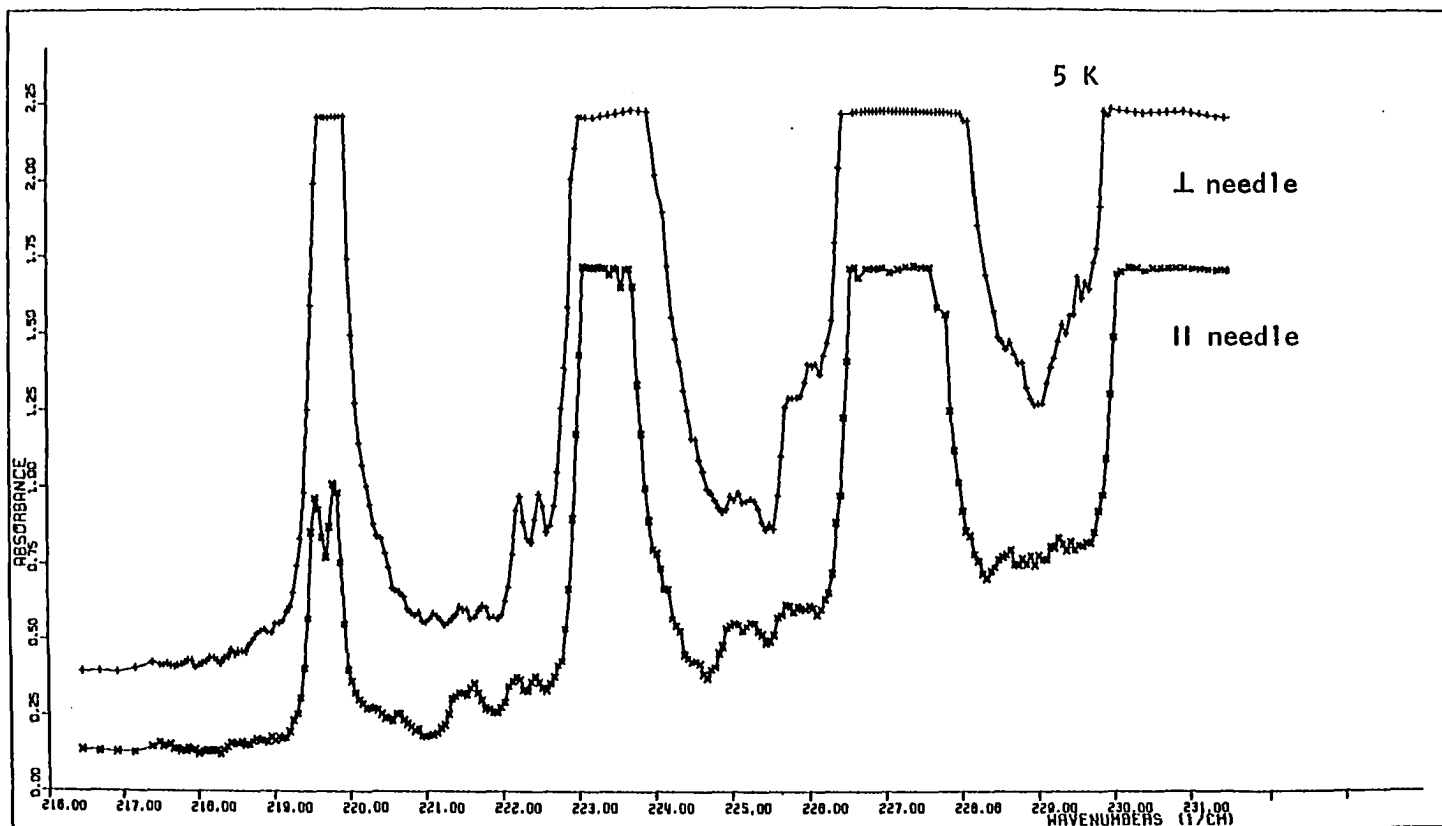


Figure 25. Polarized spectra of $\beta\text{-Mo}_2(\text{O}_2\text{CH})_4$, showing weak vibrational progressions. The crystal thickness was 36 μm

Table 16. Vibrational details in the crystal spectra of $\beta\text{-Mo}_2(\text{O}_2\text{CH})_4$ at 5 K

Assignment	$\bar{\nu}^a$, cm^{-1}	I_{\perp}/I_{\parallel}	$\Delta\bar{\nu}(0-0)^b$, cm^{-1}	$\Delta\bar{\nu}(\text{progression})^c$, cm^{-1}	$\Delta\bar{\nu}(\text{site})^d$, cm^{-1}
A_{-1}	21533 ^e		(-424)		
A_{-1}'	21561 ^e		(-421)		28
x	21882 ^f		(-75)		
A_0	21957	5.7			
A_0'	21982	5.2			25
d_0	22028		71		
d_0'	22054		72		26
e_0	22081		124		
e_0'	22104		122		23
B_0	22139	~ 0.5	182		
B_0'	22167		185		28
C_0	22214	~ 2.5	257		
C_0'	22242		260		
A_1	22316			359	
$A_1' + H_0$	22339				23

H ₀ '	22375	393		
e ₁	22432		351	
e ₁ '	22452		348	20
B ₁	22493		354	
B ₁ '	22515		348	22
C ₁	22569		355	
C ₁ '	22597		355	28
A ₂	22663			
A ₂ ' + H ₁	22694		355	31
H ₁ ' + J ₀	22727		352	
J ₀ '	22766	784		
G ₀ or G ₀ '	22822	865 or 840		

^aListed values are $\pm 15 \text{ cm}^{-1}$ for $\bar{\nu}$ and $\pm 5 \text{ cm}^{-1}$ for $\Delta\bar{\nu}$.

^bDifference of the progression origin frequency and the A₀ frequency for a particular site.

^cFrequency separation from preceding member of progression.

^dFrequency separation from adjacent site such as $\bar{\nu}(A_0') - \bar{\nu}(A_0)$.

^eObserved at temperatures above 80 K.

^fWeak transition attributed to a defect or impurity.

Table 16. Continued.

Assignment	$\bar{\nu}$, cm^{-1}	I_{\perp}/I_{\parallel}	$\Delta\bar{\nu}(0-0)$, cm^{-1}	$\Delta\bar{\nu}(\text{progression})$, cm^{-1}	$\Delta\bar{\nu}(\text{site})$, cm^{-1}
B ₂	22856			355	
C ₂	22924			355	
C ₂ '	22945			348	21
A ₃	23031			368	
A ₃ ' - H ₂	23049			355	
H ₂ ' - J ₁	23080			353	
J ₁ '	23114			348	
	23430 ^g			350	
	23795 ^g			365	
	24136 ^g			341	
	24498 ^g			362	
	24860 ^g			362	
X ₀	24265 ^h				
X ₁	not resolved			(294)	

X ₂	25853	(294)
X ₃	26178	325
X ₄	26469	291
X ₅	26788	319
X ₆	27115	327 (Av. = 308)

^gCenter of a broad band of many unresolved components.

^hFirst distinct component of a vibrational progression appearing at the beginning of an intense transition at higher energy.

of vibrational components and polarization behavior. However, e_0 and e_0' are either not as intense in the β -form as in the α -form, or they are not as highly polarized. It is conceivable that the allowing vibration of $\sim 125 \text{ cm}^{-1}$ is a phonon (lattice vibration), and thus differs in the two polymorphs. Different molecular orientations in the two forms might also account for the difference.

Though not shown in the figures, vibrational components appear above $\sim 25,000 \text{ cm}^{-1}$, as part of the next (higher frequency) spectral band. The very intense band is undoubtedly electric dipole-allowed, but the observed vibrational progression need not be. The latter portion of Table 16 lists the observed frequencies of the members of this progression, whose separations average 308 cm^{-1} . This progression may be the $\delta \rightarrow \pi^*$ ($2b_{2g} \rightarrow 5e_g$) transition, which is electric dipole-forbidden to the 1E_g excited state, but would be vibronically allowed by an ungerade vibration. This transition is calculated by Norman et al. to lie at $25,600 \text{ cm}^{-1}$ in $\text{Mo}_2(\text{O}_2\text{CH})_4$ (23), and such an assignment has been suggested for a band at $\sim 26,500 \text{ cm}^{-1}$ in the acetate complex (28). As Martin et al. noted, however, a spin-forbidden transition could also occur here, corresponding to an intense spin-allowed transition at higher energy. Norman et al. also calculated two dipole-allowed $0 \rightarrow \delta^*$ transitions to lie at $37,100 \text{ cm}^{-1}$ and $40,900 \text{ cm}^{-1}$. They observed a transition at $30,800 \text{ cm}^{-1}$ in a $\text{Mo}_2(\text{O}_2\text{CH})_4$ glass

(in 4:1 ethanol-methanol) at 80 K which they assigned as $\delta \rightarrow \delta^*$. This transition can now be assigned to one or both of the $0 \rightarrow \delta^*$ transitions. This is presumably the intense band in the crystal spectra, as well. Unfortunately, the overlap of this intense band with the progression we observed precludes the use of polarization ratios to propose a definite assignment for that transition.

Figure 26 shows a Boltzman plot based on hot band intensities observed in a thick crystal of $\beta\text{-Mo}_2(\text{O}_2\text{CH})_4$ (taken as $A_{\text{max}} \times \frac{1}{2}$). The slope yielded an origin ground state vibrational frequency of $428 \pm 23 \text{ cm}^{-1}$. This agrees with the observed appearance of the hot bands approximately 420 cm^{-1} below the band origin for each site. This supports the assignment of A_0 as the transition origin with a progression frequency corresponding to the excited state Mo-Mo stretch.

A specific assignment is proposed for the two crystal sites observed in the $\beta\text{-Mo}_2(\text{O}_2\text{CH})_4$ spectra. On the basis of the structural evidence given earlier, the A_0 origin at 21957 cm^{-1} is attributed to molecules at the general positions (β_2), and the A_0' origin at 21982 cm^{-1} is attributed to molecules at the special positions (β_1). The origin at higher energy would then correspond to the site with slightly stronger Mo-Mo bonding.

This assignment receives more credibility when we find that the transition occurs yet at higher energy in $\gamma\text{-Mo}_2(\text{O}_2\text{CH})_4$.

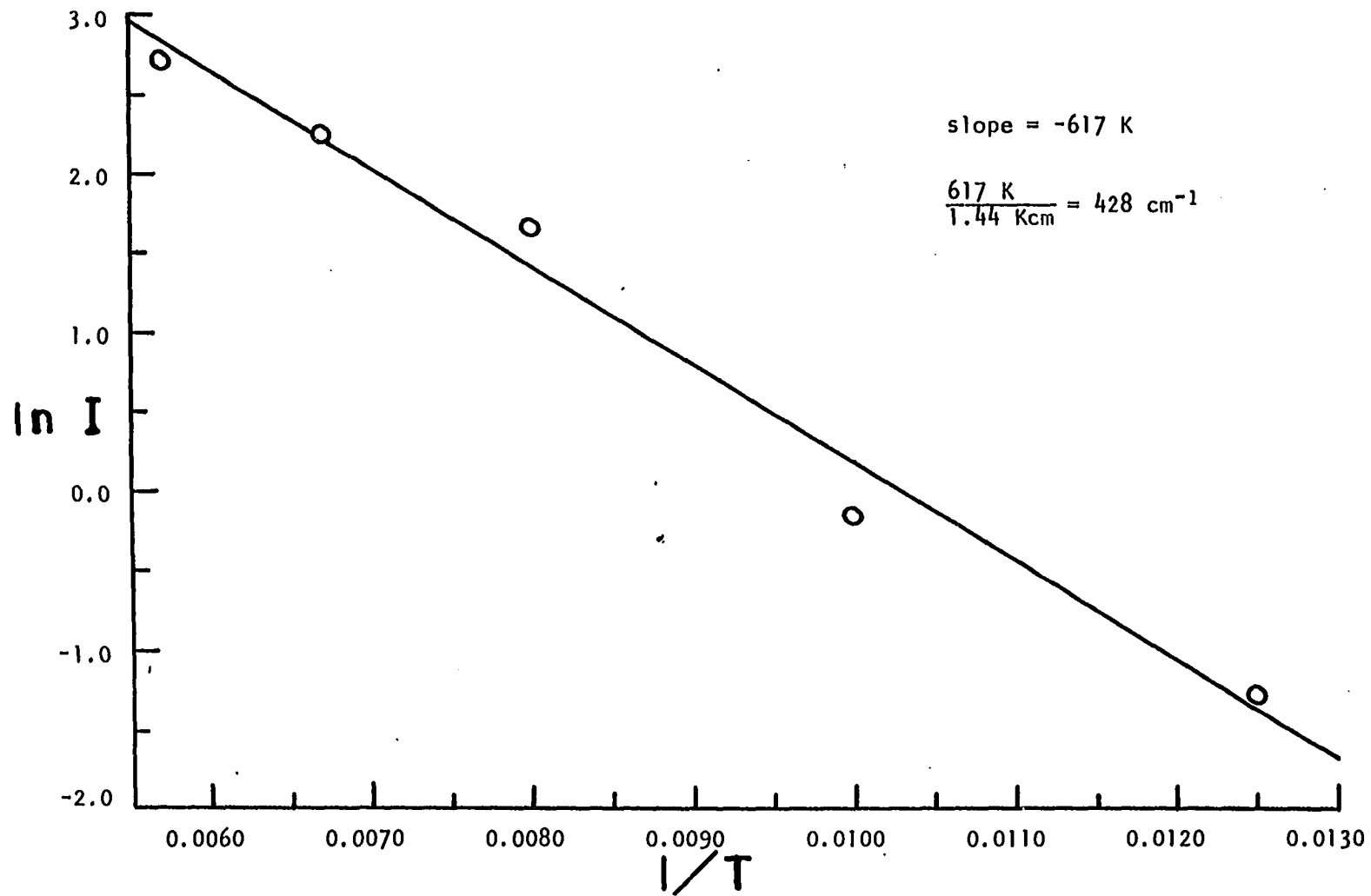


Figure 26. Boltzman plot for hot bands in $\beta\text{-Mo}_2(\text{O}_2\text{CH})_4$

Figure 27 shows the low-temperature polarized spectra obtained from a crystal of $\gamma\text{-Mo}_2(\text{O}_2\text{CH})_4$ which was $50 \pm 10 \mu\text{m}$ thick. Spectra were obtained only from one crystal. Two weak features appear at lower frequency than the band origin, which is located at 22054 cm^{-1} . These features are attributed (as before) to some kind of defect or impurity. It is worth noting that the feature at 21978 cm^{-1} could be the β -polymorph, but it is likely that the two sites would have been resolved under these conditions. Table 17 gives the details of the observed vibrational progressions in $\gamma\text{-Mo}_2(\text{O}_2\text{CH})_4$. The spectral features of this polymorph do not differ greatly from those of the other forms studied. The progression starting 460 cm^{-1} above A_0 was not observed in the other polymorphs. No corresponding Raman line has been reported. The $E_0 - A_0$ separation is 579 cm^{-1} in the γ -form, but only 520 cm^{-1} in the α -form. The acetate complex has progressions E and F built on 545 and 590 cm^{-1} vibrations. It is conceivable that the formate progressions represent two different vibrations. A frequency shift of $\sim 60 \text{ cm}^{-1}$ for the E progression allowing vibration is the alternative explanation. This shift seems large, but is perhaps not impossible. Martin et al. attributed the E_0 allowing vibration in the acetate to a ring deformation involving some motion of the Mo atoms. It is possible that the frequency of this vibration is subject to differences in axial bonding.

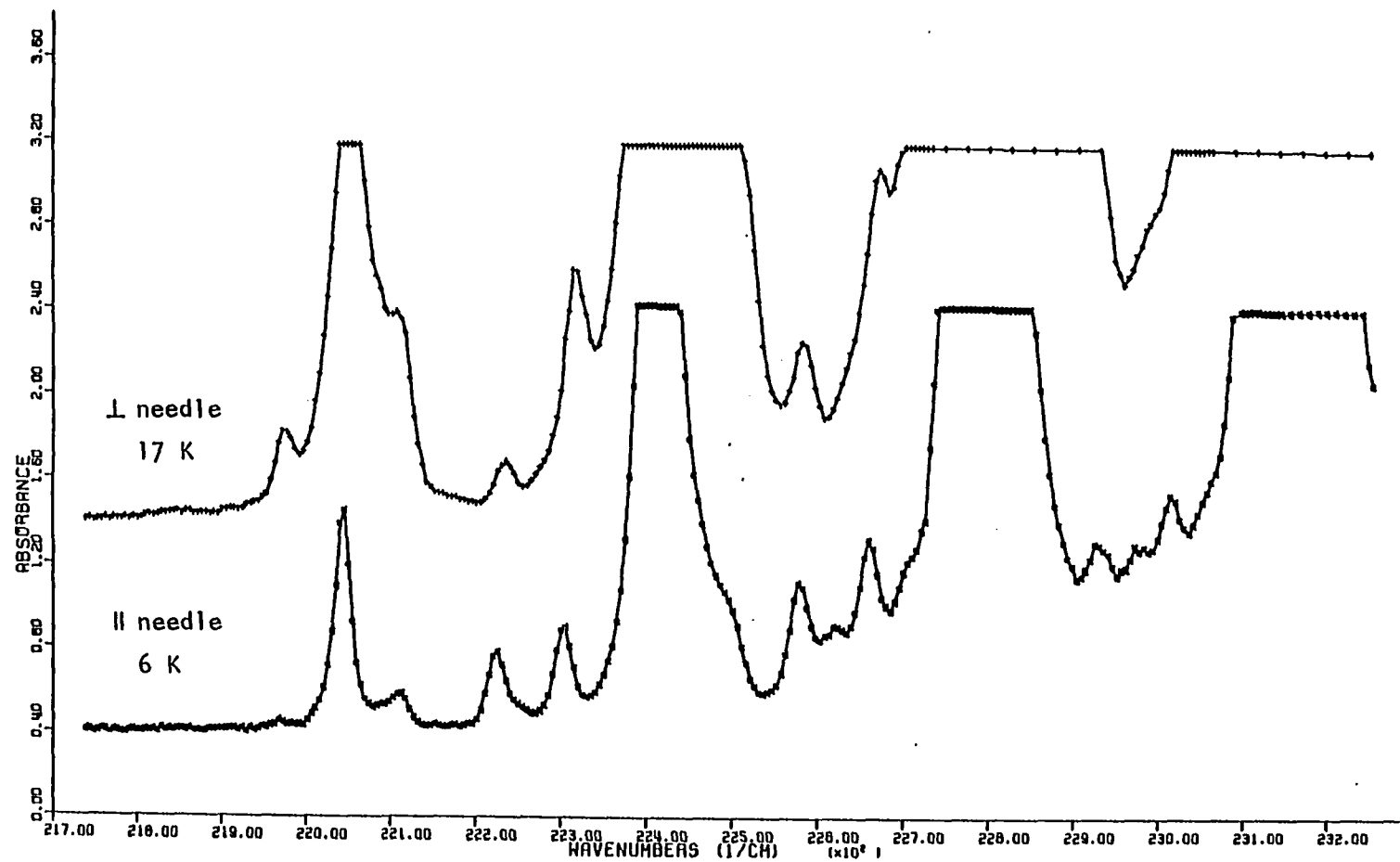


Figure 27. Polarized spectra of $\gamma\text{-Mo}_2(\text{O}_2\text{CH})_4$. The crystal thickness was $50 \pm 10 \mu\text{m}$

Table 17. Weak vibrational details in the crystal spectra of $\gamma\text{-Mo}_2(\text{O}_2\text{CH})_4$ at 6 K

Assignment	$\bar{\nu}^a$, cm^{-1}	I_{\perp}/I_{\parallel}	$\Delta\bar{\nu}(0-0)^b$, cm^{-1}	$\Delta\bar{\nu}(\text{progression})^c$, cm^{-1}
A ₋₁	21631 ^d	~6	(-423)	
C ₋₁	21671 ^d		(-424)	
x ₀	21848 ^e		(-206)	
x ₁	21978 ^e	~6	(-76)	
A ₀	22054	est. ~6	.0	
C ₀	22095		41	
d ₀	22121	~6	67	
B ₀	22236	~0.6	182	
C ₀	22314	~2	260	
D ₀	22369	~3	314	
g ₀	22514		460	
B ₁	22590			354
E ₀	22633	~2	579	
C ₁	22674			360
D ₁	22716			347

^aListed values are $\pm 15 \text{ cm}^{-1}$ for $\bar{\nu}$ and $\pm 5 \text{ cm}^{-1}$ for $\Delta\bar{\nu}$.

^bDifference of the progression origin frequency and the A₀ frequency for a particular site.

^cFrequency separation from preceding member of progression.

^dHot band observed at 75 K.

^eAttributed to an impurity or defect component.

Table 17. Continued.

Assignment	ν , cm^{-1}	I_{\perp}/I_{\parallel}	$\Delta\nu(0-0)$, cm^{-1}	$\Delta\nu(\text{progression})$, cm^{-1}
G ₀	22904		850	
B ₂	22942			352
E ₁	22986			353
C ₂	23024			350
D ₂	23064			348
E ₂	23339			353
C ₃	23377			353
D ₃	23414			350
E ₃	23688			349
C ₄ + D ₄	23734			
E ₄	24038			350
C ₅ + D ₅	24096			362
C ₆ + D ₆	24450			354
	24492 ^f			
	24558 ^f			
	24594 ^g			
	24851 ^f			359
	24913 ^g			355
	24956 ^f			362

^fComponent of a broad unresolved band.

^gCenter of a broad band of many unresolved components.

In $\gamma\text{-Mo}_2(\text{O}_2\text{CH})_4$, A_0 is found 160 cm^{-1} higher than in $\alpha\text{-Mo}_2(\text{O}_2\text{CH})_4$ and 93 cm^{-1} higher than the β_2 molecules. Thus, the observed A_0 frequency shows the Mo-Mo bond strength trend of $\gamma > \beta_1 > \beta_2 > \alpha$ as discussed in the structural results. It is interesting to note that the β_1 and γ molecules have inversion symmetry, while the β_2 and α molecules have no symmetry. This suggests that the increased axial bonding resulted in a lowering of the molecular symmetry. This point is rather speculative, however, since the pattern noted may be coincidental.

Table 18 correlates the vibrational progressions built upon A_0 in the acetate, trifluoroacetate, and formate complexes. Most of these represent vibronic components of the transition. The intensity of each progression can apparently vary greatly from one complex to another. The spectra of the three complexes now appear more similar than the gross spectral features indicate.

On the whole, the $\text{Mo}_2(\text{O}_2\text{CH})_4$ spectra are seen to be in agreement with a $\delta \rightarrow \delta^*$ assignment for the low energy transition, as proposed for the acetate complex. The A transition moment in that case was found to lie 33.9° away from the molecular z axis. Newman has shown that similar orientations in $\text{Mo}_2(\text{O}_2\text{CCF}_3)$ and $\alpha\text{-Mo}_2(\text{O}_2\text{CH})_4$ could account for the A_0 polarizations observed in those spectra (29). The A_0 polarization behavior is not greatly different in the three formate polymorphs, and we thus expect similar orientations of the respective transition

Table 18. Vibrational progressions built upon A_0 in the crystal spectra of dimolybdenum tetracarboxylate complexes^a

Progression	$\text{Mo}_2(\text{O}_2\text{CCH}_3)_4^b$	$\text{Mo}_2(\text{O}_2\text{CCF}_3)_4^c$	$\alpha\text{-Mo}_2(\text{O}_2\text{CH})_4$	$\beta\text{-Mo}_2(\text{O}_2\text{CH})_4$	$\gamma\text{-Mo}_2(\text{O}_2\text{CH})_4$
	25				
c	60		50		40
d	80		90	70	65
e	130	130 ^d	120	120	
B	175	180 ^d	190	185	180
f	255		240		
C	275	260	260	260	260
D	320		295		315
	355				
H			390	390	
g					460
E	545	500	520		580 ^e
F	590				
J			785	785	

G	865	855	850
	900		

^aGiven in cm^{-1} .

^bReference 28.

^cReference 29.

^dAssigned differently here than in the original reference.

^eMay be alternatively assigned to the F progression.

moments. No additional crystal faces were available for study, thereby limiting the amount of information available to us.

The polarized crystal spectra of $\text{Mo}_2(\text{O}_2\text{CH})_4 \cdot \text{KCl}$ at 5 K are shown in Figure 28. The spectra show one major broad progression, in striking contrast to the sharp detail observed in the $\text{Mo}_2(\text{O}_2\text{CH})_4$ spectra. This broadness was also found in the crystal spectra of $\text{K}_4\text{Mo}_2\text{Cl}_8 \cdot 2\text{H}_2\text{O}$ (24). It is presumably caused by the potassium ions in the crystal. Their strong crystal field apparently produces an increased mixing of states which participate in the transition. The vibrational progression begins at $21,743 \text{ cm}^{-1}$, showing a red shift of 151 cm^{-1} from $\alpha\text{-Mo}_2(\text{O}_2\text{CH})_4$. This is in accord with structural evidence for weakened Mo-Mo bonding. The observed progression spacing was 368 cm^{-1} . The observed polarization ratio I_1/I_2 was 0.31 (or $1/3.2$), compared with the expected z - and x, y -polarized values of 87.5 and 0.16. Thus, the polarization appears much closer to the expected x, y behavior than to z .

The vibrational data for $\text{Mo}_2(\text{O}_2\text{CH})_4 \cdot \text{KCl}$ are listed in Table 19. A weak impurity or defect progression was observed below A_0 in some crystals. A few components of a higher energy band are also listed in the Table. Comments made earlier for the corresponding band in $\beta\text{-Mo}_2(\text{O}_2\text{CH})_4$ would apply here. The three progression origins B_0 , C_0 , and E_0 were observed in a thick crystal. Since they occur here as in $\text{Mo}_2(\text{O}_2\text{CH})_4$, they

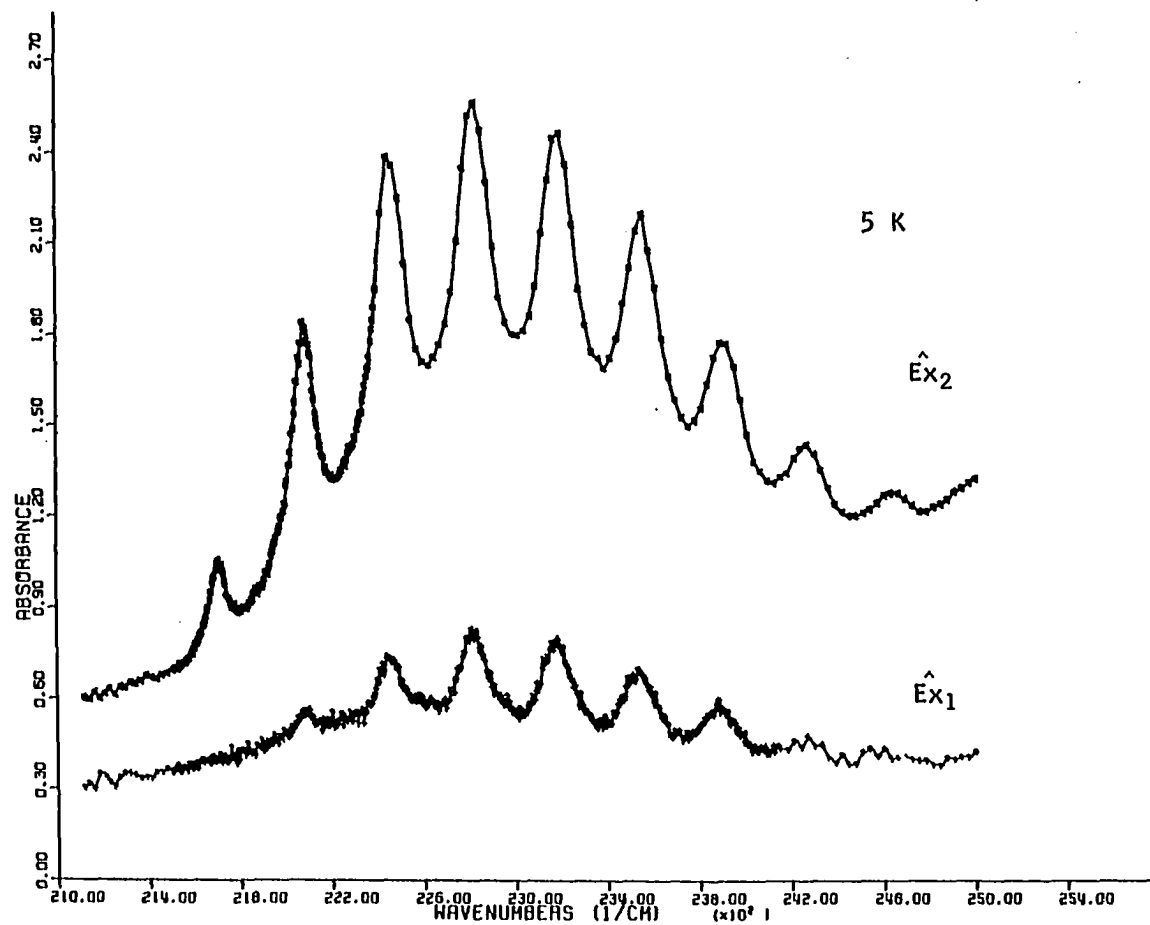


Figure 28. Polarized spectra of $\text{Mo}_2(\text{O}_2\text{CH})_4 \cdot \text{KCl}$

Table 19. Vibrational details in the crystal spectra of $\text{Mo}_2(\text{O}_2\text{CH})_4 \cdot \text{KCl}$ at 5 K

Assignment	$\bar{\nu}^a$, cm^{-1}	$\Delta\bar{\nu}(0-0)^b$, cm^{-1}	$\Delta\bar{\nu}(\text{progression})^c$, cm^{-1}
x_0^d	20286		
x_1	20640		354
x_2	21003		363
x_3	21361		358 (Av. = 358)
A_0^e	21743		
B_0^f	21924	181	
C_0^f	21992	249	
A_1	22121		378
E_0^f	22257	507	
A_2	22495		374
A_3	22865		370
A_4	23232		367
A_5	23588		356

^aListed values are $\pm 15 \text{ cm}^{-1}$ for $\bar{\nu}$ and $\pm 5 \text{ cm}^{-1}$ for $\Delta\bar{\nu}$.

^bDifference of the progression origin frequency and the A_0 frequency.

^cFrequency separation from preceding member of progression.

^dObserved in some crystals and assigned to an impurity or defect component.

^eHigher energy members of A progression may contain other unresolved components.

^fObserved in a thick crystal.

Table 19. Continued.

Assignment	$\bar{\nu}$, cm^{-1}	$\Delta\bar{\nu}(0-0)$, cm^{-1}	$\Delta\bar{\nu}(\text{progression})$, cm^{-1}
A ₆	23958		370
A ₇	24307		349
A ₈	24685		378 (Av. = 368)
X ₀ ^g	25514		
X ₁	25873		359
X ₂	26195		322
X ₃	26529		334 (Av. = 338)

^gFirst distinct component of a vibrational progression appearing at the beginning of an intense transition at higher energy.

must be due to molecular vibrations, as opposed to phonons, for example. They also indicate that this transition is much the same as in $\text{Mo}_2(\text{O}_2\text{CH})_4$, except for the line broadening. A $\delta \rightarrow \delta^*$ assignment is proposed, though not supported by the observed polarization behavior. However, the transition moment may be shifted away from the molecular z axis by the crystal field, as suggested in the acetate. We have evidence for a strong crystal field, both in the line broadness and in the apparent coordination of the potassium ion to the carboxylate oxygen atoms.

It was the goal of this research to clarify aspects of the polarized crystal spectra of dimolybdenum tetracarboxylates, and thus aid in elucidating the electronic structure of these complexes. In general, spectra of the binuclear Mo carboxylates have shown a wealth of sharp vibrational detail. The high (ideal) D_{4h} symmetry of the molecules made them attractive candidates for polarized spectroscopy, which was expected to lead to definitive conclusions concerning their electronic structure and spectroscopic behavior. Dimolybdenum tetraformate had the advantage of being the simplest carboxylate complex. For this reason, it was the complex chosen for the SCF-X α -SW calculations.

For all of the dimolybdenum tetracarboxylates, the data have proven somewhat less than ideal. The high D_{4h} molecular symmetry has been compromised by the crystal field in the solid state. For the formate complex, other effects entered in which complicated the spectra. The two intense progressions at ~ 400 and ~ 790 cm^{-1} above A_0 fell near multiples of the Mo-Mo stretch. This clustered the vibrational components and obscured some detail. The polymorphic variation and crystallographic site splitting made resolution or identification of individual lines difficult.

In spite of the difficulties, several things have been learned. The formate spectra were shown to fit the important patterns established in the acetate spectra. Thus, the $\delta \rightarrow \delta^*$

assignment is indicated for $\text{Mo}_2(\text{O}_2\text{CH})_4$. The crystal spectra of $\text{Mo}_2(\text{O}_2\text{CH})_4$ seem to provide a sensitive indicator of subtle axial bonding effects. Minor changes in the axial bonding produced significant shifts in the transition energy. Unique crystallographic sites were distinctly observed, except in $\text{Mo}_2(\text{O}_2\text{CH})_4 \cdot \text{KCl}$ where they were obscured by the line broadening. The spectra suggested the existence of a fourth polymorph, and the presence of unidentified defect or decomposition components. Dimolybdenum tetraformate was found to have considerable flexibility in crystal packing, probably due to its approximate spherical shape and absence of bulky, entangling substituents. It is possible for one particular polymorph to be preferred over another depending on the preparation or other conditions.

During the course of research, the author realized that the axial interaction in $\text{Mo}_2(\text{pivalate})_4$ was different from, but related to, that in the other complexes. At the author's suggestion, the polarized spectra of this complex are presently being investigated. This study should reveal more information concerning the spectral and/or electronic effects of axial coordination.

BIBLIOGRAPHY

1. Cotton, F. A.; Norman, J. G.; Stults, B. R.; Webb, T. R. J. Coord. Chem. 1976, 5, 217.
2. Cotton, F. A.; Curtis, N. F.; Harris, C. B.; Johnson, B. F. G.; Lippard, S. J.; Mague, J. T.; Robinson, W. R.; Wood, J. S. Science, 1964, 145, 1305.
3. Cotton, F. A. Inorg. Chem. 1965, 4, 334.
4. Cotton, F. A.; Harris, C. B. Inorg. Chem. 1965, 4, 330.
5. Figgis, B. N.; Martin, R. L. J. Chem. Soc. 1956, 3837.
6. van Niekerk, J. N.; Schoening, F. R. L.; de Wet, J. F. Acta Cryst. 1953, 6, 501.
7. Cotton, F. A.; DeBoer, B. G.; LaPrade, M. D.; Pipal, J. R.; Ucko, D. A. J. Am. Chem. Soc. 1970, 92, 2926.
8. Cotton, F. A.; Harris, C. B. Inorg. Chem. 1967, 6, 924.
9. Mortola, A. P.; Moskowitz, J. W.; Rösch, N.; Cowman, C. D.; Gray, H. B. Chem. Phys. Lett. 1975, 32, 283.
10. Cowman, C. D.; Gray, H. B. J. Am. Chem. Soc. 1973, 95, 8177.
11. Cotton, F. A.; Frenz, B. A.; Stults, B. R.; Webb, T. R. J. Am. Chem. Soc. 1976, 98, 2768.
12. Cotton, F. A. J. Less-Common Met. 1977, 54, 3.
13. Cotton, F. A. Acc. Chem. Res. 1978, 11, 225.
14. Templeton, J. L. Prog. Inorg. Chem. 1979, 26, 211.
15. Cotton, F. A.; Bratton, W. K. J. Am. Chem. Soc. 1965, 87, 921.
16. Lawton, D.; Mason, R. J. Am. Chem. Soc. 1965, 87, 921.
17. Bannister, E.; Wilkinson, G. Chem. Ind. 1960, 319.
18. Stephenson, T. A.; Bannister, E.; Wilkinson, G. J. Chem. Soc. 1964, 2538.
19. Dubicki, L.; Martin, R. L. Aust. J. Chem. 1969, 22, 1571.

20. Cotton, F. A.; Martin, D. S.; Webb, T. R.; Peters, T. J. Inorg. Chem. 1976, 15, 1199.
21. Norman, J. G.; Kolari, H. J. J. Am. Chem. Soc. 1975, 97, 33.
22. Norman, J. G.; Kolari, H. J. J. Chem. Soc., Chem. Commun. 1975, 649.
23. Norman, J. G.; Kolari, H. J.; Gray, H. B.; Trogler, W. C. Inorg. Chem. 1977, 16, 987.
24. Fanwick, P. E.; Martin, D. S.; Cotton, F. A.; Webb, T. R. Inorg. Chem. 1977, 16, 2103.
25. Cotton, F. A.; Martin, D. S.; Fanwick, P. E.; Peters, T. J.; Webb, T. R. J. Am. Chem. Soc. 1976, 98, 4681.
26. Fanwick, P. E.; Martin, D. S.; Webb, T. R.; Robbins, G. A.; Newman, R. A. Inorg. Chem. 1978, 17, 2723.
27. Trogler, W. C.; Solomon, E. I.; Trajberg, I.; Ballhausen, C. J.; Gray, H. B. Inorg. Chem. 1977, 16, 828.
28. Martin, D. S.; Newman, R. A.; Fanwick, P. E. Inorg. Chem. 1979, 18, 2511.
29. Newman, R. A. Ph.D. Dissertation, Iowa State University, Ames, Iowa, 1981.
30. Bino, A.; Cotton, F. A.; Fanwick, P. E. Inorg. Chem. 1980, 19, 1215.
31. Bowen, A. R.; Taube, H. Inorg. Chem. 1974, 13, 2245.
32. Cotton, F. A.; Webb, T. R. Inorg. Chem. 1976, 15, 68.
33. Erwin, D. K.; Geoffroy, G. L.; Gray, H. B.; Hammond, G. S.; Solomon, E. I.; Trogler, W. C.; Zagars, A. A. J. Am. Chem. Soc. 1977, 99, 3620.
34. Sattelberger, A. P.; Fackler, J. P. J. Am. Chem. Soc. 1977, 99, 1258.
35. Cowman, C. D.; Trogler, W. C.; Gray, H. B. Israel J. Chem. 1977, 15, 308.
36. Böhmer, W. H.; Madeja, K.; Kurras, E.; Rosenthal, U. Z. Chem. 1978, 18, 453.

37. Cotton, F. A.; Fanwick, P. E. J. Am. Chem. Soc. 1979, 101, 5252.
38. Bino, A.; Cotton, F. A.; Fanwick, P. E. Inorg. Chem. 1979, 18, 3558.
39. Noodleman, L.; Norman, J. G. J. Chem. Phys. 1979, 70, 4903.
40. Robbins, G. A. M.S. Thesis, Iowa State University, Ames, Iowa, 1978.
41. Jacobson, R. A. "An Algorithm For Automatic Indexing and Bravais Lattice Selection: the programs BLIND and ALICE", Ames Laboratory-USAEC Report IS-3469, Iowa State University, Ames, Iowa, 1974.
42. "Crystal Data Determinative Tables", 2nd Ed.; American Cryst. Assoc., Williams and Heinz Map Corp.: Washington, D.C., 1963; pp. 2, 3.
43. Lawton, S. L.; Jacobson, R. A. Inorg. Chem. 1968, 7, 2124.
44. Hanson, H. P.; Herman, F.; Lea, J. D.; Skillman, S. Acta Cryst. 1960, 17, 1040.
45. Templeton, D. H. "International Tables for X-ray Crystallography"; The Kynoch Press: Birmingham, England, 1962; Vol. III.
46. Templeton, D. H. "International Tables for X-ray Crystallography"; The Kynoch Press: Birmingham, England, 1962; Vol. III, Table 3.3.2c, pp. 215, 216.
47. Stewart, R. F.; Davidson, E. R.; Simpson, W. T. J. Chem. Phys., 1965, 42, 3175.
48. Johnson, C. K. AEC Report ORNL-3794, Oak Ridge Tenn., March 1971 (second revision).
49. Takusagawa, F. Ames Laboratory, USDOE, Iowa State University, Ames, Iowa, unpublished.
50. Howells, E. R.; Phillips, D. C.; Rogers, D. Acta Cryst. 1950, 3, 210.
51. Lapp, R. L.; Jacobson, R. A. "ALLS: A Generalized Crystallographic Least-Squares Program", USDOE Report IS-4708, Iowa State University, Ames, Iowa, 1979 (preliminary version).
52. Hubbard, C. R.; Quicksall, C. O.; Jacobson, R. A. "The Fast Fourier Algorithm and the Programs ALFF, ALFFDP, ALFFPROJ, ALFFT AND FRIEDEL", Ames Laboratory-USAEC Report IS-2625, Iowa State University, Ames, Iowa, 1971.

53. Busing, W. R.; Martin, K. O.; Levy, H. A. "ORFFE, A Fortran Crystallographic Function and Error Program: USAEC Report ORNL-TM-306, Oak Ridge National Laboratory, Oak Ridge, Tennessee, 1964.
54. Lapp, R. L.; Jacobson, R. A. "ALLS: A Generalized Crystallographic Least-Squares Program", USDOE Report IS-4798, Iowa State University, Ames, Iowa, 1979.
55. Powell, D. R.; Jacobson, R. A. "FOUR: A Generalized Crystallographic Fourier Program:", Ames Laboratory-DOE Report IS-4737, Iowa State University, Ames, Iowa, 1980.
56. Jenson, W. private communication, South Dakota State University, Brookings, South Dakota.
57. Cotton, F. A.; Thompson, J. L. Inorg. Chem. 1981, 20, 3887.
58. Cotton, F. A.; Mester, E. C.; Webb, T. R. Acta Cryst. 1974, B30, 2768.
59. Cotton, F. A.; Norman, J. G. J. Coord. Chem. 1971, 1, 161.
60. Presented in part at the 15th Midwest Regional ACS Meeting, St. Louis, Missouri, November, 1979.
61. Trogler, W. C.; Gray, H. B. Accts. Chem. Res. 1978, 11, 232.
62. Bratton, W. K.; Cotton, F. A.; Debeau, M. J. Coord. Chem. 1971, 1, 121.
63. Ketteringham, A. P.; Oldham, C. J. C. S. Dalton 1973, 1067.

ACKNOWLEDGMENTS

The author gratefully acknowledges the advice and assistance of Dr. R. A. Jacobson and members of the X-ray crystallography group with many aspects of the crystal structures.

The author wishes to thank the members of Radiochemistry Group II for their help and advice in the course of the research and for the interesting discussions and friendship which they provided.

The advice, encouragement, and assistance provided throughout the author's graduate career by Dr. Don S. Martin is greatly appreciated.

The author wishes to thank his parents for their encouragement and wholehearted support throughout his academic career.

The author is indebted to his wife, Marie, for her continued patience, encouragement, and support. Her diligent and skillful effort in preparing the manuscript is greatly appreciated.

APPENDIX A: OBSERVED AND CALCULATED STRUCTURE FACTORS
FOR $\beta\text{-Mo}_2(\text{O}_2\text{CH})_4$

H = 6	7-5	53	53	2-8	164	172	8-2	28	27	4-5	129	123	1-14	12	15	9-6	55	53
K L FO	7-7	69	66	2-9	54	55	8-5	22	22	4-6	163	154	1-15	97	103	9-7	42	41
5-0	7-9	44	46	2-10	49	53	8-6	61	60	4-7	214	207	1-16	27	30	9-8	116	119
5-1	7-10	16	17	2-12	104	107	8-7	127	123	4-8	11	13	1-17	23	17	9-9	44	45
5-2	7-11	11	11	2-13	12	17	8-8	74	71	4-10	118	120	1-18	21	18	9-10	25	23
5-3	7-12	11	11	2-14	108	114	8-9	28	25	4-11	31	25	0-0	90	48	9-11	117	117
5-4	7-13	11	11	1-0	44	40	8-10	41	38	4-12	22	23	0-2	212	201	9-12	140	138
5-5	7-14	11	11	1-1	82	82	8-11	7	8	4-13	76	75	0-4	84	92	9-13	22	20
5-6	7-15	11	11	1-2	37	34	8-12	76	74	4-14	23	23	0-6	113	113	9-14	15	15
5-7	7-16	11	11	1-3	44	40	8-13	91	90	4-15	10	13	0-8	50	54	9-15	40	39
5-8	7-17	11	11	1-4	14	16	7-0	9	8	4-16	54	53	0-10	115	114	8-0	102	99
5-9	7-18	11	11	1-5	166	170	7-1	21	23	3-0	71	70	0-12	60	63	8-1	38	34
5-10	7-19	11	11	1-6	19	18	7-2	137	131	3-1	57	57	0-14	19	18	8-2	53	55
5-11	7-20	11	11	1-7	46	45	7-3	147	143	3-2	116	112	0-16	125	130	8-3	38	36
5-12	7-21	11	11	1-8	20	22	7-4	90	87	3-3	134	130	0-18	125	124	8-4	30	31
5-13	7-22	11	11	1-9	70	68	7-5	12	10	3-4	127	121	0-18	125	124	8-5	51	48
5-14	7-23	11	11	1-11	169	169	7-6	37	43	3-5	86	47				8-6	62	58
5-15	7-24	11	11	1-12	9	13	7-7	16	16	3-6	145	140	K L	FO	FC	8-7	23	24
5-16	7-25	11	11	1-13	47	50	7-8	44	43	3-7	67	67	13-0	92	96	8-8	87	85
5-17	7-26	11	11	1-14	22	22	7-9	125	119	3-8	69	70	13-1	19	22	8-9	122	121
5-18	7-27	11	11	1-15	82	87	7-10	121	117	3-9	69	69	13-2	106	111	8-10	95	89
5-19	7-28	11	11	0-0	119	114	7-11	49	47	3-10	95	97	12-0	26	26	8-11	94	98
5-20	7-29	11	11	0-2	188	185	7-12	32	32	3-11	114	109	12-1	36	35	8-12	54	49
5-21	7-30	11	11	0-4	86	83	7-13	14	17	3-12	8	9	12-2	44	45	8-13	36	34
5-22	7-31	11	11	0-6	16	13	7-14	7	12	3-13	43	42	12-3	55	55	8-14	91	90
5-23	7-32	11	11	0-8	141	144	6-0	126	126	3-14	65	63	12-4	23	22	8-15	109	102
5-24	7-33	11	11	0-10	40	41	6-1	24	25	3-15	11	11	12-5	135	149	8-16	74	71
5-25	7-34	11	11	0-12	103	109	6-2	9	10	3-16	69	70	12-6	13	13	7-1	95	95
5-26	7-35	11	11	0-14	114	122	6-3	101	97	2-0	69	70	12-7	15	19	7-2	26	23
5-27	7-36	11	11	0-12	114	122	6-4	101	97	2-1	66	61	12-8	42	43	7-3	25	28
5-28	7-37	11	11	0-13	47	50	6-5	180	174	2-2	185	197	11-0	85	90	7-4	9	9
5-29	7-38	11	11	0-14	39	40	6-6	8	25	2-3	46	47	11-1	27	28	7-5	51	48
5-30	7-39	11	11	0-15	67	71	6-7	189	174	2-4	65	71	11-2	117	122	7-6	155	141
5-31	7-40	11	11	0-16	102	103	6-8	19	16	2-5	88	59	11-4	19	20	7-7	19	17
5-32	7-41	11	11	0-17	102	103	6-9	19	16	2-6	102	105	11-5	89	88	7-8	70	64
5-33	7-42	11	11	0-18	18	19	6-10	35	36	2-7	74	77	11-6	8	6	7-9	66	65
5-34	7-43	11	11	0-19	44	46	6-11	74	72	2-8	26	24	11-7	27	31	7-10	65	64
5-35	7-44	11	11	0-20	73	77	6-12	30	39	2-9	12	12	11-8	126	123	7-11	94	91
5-36	7-45	11	11	0-21	38	45	6-13	14	15	2-10	138	138	11-9	23	24	7-12	145	136
5-37	7-46	11	11	0-22	15	15	6-14	32	32	2-11	47	48	11-10	16	16	7-13	104	94
5-38	7-47	11	11	0-23	4	5	6-15	63	56	2-12	19	17	11-11	83	63	7-14	16	17
5-39	7-48	11	11	0-24	51	54	5-0	83	86	2-13	85	83	10-0	57	56	7-15	43	44
5-40	7-49	11	11	0-25	101	103	5-1	126	121	2-14	9	15	10-1	31	32	7-16	37	36
5-41	7-50	11	11	0-26	44	46	5-2	168	160	2-16	95	100	10-2	59	57	7-17	30	33
5-42	7-51	11	11	0-27	44	46	5-3	139	132	2-18	94	97	10-3	22	22	6-0	113	114
5-43	7-52	11	11	0-28	34	35	5-4	16	16	2-19	25	27	10-4	28	27	6-1	13	14
5-44	7-53	11	11	0-29	16	16	5-5	17	16	1-0	25	27	10-5	133	135	6-2	61	61
5-45	7-54	11	11	0-30	95	95	5-6	85	85	1-1	14	14	10-6	9	11	6-3	114	109
5-46	7-55	11	11	0-31	38	39	5-7	79	76	1-2	63	62	10-7	74	74	6-4	149	146
5-47	7-56	11	11	0-32	140	139	5-8	132	128	1-3	139	141	10-8	74	74	6-5	32	33
5-48	7-57	11	11	0-33	44	46	5-9	16	15	1-4	128	127	10-9	73	79	6-6	93	88
5-49	7-58	11	11	0-34	26	26	5-10	16	15	1-5	138	142	10-10	57	55	6-7	51	51
5-50	7-59	11	11	0-35	15	19	5-11	42	44	1-6	9	9	10-11	87	82	6-8	110	105
5-51	7-60	11	11	0-36	23	22	5-12	28	27	1-7	46	67	10-12	49	51	6-9	171	163
5-52	7-61	11	11	0-37	89	87	4-0	83	85	1-8	19	18	9-0	50	51	6-10	36	32
5-53	7-62	11	11	0-38	93	96	4-1	63	62	1-9	26	29	9-1	10	3	6-11	87	87
5-54	7-63	11	11	0-39	93	96	4-2	107	104	1-10	35	33	9-2	60	67	6-12	42	41
5-55	7-64	11	11	0-40	142	142	4-3	33	38	1-11	12	13	9-3	16	13	6-13	38	36
5-56	7-65	11	11	0-41	29	26	4-4	32	32	1-12	175	187	9-4	5	68	6-14	26	25
5-57	7-66	11	11	0-42	29	26	4-5	32	32	1-13	175	187	9-5	5	68	6-15	38	36
5-58	7-67	11	11	0-43	29	26	4-6	32	32	1-14	175	187	9-6	5	68	6-16	38	36

6-15	123	119	3-19	92	91	12	0	54	50	0	-5	53	9	-7	129	122	2	-5	110	111	13	-1	35	36					
6-16	116	111	3-20	15	14	12	-1	50	60	0	-6	74	66	5	-8	69	2	-6	94	99	13	-2	18	16					
6-17	117	10	2	0	31	32	58	60	60	0	-7	35	37	5	-5	30	2	-7	23	22	13	-3	15	16					
6-18	9	12	2	-1	35	34	12	3	121	122	8	-8	27	32	19	19	2	-8	107	177	13	-4	30	30					
5	0	54	2	-2	39	42	12	-4	24	24	8	-9	36	38	10	107	2	-9	56	58	13	-5	37	37					
5	-1	227	2	-4	201	204	12	-5	17	18	8	-10	11	11	17	102	2	-10	266	248	13	-7	22	23					
5	-2	8	2	-5	30	34	12	-6	20	19	8	-12	62	62	17	102	2	-11	59	65	13	-8	21	23					
5	-3	31	2	-6	21	20	12	-7	93	97	8	-13	24	25	10	102	2	-12	106	106	13	-10	74	80					
5	-4	208	2	-8	11	10	12	-8	21	19	8	-14	84	81	10	106	2	-13	18	20	12	-1	121	120					
5	-5	78	2	-9	110	108	12	-9	45	46	8	-15	77	70	10	106	2	-14	101	166	12	-2	76	75					
5	-6	113	2	-10	111	111	12	-10	53	62	8	-16	21	20	11	111	2	-15	43	44	12	-3	21	20					
5	-7	54	2	-10	60	58	11	0	124	123	8	-17	8	10	11	111	2	-16	70	69	12	-4	55	58					
5	-8	70	2	-12	92	89	11	-2	25	24	8	-18	45	44	10	111	2	-17	19	21	12	-5	35	35					
5	-9	14	2	-13	42	44	11	-3	30	29	7	0	186	190	5	51	2	-18	6	7	12	-7	26	26					
5	-10	31	2	-14	39	39	11	-4	86	84	7	-1	26	22	4	27	2	-19	20	18	12	-8	72	71					
5	-12	115	116	2	-15	52	55	11	-5	48	43	7	-2	119	119	4	-1	112	119	2	-20	46	47	37	36				
5	-13	68	71	2	-16	96	96	11	-6	101	102	7	-3	86	90	4	-2	111	115	2	-21	48	47	12	-9	37	36		
5	-14	26	26	2	-19	23	24	11	-7	9	10	7	-4	21	18	4	-3	169	164	2	-22	7	7	12	-10	51	53		
5	-15	45	43	2	-20	79	78	11	-8	18	16	7	-5	49	51	4	-4	188	182	1	0	92	97	12	-11	15	16		
5	-16	55	53	1	0	32	32	11	-9	30	31	7	-6	113	109	4	-5	104	110	1	-1	162	160	12	-12	8	14		
5	-18	100	98	1	-1	874	399	11	-10	77	76	7	-7	70	66	4	-6	54	58	1	-2	81	82	11	0	50	49		
5	-19	97	100	1	-2	56	54	11	-11	14	14	7	-8	31	32	4	-7	45	46	1	-3	186	197	11	-1	85	86		
4	0	43	44	1	-3	23	23	11	-12	11	13	7	-9	52	50	4	-8	111	108	1	-4	67	66	11	-4	70	69		
4	-1	33	32	1	-4	30	29	11	-13	36	33	7	-10	38	37	4	-9	22	21	1	-5	59	65	11	-5	90	84		
4	-2	7	8	1	-5	24	24	11	-14	46	49	7	-11	60	63	4	-10	177	169	1	-6	91	92	11	-6	36	33		
4	-3	82	81	1	-6	9	10	10	0	115	110	7	-12	37	36	4	-11	70	68	1	-7	202	305	11	-7	48	49		
4	-4	209	202	1	-7	209	203	10	-1	12	14	7	-13	16	14	4	-12	139	130	1	-8	47	50	11	-8	43	40		
4	-5	29	30	1	-8	5	5	10	-2	97	94	7	-14	28	26	4	-13	69	65	1	-9	146	160	11	-9	9	7		
4	-6	42	43	1	-9	67	90	10	-3	129	124	7	-15	29	28	4	-14	119	117	1	-10	186	190	11	-10	93	90		
4	-7	37	36	1	-10	37	38	10	-4	8	6	7	-16	25	23	4	-15	79	76	1	-11	201	190	11	-11	67	68		
4	-8	71	71	1	-11	14	15	10	-5	15	18	7	-17	84	81	4	-16	118	119	1	-12	70	70	11	-12	39	40		
4	-9	184	174	1	-12	48	52	10	-6	39	38	7	-18	91	92	4	-17	149	149	1	-13	149	158	11	-13	46	45		
4	-10	50	47	1	-13	54	54	10	-7	66	60	7	-19	44	44	4	-18	177	169	1	-14	12	12	11	-14	46	45		
4	-11	29	29	1	-15	32	30	10	-8	20	17	6	0	15	12	4	-19	144	144	1	-15	54	53	11	-15	10	11		
4	-12	80	87	1	-16	10	15	10	-9	58	58	6	-1	6	9	3	-20	171	171	1	-16	15	14	11	-16	22	23		
4	-13	6	7	1	-17	82	82	10	-11	27	26	6	-2	124	119	3	-21	71	71	1	-17	182	111	10	-17	10	11		
4	-14	22	20	1	-18	84	87	10	-12	50	47	6	-3	222	222	3	-22	143	143	1	-18	182	111	10	-18	10	10		
4	-15	119	115	0	0	68	61	10	-13	59	57	6	-4	62	61	3	-23	144	144	1	-19	24	23	10	-2	186	168		
4	-16	121	114	0	0	68	61	10	-13	59	57	6	-5	102	99	3	-24	144	144	1	-20	30	31	10	-3	34	34		
4	-17	10	9	0	-2	6	7	10	-14	52	51	6	-6	5	4	3	-25	153	151	1	-21	10	13	10	-4	76	82		
4	-18	7	8	0	-4	408	373	10	-15	62	57	6	-7	9	10	3	-26	153	151	1	-22	0	0	186	182	10	-6	12	13
4	-19	7	8	0	-6	28	28	9	0	160	154	6	-8	33	32	3	-27	120	120	0	-2	52	58	10	-7	10	10		
4	-20	52	51	0	-10	58	60	9	-2	55	50	6	-9	12	9	3	-28	275	275	0	-4	323	323	10	-8	132	128		
3	0	82	79	0	-14	56	56	9	-4	35	38	6	-10	67	62	3	-29	96	94	0	-6	153	167	10	-9	76	73		
3	-1	334	327	0	-16	105	99	9	-5	48	43	3	-9	72	78	0	-30	72	78	0	-8	130	145	10	-10	66	65		
3	-2	86	81	0	-18	31	35	9	-6	103	100	3	-11	21	207	0	-31	207	207	0	-10	246	247	10	-11	29	28		
3	-4	14	13	0	-20	77	86	9	-7	30	31	6	-12	44	42	3	-12	207	207	0	-12	201	191	10	-13	189	121		
3	-5	31	29	3	-6	101	101	9	-8	12	8	6	-14	109	100	3	-13	135	128	0	-14	197	177	10	-14	36	35		
3	-6	94	101	3	-9	65	62	9	-9	65	62	6	-15	21	20	3	-14	51	51	0	-16	91	92	10	-15	38	36		
3	-7	138	136	14	0	21	23	9	-10	92	84	6	-16	64	64	3	-16	9	8	0	-18	8	10	10	-16	10	9		
3	-9	91	94	14	-1	52	55	9	-11	57	53	6	-17	64	64	3	-17	98	98	0	-20	42	43	9	0	16	16		
3	-10	17	15	13	0	91	97	9	-12	29	28	6	-18	36	36	3	-18	78	78	0	-22	42	43	9	0	16	16		
3	-12	121	114	13	-3	19	19	9	-15	44	45	5	0	182	179	3	-20	50	49	0	-24	42	43	9	0	16	16		
3	-13	49	45	13	-4	90	92	9	-17	44	44	5	-1	34	34	3	-21	50	49	0	-26	42	43	9	0	16	16		
3	-15	36	40	13	-5	47	48	8	0	78	73	5	-3	5	6	2	-22	21	23	14	-1	57	62	9	-2	64	64		
3	-16	37	38	13	-6	88	90	8	-2	112	117	5	-4	56	56	2	-23	21	23	14	-2	17	14	9	-4	109	108		
3	-17	51	51	13	-7	9	8	0	-3	193	184	5	-5	44	44	2	-24	133	133	14	-3	20	22	9	-5	206	190		
3	-18	57	57	13	-8	60	60	6	-4	193	184	5	-6	44	44	2	-25	133	133	14	-4	23	24	9	-6	116	114		
3	-19	56	57	13	-9	55	55	6	-4	193	184	5	-7	44	44	2	-26	133	133	14	-5	16	16	9	-7	103	84		
3	-20	56	57	13	-10	55	55	6	-4	193	184	5	-8	44	44	2	-27	133	133	14	-6	16	16	9	-8	103	84		
3	-21	56	57	13	-11	55	55	6	-4	193	184	5	-9	44	44	2	-28	133	133	14	-7	16	16	9	-9	103	84		

7-20	44	43	5-9	66	70	4-17	94	94	2-2	36	38	1-12	8	11	12-2	31	32	0-1	67	66
7-20	44	43	5-10	20	21	4-17	94	94	2-4	60	63	1-13	68	68	12-3	120	122	0-2	75	62
6-0	162	162	5-10	19	21	4-18	109	108	2-4	61	63	1-13	66	68	12-4	35	34	0-3	40	40
6-1	14	17	5-11	78	77	4-20	10	5	2-5	140	161	1-14	56	57	12-5	98	100	0-4	36	33
6-1	13	17	5-12	38	38	4-20	11	5	2-6	250	279	1-15	118	121	12-7	61	61	0-5	130	125
6-2	35	36	5-12	39	38	4-22	66	64	2-6	251	279	1-15	120	121	12-8	37	37	0-6	56	56
6-2	33	36	5-13	48	49	4-22	64	64	2-7	54	57	1-16	46	48	12-9	130	136	0-7	79	79
6-3	4	5	5-13	49	49	3-1	50	55	2-7	53	57	1-16	46	48	12-10	6	1	0-8	46	43
6-4	204	201	5-14	166	157	3-1	50	55	2-8	145	153	1-17	47	48	12-11	41	42	0-9	85	81
6-4	214	201	5-14	162	157	3-2	125	128	2-8	145	153	1-17	14	12	12-13	16	22	0-10	68	65
6-5	198	200	5-15	93	97	3-2	127	128	2-9	38	41	1-18	33	31	11-0	50	49	0-11	23	21
6-5	192	200	5-15	100	97	3-3	329	347	2-9	36	41	1-18	33	31	11-1	0	50	0-12	24	24
6-6	37	36	5-16	21	20	3-3	349	347	2-10	35	36	1-19	114	120	11-2	129	138	0-13	42	41
6-6	36	36	5-16	21	20	3-4	14	15	2-10	36	36	1-19	114	120	11-3	42	41	0-14	78	77
6-7	102	102	5-17	8	10	3-4	14	15	2-11	119	117	1-21	69	69	11-4	0	132	0-15	71	76
6-7	100	102	5-17	8	10	3-5	142	157	2-11	119	117	1-21	69	69	11-5	50	51	0-16	97	101
6-8	10	17	5-18	21	21	3-5	147	157	2-12	71	78	1-22	14	16	11-6	31	30	0-17	93	51
6-8	10	17	5-18	21	21	3-6	123	126	2-12	71	75	1-22	14	16	11-7	47	51	0-18	93	51
6-9	78	79	5-19	69	64	3-6	116	126	2-13	6	7	1-23	43	43	11-8	97	100	0-19	21	16
6-9	78	79	5-19	66	64	3-7	129	140	2-13	6	7	1-23	43	43	11-9	97	100	0-20	48	51
6-10	90	90	5-20	52	56	3-7	140	140	2-14	5	6	0-2	65	76	11-10	23	25	7-1	128	129
6-10	90	90	5-20	52	56	3-8	271	276	2-15	63	65	0-2	65	76	11-11	46	49	7-2	100	105
6-11	204	196	5-21	69	71	3-8	279	277	2-15	64	65	0-4	63	71	11-12	44	46	7-3	48	50
6-11	208	196	5-21	69	71	3-9	279	277	2-16	110	99	0-4	63	71	11-13	44	46	7-4	34	36
6-12	79	79	5-22	17	21	3-9	102	95	2-16	99	99	0-6	78	88	10-0	7	7	7-5	42	46
6-12	82	80	5-22	18	21	3-10	102	95	2-17	69	73	0-6	78	88	10-1	19	18	7-6	45	45
6-13	33	32	4-0	99	112	3-10	6	6	2-17	69	73	0-6	78	88	10-2	69	69	7-7	13	14
6-13	33	32	4-0	102	112	3-11	73	76	2-18	96	99	0-8	49	56	10-3	61	59	7-8	69	77
6-14	61	61	4-1	47	46	3-11	78	76	2-18	96	99	0-8	51	56	10-4	57	55	7-9	56	55
6-14	61	61	4-1	47	46	3-12	21	19	2-19	14	17	0-10	18	19	10-5	110	99	7-10	65	63
6-15	7	8	4-2	69	72	3-12	19	19	2-19	14	17	0-10	18	19	10-6	21	21	7-11	29	28
6-16	21	21	4-2	68	72	3-12	19	19	2-19	14	17	0-10	18	19	10-7	32	30	7-12	19	21
6-16	21	21	4-2	68	72	3-13	43	46	2-20	26	26	0-12	36	38	10-8	67	65	7-13	115	111
6-17	107	100	4-3	116	124	3-13	45	45	2-20	24	26	0-12	36	38	10-9	150	141	7-14	61	79
6-17	107	100	4-3	116	124	3-14	134	137	2-22	119	119	0-14	27	25	10-10	30	31	7-15	41	41
6-18	115	118	4-4	124	129	3-14	142	137	2-22	115	119	0-14	26	25	10-11	28	24	7-16	57	62
6-18	115	118	4-4	124	129	3-15	186	145	1-1	39	43	0-16	101	102	10-12	53	52	7-17	94	88
6-18	124	118	4-5	290	283	3-15	187	149	1-1	39	43	0-16	92	102	10-13	16	17	7-18	37	35
6-19	25	28	4-5	277	283	3-16	49	48	1-2	51	52	0-18	82	85	10-14	68	68	7-19	32	28
6-19	27	28	4-6	261	274	3-16	52	48	1-2	51	52	0-18	82	85	10-15	26	27	7-20	126	116
6-21	29	31	4-6	270	274	3-17	29	29	1-3	497	608	0-20	41	42	9-0	15	16	6-1	143	140
6-21	30	31	4-7	7	8	3-17	29	29	1-3	452	608	0-22	168	171	9-1	171	169	6-2	22	22
5-1	97	101	4-7	8	8	3-18	42	43	1-4	36	36	0-22	163	171	9-2	171	166	6-3	42	42
5-2	144	139	4-8	165	159	3-18	44	43	1-4	35	36	0-22	163	171	9-3	44	45	6-4	90	88
5-2	144	139	4-8	167	159	3-19	57	94	1-5	72	74	K	L	FD	9-4	29	29	6-5	151	145
5-3	235	247	4-9	86	87	3-19	101	94	1-5	71	74	K	L	FD	9-5	59	57	6-6	92	95
5-3	249	247	4-9	87	87	3-20	30	30	1-6	152	159	14-3	132	159	9-6	52	52	6-7	81	86
5-4	65	69	4-10	68	71	3-20	32	30	1-6	149	155	14-5	92	93	9-7	37	37	6-8	18	16
5-4	70	69	4-11	263	238	3-21	55	53	1-7	45	46	13-0	75	76	9-8	78	75	6-9	34	32
5-5	5	2	4-11	245	238	3-22	16	14	1-8	71	76	13-1	16	17	9-10	20	18	6-10	146	138
5-5	5	2	4-12	94	100	3-22	14	14	1-8	71	76	13-2	123	124	9-11	85	82	6-11	18	15
5-6	33	33	4-12	102	100	3-23	12	11	1-8	74	76	13-3	9	14	9-12	64	61	6-12	33	31
5-6	32	33	4-14	14	12	3-23	7	11	1-9	110	111	13-4	50	50	9-13	60	64	6-13	107	101
5-7	170	170	4-14	14	12	2-0	501	601	1-10	13	13	13-5	33	34	9-14	102	98	6-14	25	20
5-7	170	170	4-15	57	56	2-0	480	601	1-10	13	13	13-6	167	158	9-15	65	62	6-15	22	21
5-8	283	275	4-15	52	56	2-1	50	52	1-11	70	72	13-7	28	26	9-16	26	24	6-16	94	83
5-8	288	275	4-16	49	50	2-1	50	52	1-11	71	72	13-8	37	37	9-17	65	66	6-17	102	105
5-9	70	70	4-16	51	50	2-2	37	36	1-12	10	11	13-9	44	47	9-18	25	28	6-18	40	45
5-9	70	70	4-16	51	50	2-2	37	36	1-12	10	11	13-10	12	10	9-19	0	0	6-19	44	44

9-9	39	38	6-9	102	170	3-8	75	74	0-6	102	109	12-10	94	91	10-11	128	121	8-6	44	40	
9-10	48	46	6-10	86	79	3-9	206	217	0-8	71	81	12-10	89	91	10-12	97	97	8-7	141	135	
9-11	93	88	6-11	10	19	3-10	11	10	0-10	59	61	12-11	76	77	10-12	100	47	8-7	139	135	
9-12	64	67	6-12	131	120	3-11	41	42	0-12	260	260	12-11	78	77	10-13	46	44	8-8	13	11	
9-13	35	32	6-13	18	10	3-12	110	112	0-14	143	140	12-12	57	61	10-13	46	44	8-8	12	11	
9-14	33	34	6-15	94	90	3-13	35	34	0-16	34	33	12-12	58	61	10-14	15	17	8-10	100	96	
9-15	8	9	6-17	83	75	3-14	11	11	0-18	46	45	12-13	36	36	10-14	15	17	8-10	07	96	
9-16	79	83	6-18	12	11	3-15	149	146	0-20	138	148	12-13	35	36	10-15	11	12	8-11	143	133	
9-17	10	14	6-19	15	16	3-17	138	138				11-1	50	52	10-15	9	12	8-11	142	133	
9-18	13	18	6-20	47	47	3-18	63	63				11-1	52	52	10-16	37	30	0-12	84	80	
8-0	42	44	6-21	10	11	3-19	18	17				11-2	67	64	10-16	38	38	8-12	79	80	
8-1	203	200	5-0	86	95	3-20	57	57	K	L	FO	FC	11-2	64	64	10-17	57	56	8-14	35	35
8-2	275	262	5-1	73	77	3-21	7	8	14	0	15	16	11-2	64	64	10-17	57	56	8-14	35	35
8-3	112	113	5-2	94	94	3-22	19	21	14	-1	83	89	11-3	28	28	9-1	69	71	8-16	53	50
8-4	68	66	5-3	52	57	2-0	88	95	14	-1	83	89	11-3	28	28	9-1	71	71	8-16	51	50
8-5	103	98	5-4	117	125	2-1	10	12	14	-2	39	40	11-4	113	109	9-2	28	27	8-17	98	95
8-6	74	72	5-5	249	231	2-2	89	91	14	-2	37	40	11-5	6	4	9-2	27	27	8-17	98	95
8-7	78	78	5-6	184	195	2-4	69	71	14	-3	8	12	11-6	25	25	9-3	24	23	8-18	111	107
8-8	147	138	5-7	45	46	2-5	159	175	14	-4	26	28	11-6	24	25	9-3	22	23	8-18	109	107
8-9	121	118	5-8	47	44	2-6	188	204	14	-4	25	28	11-7	81	81	9-4	90	97	8-19	36	36
8-10	66	63	5-9	180	180	2-7	136	140	14	-5	28	28	11-7	81	81	9-4	100	97	8-19	35	36
8-11	21	20	5-10	49	47	2-8	175	167	14	-5	28	28	11-8	90	87	9-5	20	23	7-1	75	76
8-12	55	51	5-11	37	39	2-9	25	33	14	-6	27	26	11-8	92	87	9-5	23	23	7-1	75	76
8-13	63	62	5-12	172	156	2-10	117	114	14	-6	28	26	11-9	44	43	9-6	35	33	7-2	84	87
8-14	30	33	5-13	13	12	2-11	72	70	14	-7	114	119	11-9	43	43	9-6	38	33	7-2	84	87
8-15	76	75	5-15	81	82	2-12	280	232	14	-7	112	119	11-10	95	96	9-7	115	101	7-3	82	83
8-16	11	12	5-16	10	13	2-14	108	109	13	-1	16	16	11-10	90	96	9-7	106	101	7-3	85	83
8-17	51	54	5-17	100	94	2-15	95	93	13	-1	18	16	11-11	12	12	9-8	149	151	7-4	79	82
8-18	16	15	5-18	60	56	2-16	17	16	13	-2	38	39	11-11	12	12	9-8	167	151	7-4	86	82
8-19	42	44	5-19	11	9	2-17	22	24	13	-2	38	39	11-12	13	13	9-9	66	57	7-5	15	15
7-0	46	51	5-20	67	68	2-18	61	62	13	-3	33	36	11-12	18	13	9-9	69	57	7-5	15	15
7-1	28	26	5-21	23	24	2-20	145	140	13	-3	35	36	11-13	68	66	9-10	75	76	7-6	38	38
7-2	223	218	4-0	19	18	2-21	12	17	13	-4	143	143	11-13	65	66	9-10	81	76	7-6	38	38
7-3	17	12	4-1	82	90	2-23	21	27	13	-4	148	143	11-14	79	78	9-11	14	17	7-7	139	139
7-4	142	156	4-2	126	137	1-0	34	34	13	-5	16	18	11-14	78	78	9-11	16	17	7-7	155	139
7-5	304	271	4-3	134	149	1-1	339	337	13	-5	18	18	11-15	69	69	9-12	9	11	7-8	165	165
7-6	201	176	4-4	46	47	1-2	63	62	13	-6	9	11	11-15	70	69	9-13	86	86	7-8	168	165
7-7	112	114	4-5	84	89	1-3	40	45	13	-6	9	11	10-0	43	40	9-13	82	86	7-9	97	95
7-8	44	44	4-6	149	156	1-4	141	140	13	-7	40	40	10-0	37	40	9-14	120	117	7-9	88	95
7-9	128	121	4-7	88	92	1-5	126	131	13	-7	37	40	10-1	135	124	9-14	119	117	7-10	52	52
7-10	51	49	4-8	150	141	1-6	13	15	13	-8	14	16	10-1	130	124	9-15	110	111	7-10	64	52
7-11	65	62	4-9	161	160	1-7	122	123	13	-8	16	16	10-2	46	44	9-15	120	111	7-11	40	38
7-12	120	113	4-10	32	30	1-8	48	50	13	-9	17	19	10-2	48	44	9-17	14	15	7-11	39	38
7-13	22	23	4-11	7	4	1-9	238	251	13	-9	18	19	10-3	8	9	9-17	17	15	7-12	22	22
7-14	36	39	4-12	191	179	1-10	9	10	13	-10	83	82	10-4	56	51	9-18	12	12	7-12	22	22
7-15	36	34	4-14	45	42	1-11	46	50	13	-10	82	82	10-4	56	51	9-18	11	12	7-13	106	94
7-16	56	58	4-15	109	108	1-12	27	30	13	-11	7	10	10-5	75	72	8-0	23	25	7-13	98	94
7-17	26	24	4-17	44	42	1-13	32	35	13	-11	11	10	10-5	75	72	8-0	24	25	7-14	150	140
7-18	39	35	4-18	40	40	1-15	140	152	12	0	15	18	10-6	19	19	8-1	29	28	7-14	149	140
7-20	58	54	4-20	114	106	1-17	105	111	12	0	19	18	10-6	18	19	8-1	29	28	7-15	94	92
6-0	74	72	4-21	26	26	1-18	26	29	12	-1	106	106	10-7	102	103	8-2	5	5	7-15	95	92
6-1	175	169	3-0	107	119	1-19	6	8	12	-1	107	106	10-7	113	103	8-2	6	5	7-16	40	40
6-2	309	269	3-1	6	8	1-20	19	17	12	-3	7	3	10-8	21	20	8-3	44	45	7-16	37	40
6-3	154	155	3-2	21	16	1-21	6	8	12	-4	45	44	10-8	19	20	8-3	45	45	7-17	40	39
6-4	24	21	3-3	137	150	1-22	10	13	12	-4	43	44	10-9	25	29	8-4	118	128	7-17	40	39
6-5	126	130	3-4	140	148	1-23	133	134	12	-6	27	29	10-9	27	29	8-4	122	128	7-18	12	6
6-6	124	123	3-5	162	178	0-0	161	153	12	-6	28	29	10-10	120	117	8-5	129	123	7-18	9	6
6-7	146	133	3-6	106	111	0-2	206	213	12	-7	129	126	10-10	114	117	8-5	117	123	7-19	18	20
6-8	95	89	3-7	108	110	0-4	144	147	12	-7	137	126	10-11	131	121	8-6	46	40	7-19	20	20

6-20	94	94	3-17	42	45	0-16	150	177	9-7	103	97	6-15	32	29	3-13	73	72	0-14	165	158
6-21	54	52	3-18	52	53	0-18	50	52	9-8	76	76	6-16	33	34	3-14	88	86	0-16	126	123
5-0	87	95	3-19	83	83	0-20	29	29	9-9	72	74	6-17	50	50	3-15	62	66	0-18	34	32
6-1	124	128	3-20	51	50	0-22	20	22	9-10	30	30	6-18	18	20	3-16	41	42	0-20	10	12
5-2	200	191	3-22	29	30				9-11	61	61	6-19	76	76	3-17	53	54	0-22	94	103
5-3	147	148	2-0	102	95				9-12	108	115	6-20	47	46	3-18	26	27			
5-4	133	142	2-1	56	56				9-13	67	66	5-0	181	179	3-19	115	109			
5-5	192	178	2-2	284	262				9-14	44	41	5-1	176	173	3-20	22	21			
5-6	74	75	2-3	88	93				9-16	50	51	5-2	158	148	3-21	33	34			
5-7	75	77	2-4	53	54				6-0	73	73	5-3	40	37	2-0	137	133			
5-8	17	17	2-5	88	97				6-1	162	154	5-4	178	171	2-1	137	133			
5-9	110	113	2-6	218	224				6-2	14	14	5-5	139	134	2-2	145	133			
5-10	119	110	2-7	78	83				6-3	77	78	5-6	49	50	2-3	149	147			
5-11	42	40	2-8	176	172				6-4	175	169	5-7	179	168	2-4	146	140			
5-12	17	15	2-9	13	14				6-5	68	65	5-8	181	174	2-5	61	64			
5-13	153	140	2-10	251	234				6-6	81	78	5-9	47	47	2-6	114	115			
5-14	26	24	2-11	63	61				6-7	77	75	5-11	130	122	2-7	60	62			
5-15	8	10	2-12	165	171				6-8	91	95	5-12	17	18	2-8	287	257			
5-16	70	65	2-13	36	37				6-10	82	80	5-13	28	25	2-9	20	20			
5-17	55	56	2-14	27	24				6-11	95	94	5-14	96	94	2-10	39	36			
5-18	41	42	2-15	30	31				6-12	28	30	5-15	9	10	2-11	92	90			
5-19	40	43	2-16	183	169				6-13	9	12	5-16	37	40	2-12	82	82			
5-20	93	104	2-17	83	81				6-14	40	40	5-17	16	15	2-14	155	157			
5-21	24	27	2-18	36	36				6-15	78	73	5-19	58	65	2-15	7	8			
4-0	19	18	2-19	22	23				6-16	21	21	5-20	28	27	2-16	128	123			
4-1	88	88	2-20	21	21				6-17	33	36	5-21	16	18	2-17	22	21			
4-2	161	161	2-21	29	28				6-18	9	10	4-0	26	27	2-18	52	56			
4-3	142	145	2-23	23	28				7-0	197	198	4-1	155	161	2-19	36	35			
4-4	43	42	1-0	33	34				7-1	199	192	4-2	80	78	2-21	18	21			
4-5	159	158	1-1	146	141				7-2	65	66	4-3	200	190	2-22	85	89			
4-6	243	236	1-2	58	55				7-3	20	19	4-4	184	172	1-0	96	87			
4-7	150	138	1-3	110	114				7-4	197	181	4-5	273	247	1-1	168	167			
4-8	113	104	1-4	30	30				7-5	54	52	4-6	18	19	1-2	57	58			
4-10	210	201	1-5	42	46				7-6	52	50	4-7	86	86	1-3	171	171			
4-12	125	119	1-6	12	10				7-7	136	130	4-8	187	178	1-4	66	68			
4-13	70	68	1-7	146	157				7-8	133	137	4-9	41	39	1-5	257	255			
4-14	43	43	1-8	22	23				7-9	64	59	4-10	94	83	1-6	44	45			
4-15	21	20	1-9	189	212				7-10	37	35	4-11	110	104	1-7	51	52			
4-16	123	116	1-10	37	39				7-11	83	87	4-12	56	54	1-8	30	30			
4-17	87	84	1-11	206	213				7-12	49	49	4-13	21	22	1-9	82	83			
4-19	59	62	1-12	11	13				7-13	39	39	4-14	119	111	1-10	21	21			
4-20	49	47	1-13	257	268				7-14	59	60	4-16	110	108	1-11	313	288			
4-21	51	52	1-14	15	16				7-15	8	5	4-17	56	52	1-12	16	16			
3-0	113	119	1-15	100	110				7-16	46	45	4-18	49	49	1-13	151	152			
3-1	69	69	1-16	19	23				7-18	32	30	4-19	68	64	1-14	26	26			
3-2	174	162	1-17	34	35				7-19	10	15	4-20	22	22	1-15	78	77			
3-3	295	304	1-18	29	30				6-0	16	12	4-21	33	34	1-16	22	22			
3-4	196	182	1-19	71	72				6-1	206	198	3-0	149	143	1-17	46	47			
3-5	319	329	1-20	19	18				6-2	13	9	3-1	158	153	1-18	11	11			
3-6	46	45	1-21	11	12				6-3	98	101	3-2	140	142	1-19	125	125			
3-7	178	178	1-23	23	23				6-4	260	245	3-3	8	10	1-21	21	22			
3-9	166	189	0-0	168	153				6-5	233	210	3-4	162	155	1-22	12	15			
3-10	81	81	0-2	326	330				6-6	74	75	3-5	260	242	0-0	197	182			
3-11	9	13	0-4	28	30				6-7	106	98	3-6	81	83	0-2	104	100			
3-12	8	3	0-6	123	132				6-8	159	151	3-7	120	122	0-4	212	190			
3-13	199	189	0-8	173	177				6-10	57	54	3-8	142	122	0-6	159	160			
3-14	25	25	0-10	264	259				6-11	100	90	3-9	95	98	0-8	319	336			
3-15	85	80	0-12	153	167				6-12	12	9	3-11	208	194	0-10	164	160			
3-16	52	51	0-14	48	50				6-14	58	56	3-12	9	8	0-12	84	88			

8 0	100	99	5-18	25	24	2-20	60	61	8 -3	42	41	4 -6	97	93	1-14	26	25	5 -6	96	99
8 -1	33	30	5-19	8	10	1 0	33	32	8 -4	26	27	4 -7	45	42	1-15	106	105	8 -7	160	159
8 -2	34	34	4 0	42	44	1 -1	66	59	8 -5	69	71	4 -8	83	78	1-17	46	46	5 -8	15	12
8 -3	29	30	4 -1	55	53	1 -2	54	47	8 -6	10	13	4 -9	100	94	1-18	8	11	5 -9	24	25
8 -5	39	37	4 -2	239	217	1 -3	114	117	8 -7	47	46	4-11	16	16	0 0	45	46	5-10	65	66
8 -6	121	113	4 -3	54	52	1 -4	39	39	8 -9	57	54	4-12	174	154	0 -2	122	122	5-11	28	31
8 -7	113	125	4 -4	49	47	1 -5	256	243	8-10	50	50	4-13	43	44	0 -4	291	247	4 0	57	56
8 -8	118	114	4 -5	48	46	1 -6	7	6	8-11	42	40	4-14	33	29	0 -6	159	141	4 -1	60	59
8 -9	49	50	4 -6	159	148	1 -7	71	70	8-12	60	60	4-15	86	86	0 -8	119	124	4 -2	13	13
0-11	12	9	4 -7	204	188	1 -8	21	20	8-13	26	28	4-16	59	57	0-10	91	88	4 -3	93	90
8-12	85	82	4 -8	62	59	1 -9	70	70	7 0	9	8	4-17	42	46	0-12	191	186	4 -4	84	85
8-13	154	149	4 -9	6	4	1-10	78	81	7 -1	16	18	3 0	72	70	0-14	52	55	4 -5	15	16
8-14	98	94	4-13	166	155	1-11	13	13	7 -2	41	40	3 -1	220	204	0-16	56	53	4 -6	71	71
7 -1	60	58	4-14	130	123	1-12	33	36	7 -3	69	65	3 -2	73	76	0-18	56	63	4 -7	111	107
7 -2	18	16	4-15	7	8	1-13	8	10	7 -4	151	147	3 -4	75	68				4 -8	43	45
7 -3	141	132	4-16	14	14	1-14	12	14	7 -5	63	69	3 -5	91	89				4 -9	64	64
7 -4	132	136	4-17	7	4	1-15	82	84	7 -6	82	79	3 -6	102	103				4-10	145	145
7 -5	10	7	4-18	76	79	1-16	21	20	7 -8	39	39	3 -7	70	69				4-12	29	30
7 -6	26	25	4-19	59	60	1-17	85	87	7 -9	51	50	3 -8	42	42				4-13	58	64
7 -8	66	64	3 0	84	79	0 0	65	61	7-10	6	6	3 -9	213	203				3 0	84	82
7 -9	108	106	3 -1	69	66	0 -2	470	359	7-11	10	12	3-10	29	29				3 -1	16	19
7-10	179	166	3 -2	21	21	0 -4	34	36	7-12	72	73	3-11	85	84				3 -2	39	37
7-11	108	100	3 -3	75	80	0 -6	127	127	7-13	55	57	3-12	58	52				3 -3	86	78
7-13	14	13	3 -4	40	40	0 -8	128	128	7-14	17	18	3-13	29	29				3 -4	97	95
7-14	20	22	3 -5	186	171	0-10	50	48	6 0	115	126	3-14	40	41				3 -5	36	36
7-15	22	22	3 -6	23	22	0-12	7	9	6 -1	146	156	3-15	133	127				3 -6	78	77
7-16	97	100	3 -7	62	58	0-14	39	40	6 -2	14	13	3-16	35	36				3 -7	151	151
7-17	85	89	3 -8	8	7	0-18	162	159	6 -3	87	87	3-17	17	17				3 -8	24	25
6 0	110	114	3 -9	89	83	0-20	66	73	6 -4	47	40	3-18	52	54				3-10	56	59
6 -1	76	77	3-10	163	153				6 -5	25	27	2 0	70	70				3-11	90	89
6 -2	130	130	3-11	43	45				6 -6	56	51	2 -1	110	110				3-12	27	26
6 -4	30	28	3-12	15	16				6 -7	68	65	2 -2	115	106				3-13	118	119
6 -5	54	55	3-13	17	15				6 -8	37	38	2 -3	28	27				3-14	10	16
6 -6	187	171	3-14	11	11				6 -9	61	60	2 -4	206	183				2 0	74	72
6 -7	197	182	3-15	75	74				6-12	84	86	2 -5	7	8				2 -1	42	42
6 -8	37	36	3-16	108	107				6-13	49	50	2 -6	151	140				2 -2	45	43
6 -9	8	10	3-17	83	87				6-15	86	86	2 -8	124	115				2 -3	71	69
6-10	32	30	3-18	20	20				6-16	77	84	2 -9	134	133				2 -4	99	94
6-11	10	9	3-19	11	12				5 0	60	56	2-10	36	35				2 -5	29	28
6-12	34	33	3-20	16	18				5 -1	82	83	2-11	25	24				2 -6	42	39
6-13	167	156	2 0	33	32				5 -3	28	28	2-12	210	197				2 -7	14	13
6-14	131	125	2 -1	19	18				5 -4	93	89	2-13	32	32				2 -8	83	85
6-15	20	19	2 -2	371	315				5 -5	74	68	2-14	60	59				2 -9	35	31
6-18	37	39	2 -3	71	70				5 -6	100	92	2-16	38	40				2-10	183	173
5 0	56	55	2 -4	41	41				5 -7	54	52	2-17	10	18				2-12	56	60
5 -1	8	9	2 -5	23	24				5 -8	5	4	2-18	57	60				2-13	75	70
5 -2	19	18	2 -6	105	103				5 -9	92	92	1 0	27	27				2-14	89	91
5 -3	156	143	2 -7	122	110				5-10	19	17	1 -1	280	241				1 0	48	48
5 -4	205	186	2 -8	92	92				5-11	30	31	1 -2	56	50				1 -1	37	36
5 -5	90	86	2 -9	32	32				5-12	70	69	1 -3	60	56				1 -2	26	26
5 -6	11	9	2-10	51	49				5-13	50	51	1 -4	62	55				1 -3	74	70
5 -8	24	21	2-11	34	37				5-14	28	29	1 -5	117	110				1 -4	17	16
5 -9	108	101	2-13	96	90				5-15	116	118	1 -6	69	69				1 -5	66	65
5-10	147	133	2-14	72	71				5-16	70	71	1 -7	165	155				1 -6	29	27
5-11	58	57	2-15	14	17				A 0	93	85	1 -8	34	37				1 -7	137	130
5-12	11	13	2-16	11	11				4 -1	96	90	1 -9	243	224				1 -8	22	23
5-15	34	31	2-17	6	6				4 -2	46	45	1-10	43	43				1 -9	28	29
5-16	159	154	2-18	127	128				4 -3	62	60	1-11	103	103				1-10	16	18
5-17	110	112	2-19	27	29				4 -4	109	103	1-12	14	14				1-11	110	110

6-0	100	99	24	25	24	2-20	60	61	42	41	4-6	97	93	1-14	26	25	5-5	96	99	1-12	21	23		
6-1	33	30	8	10	10	1-0	33	32	26	27	4-7	45	42	1-15	106	105	5-7	100	159	1-13	126	120		
6-2	34	34	4	4	4	1-1	66	59	60	71	4-8	83	78	1-18	4	46	5-8	15	12	1-14	22	21		
6-3	29	30	4	5	5	1-2	54	47	10	13	4-9	100	94	1-18	8	11	5-9	24	25	1-15	74	80		
6-4	39	37	4	2	2	1-3	114	117	47	46	4-11	16	16	0	45	48	5-10	65	66	0	109	114		
6-5	121	113	4	3	3	1-4	39	39	57	54	4-12	174	154	0	2	122	122	5-11	28	31	0	88	88	
6-6	113	125	4	4	4	1-5	256	243	40	50	4-13	43	44	0	2	251	247	4	60	56	0	151	140	
6-7	113	125	4	4	4	1-6	7	6	40	40	4-14	33	29	0	6	159	141	4	60	59	0	6	2	
6-8	118	114	4	4	4	1-7	71	70	60	60	4-15	85	86	0	10	124		4	60	59	0	6	2	
6-9	99	50	4	7	7	1-8	21	20	26	28	4-16	59	57	0	10	91	88	4	60	59	0	6	2	
6-10	85	82	4	6	6	1-9	70	70	9	8	4-17	42	46	0	10	191	186	4	60	59	0	6	2	
6-11	12	9	4	6	6	1-10	78	81	16	16	3	0	72	0	191	186	4	60	59	0	6	2		
6-12	85	82	4	6	6	1-11	13	13	41	40	3	1	220	204	0	16	56	53	4	60	59	0	6	2
6-13	154	149	4	6	6	1-12	33	36	89	65	3	2	73	76	0	16	56	53	4	60	59	0	6	2
6-14	98	94	4	6	6	1-13	3	3	151	147	3	4	78	68	0	16	56	53	4	60	59	0	6	2
6-15	60	58	4	6	6	1-14	12	14	63	69	3	5	91	89	0	16	56	53	4	60	59	0	6	2
6-16	18	16	4	6	6	1-15	14	14	82	84	3	5	102	103	0	16	56	53	4	60	59	0	6	2
6-17	132	136	4	6	6	1-16	82	84	7	6	3	5	102	103	0	16	56	53	4	60	59	0	6	2
6-18	10	7	4	6	6	1-17	21	20	6	6	3	5	102	103	0	16	56	53	4	60	59	0	6	2
6-19	26	25	4	6	6	1-18	76	79	7	7	3	5	102	103	0	16	56	53	4	60	59	0	6	2
6-20	66	64	3	6	6	1-19	85	87	7	7	3	5	102	103	0	16	56	53	4	60	59	0	6	2
6-21	108	106	3	6	6	1-20	65	61	6	6	3	5	102	103	0	16	56	53	4	60	59	0	6	2
6-22	108	100	3	6	6	1-21	21	21	10	12	3	5	102	103	0	16	56	53	4	60	59	0	6	2
6-23	14	13	3	6	6	1-22	40	40	7	7	3	5	102	103	0	16	56	53	4	60	59	0	6	2
6-24	20	22	3	6	6	1-23	127	127	7	7	3	5	102	103	0	16	56	53	4	60	59	0	6	2
6-25	22	22	3	6	6	1-24	80	48	6	6	3	5	102	103	0	16	56	53	4	60	59	0	6	2
6-26	97	100	3	6	6	1-25	7	9	17	18	3	5	102	103	0	16	56	53	4	60	59	0	6	2
6-27	85	89	3	6	6	1-26	58	58	6	6	3	5	102	103	0	16	56	53	4	60	59	0	6	2
6-28	118	114	3	6	6	1-27	162	159	6	6	3	5	102	103	0	16	56	53	4	60	59	0	6	2
6-29	118	114	3	6	6	1-28	66	73	6	6	3	5	102	103	0	16	56	53	4	60	59	0	6	2
6-30	130	130	3	6	6	1-29	153	153	6	6	3	5	102	103	0	16	56	53	4	60	59	0	6	2
6-31	43	45	3	6	6	1-30	43	45	6	6	3	5	102	103	0	16	56	53	4	60	59	0	6	2
6-32	15	16	3	6	6	1-31	15	16	6	6	3	5	102	103	0	16	56	53	4	60	59	0	6	2
6-33	17	15	3	6	6	1-32	15	16	6	6	3	5	102	103	0	16	56	53	4	60	59	0	6	2
6-34	11	11	3	6	6	1-33	11	11	6	6	3	5	102	103	0	16	56	53	4	60	59	0	6	2
6-35	107	182	3	6	6	1-34	75	74	11	11	6	6	6	6	6	6	6	6	6	6	6	6	6	6
6-36	37	36	3	6	6	1-35	108	107	11	11	6	6	6	6	6	6	6	6	6	6	6	6	6	6
6-37	8	10	3	6	6	1-36	11	11	11	11	6	6	6	6	6	6	6	6	6	6	6	6	6	6
6-38	32	30	3	6	6	1-37	20	20	10	10	6	6	6	6	6	6	6	6	6	6	6	6	6	6
6-39	10	9	3	6	6	1-38	10	9	10	10	6	6	6	6	6	6	6	6	6	6	6	6	6	6
6-40	34	33	3	6	6	1-39	93	96	10	10	6	6	6	6	6	6	6	6	6	6	6	6	6	6
6-41	10	9	3	6	6	1-40	25	29	16	16	6	6	6	6	6	6	6	6	6	6	6	6	6	6
6-42	34	33	3	6	6	1-41	30	29	16	16	6	6	6	6	6	6	6	6	6	6	6	6	6	6
6-43	107	186	2	6	6	1-42	30	29	16	16	6	6	6	6	6	6	6	6	6	6	6	6	6	6
6-44	131	126	2	6	6	1-43	109	108	16	16	6	6	6	6	6	6	6	6	6	6	6	6	6	6
6-45	20	19	2	6	6	1-44	371	315	10	10	6	6	6	6	6	6	6	6	6	6	6	6	6	6
6-46	37	39	2	6	6	1-45	70	70	10	10	6	6	6	6	6	6	6	6	6	6	6	6	6	6
6-47	56	55	2	6	6	1-46	41	41	10	10	6	6	6	6	6	6	6	6	6	6	6	6	6	6
6-48	8	9	2	6	6	1-47	8	8	10	10	6	6	6	6	6	6	6	6	6	6	6	6	6	6
6-49	18	18	2	6	6	1-48	42	42	10	10	6	6	6	6	6	6	6	6	6	6	6	6	6	6
6-50	156	143	2	6	6	1-49	122	110	10	10	6	6	6	6	6	6	6	6	6	6	6	6	6	6
6-51	205	180	2	6	6	1-50	92	92	10	10	6	6	6	6	6	6	6	6	6	6	6	6	6	6
6-52	90	86	2	6	6	1-51	32	32	10	10	6	6	6	6	6	6	6	6	6	6	6	6	6	6
6-53	11	9	2	6	6	1-52	51	49	10	10	6	6	6	6	6	6	6	6	6	6	6	6	6	6
6-54	24	21	2	6	6	1-53	34	37	10	10	6	6	6	6	6	6	6	6	6	6	6	6	6	6
6-55	108	101	2	6	6	1-54	96	90	10	10	6	6	6	6	6	6	6	6	6	6	6	6	6	6
6-56	147	133	2	6	6	1-55	72	71	10	10	6	6	6	6	6	6	6	6	6	6	6	6	6	6
6-57	58	57	2	6	6	1-56	14	14	10	10	6	6	6	6	6	6	6	6	6	6	6	6	6	6
6-58	11	13	2	6	6	1-57	11	11	10	10	6	6	6	6	6	6	6	6	6	6	6	6	6	6
6-59	34	31	2	6	6	1-58	26	28	10	10	6	6	6	6	6	6	6	6	6	6	6	6	6	6
6-60	159	154	2	6	6	1-59	146	142	10	10	6	6	6	6	6	6	6	6	6	6	6	6	6	6
6-61	110	112	2	6	6	1-60	127	128	10	10	6	6	6	6	6	6	6	6	6	6	6	6	6	6
6-62	110	112	2	6	6	1-61	49	48	10	10	6	6	6	6	6	6	6	6	6	6	6	6	6	6
6-63	110	112	2	6	6	1-62	49	48	10	10	6	6	6	6	6	6	6	6	6	6	6	6	6	6

H = -4

K L

H = -6

K L

H = -5

K L

H = -6

K L

H = -5

K L

H = -6

K L

APPENDIX B: OBSERVED AND CALCULATED STRUCTURE FACTORS
FOR $\gamma\text{-Mo}_2(\text{O}_2\text{CH})_4$

APPENDIX C

For the special positions of $\beta\text{-Mo}_2(\text{O}_2\text{CH})_4$, $\phi_1^{\sim}(k)$ and $\phi_2^{\sim}(k)$ designate Frenkel exciton bands of states for the two symmetry equivalent molecular transitions, where k is the wave vector.

The two Davydov bands may be represented by

$$\phi_1^{\sim}(k) = (\phi_1^{\sim}(k) + \phi_2^{\sim}(k))/\sqrt{2}$$

and

$$\phi_{II}^{\sim}(k) = (\phi_1^{\sim}(k) - \phi_2^{\sim}(k))/\sqrt{2}.$$

Transitions are allowed only to the two Davydov states $\phi_1^{\sim}(0)$ and $\phi_{II}^{\sim}(0)$. If μ_1 and μ_2 represent electric dipole operators for the symmetry related molecules, the corresponding transition moment vectors μ_1 and μ_2 are given by $\mu_1 = \langle \phi_1^{\sim} | \mu_1 | \phi_1^{\circ} \rangle$ and $\mu_2 = \langle \phi_2^{\sim} | \mu_2 | \phi_2^{\circ} \rangle$. Here, ϕ_1^{\sim} and ϕ_1° are the excited- and ground-state molecular wavefunctions for molecule 1, and ϕ_2^{\sim} and ϕ_2° represent the corresponding molecule 2 wavefunctions. The vector μ_1 may be expressed by $\mu_1 = x\hat{a} + y\hat{b} + z\hat{c}$, where \hat{a} , \hat{b} , and \hat{c} are the crystallographic unit vectors. The glide operation in $P2_1/c$ transforms the vector μ_1 into μ_2 for molecule 2, expressed as $\mu_2 = x\hat{a} - y\hat{b} + z\hat{c}$. The transition moments from the ground state ϕ° to the Davydov states $\phi_1^{\sim}(0)$ and $\phi_{II}^{\sim}(0)$ are found by

$$\mu_1 = \langle \phi_1^{\sim}(0) | (\mu_1 + \mu_2) | \phi^{\circ} \rangle = \sqrt{N/2}(\mu_1 + \mu_2) = \sqrt{2N} (x\hat{a} + z\hat{c})$$

and

$$\mu_{II} = \langle \phi_{II}^{\sim}(0) | (\mu_1 + \mu_2) | \phi^{\circ} \rangle = (\mu_1 - \mu_2)/\sqrt{2} = \sqrt{2N} (y\hat{b}).$$

N is the number of unit cells in the crystal, and the \sqrt{N} factor results from normalization of the exciton wavefunction.

The general position molecules are treated similarly. The Frenkel exciton bands $\phi_3^-(k)$, $\phi_4^-(k)$, $\phi_5^-(k)$, and $\phi_6^-(k)$ result in four Davydov states:

$$\phi_{III}^-(0) = (\phi_3^-(0) + \phi_4^-(0) + \phi_5^-(0) + \phi_6^-(0))/2$$

$$\phi_{IV}^-(0) = (\phi_3^-(0) + \phi_4^-(0) - \phi_5^-(0) - \phi_6^-(0))/2$$

$$\phi_V^-(0) = (\phi_3^-(0) - \phi_4^-(0) + \phi_5^-(0) - \phi_6^-(0))/2$$

$$\phi_{VI}^-(0) = (\phi_3^-(0) - \phi_4^-(0) - \phi_5^-(0) + \phi_6^-(0))/2.$$

The four symmetry-related molecular transition moments are:

$$\mu_3 = x\hat{a} + y\hat{b} + z\hat{c}$$

$$\mu_4 = -x\hat{a} - y\hat{b} - z\hat{c}$$

$$\mu_5 = -x\hat{a} + y\hat{b} - z\hat{c}$$

$$\mu_6 = x\hat{a} - y\hat{b} + z\hat{c}.$$

As before, $\mu_3 = \langle \phi_3^- | \mu_3 | \phi_3^0 \rangle$, and so on. The transition moments from the ground state to the Davydov states are found by:

$$\begin{aligned} \mu_{III} &= \langle \phi_{III}^-(0) | (\mu_3 + \mu_4 + \mu_5 + \mu_6) | \phi^0 \rangle \\ &= (1/2)\sqrt{N} (\mu_3 + \mu_4 + \mu_5 + \mu_6) = 0 \end{aligned}$$

$$\begin{aligned} \mu_{IV} &= \langle \phi_{IV}^-(0) | (\mu_3 + \mu_4 + \mu_5 + \mu_6) | \phi^0 \rangle \\ &= (1/2)\sqrt{N} (\mu_3 + \mu_4 - \mu_5 - \mu_6) = 0 \end{aligned}$$

$$\begin{aligned} \mu_V &= \langle \phi_V^-(0) | (\mu_3 + \mu_4 + \mu_5 + \mu_6) | \phi^0 \rangle \\ &= (1/2)\sqrt{N} (\mu_3 - \mu_4 + \mu_5 - \mu_6) = 2\sqrt{N} y\hat{b} \end{aligned}$$

$$\begin{aligned} \mu_{VI} &= \langle \phi_{VI}^-(0) | (\mu_3 + \mu_4 + \mu_5 + \mu_6) | \phi^0 \rangle \\ &= (1/2)\sqrt{N} (\mu_3 - \mu_4 - \mu_5 + \mu_6) = 2\sqrt{N} (x\hat{a} + z\hat{c}). \end{aligned}$$